Shashank Shekhar Harivyasi

EMPLOYING AB-INITIO METHODS TO STUDY DISTINCT SCENARIOS OF ADSORPTION OF ORGANIC MOLECULES ON INORGANIC SURFACES

DISSERTATION

zur Erlangung des akademischen Grades
Doktor der Naturwissenschaften
eingereicht an der

Technischen Universität Graz

Betreuer

Ao.Univ.-Prof. Dipl.-Ing. Dr.techn. Egbert Zojer

Institut für Festkörperphysik

Graz, Juni 2018

AFFIDAVIT | EIDESSTATTLICHE ERKLÄRUNG

I declare that I have authored this thesis independently, that I have not used other than the declared sources/resources, and that I have explicitly indicated all material which has been quoted either literally or by content from the sources used. The text document uploaded to TUGRAZonline is identical to the present doctoral thesis.

Ich erkläre an Eides statt, dass ich die vorliegende Arbeit selbstständig verfasst, andere als die angegebenen Quellen/Hilfsmittel nicht benutzt, und die den benutzten Quellen wörtlich und inhaltlich entnommenen Stellen als solche kenntlich gemacht habe. Das in TUGRAZonline hochgeladene Textdokument ist mit der vorliegenden Dissertation identisch.

Graz, May/Mai 3, 2018

Shashank Shekhar Harivyasi

To the Beauty of $\infty - \infty = \infty$

And to my Grandparents.

ABSTRACT

In this work, we study two distinct scenarios of adsorption of organic molecules on metal surfaces — non-planar Chloro boron-subphthalocyanine (ClB-SubPc) molecules on a Cu(111) surface as well as a perfluoroanthracenylaminoalkane thiolate self-assembled monolayer (SAM) that forms on Au(111) — using different methodologies albeit with similar motivation: simulating experimentally relevant systems.

In case of ClB-SubPc on Cu(111), our goal was to develop an understanding of the registry between adsorbate and the substrate, to develop on results from scanning tunneling microscopy (STM) experiments as well as to explore the interfacial electronic structure. We found that the registry is governed by interaction between the molecule's nitrogen atom atoms and the six-fold symmetry of the underlying substrate. By comparing simulated STM results with those experiments, we found that adsorption on Cu(111) leads to dechlorination of the ClB-SubPc molecule, resulting in formation of two chemically different moieties on the surface. To explore the evolution of interfacial electronic structure in relation to the molecule's peculiar geometry, we introduced a novel methodology and found the adsorption of this molecule is an unusual case of van der Waals-interaction activated strong electronic interaction.

For the perfluoroanthracenylaminoalkane thiolate SAM, our main goal was to be able to simulate its near edge X-ray absorption fine structure spectra in order to experimental understanding of the system. This work was a partial success because of the limitations of the presently available methodology. However, we were able identify the source of the problem and future improvements to the methodology might resolve the issue.

ZUSAMMENFASSUNG

In dieser Arbeit untersuchen wir zwei verschiedene Fälle von Adsorption organischer Moleküle auf Metalloberflächen: nicht-planare Chlor-Bor-Subphthalocyanin (ClB-SubPc) Moleküle auf einer Cu(111) Oberfläche sowie eine selbstassemblierte Monolage aus Perfluoranthracenylaminoalkan-Thiolat, die sich auf Au(111) formiert. Die Untersuchung geschieht mit verschiedenen Methoden, wenn auch mit ähnlicher Motivation, nämlich der Simulation experimentell relevanter Systeme.

Im Fall von ClB-SubPc auf Cu (111) war unser Ziel, ein Verständnis der Anordnung des Adsorbats auf dem Substrat zu entwickeln, Ergebnisse aus Rastertunnelmikroskopie (STM) Experimenten zu interpretieren und die elektronische Struktur an der Grenzfläche zu verstehen. Dabei fanden wir heraus, dass die Anordnung des Moleküls durch die Wechselwirkung zwischen den Stickstoffatomen des Moleküls sowie durch die sechszählige Symmetrie des Substrats bestimmt wird. Durch den Vergleich simulierter STM-Bilder mit denen aus Experimenten fanden wir heraus, dass die Adsorption an Cu(111) zur Dechlorinierung des ClB-SubPc-Moleküls

führt. Dies hat zur Folge, dass zwei chemisch unterschiedliche Spezies auf der Oberfläche zu finden sind. Um den Zusammenhang zwischen der elektronischen Struktur der Grenzfläche und der besonderen Geometrie des Moleküls zu untersuchen, haben wir in eine neuartige Methode entwickelt. Dabei stellte sich heraus, dass die Adsorption dieses Moleküls ein ungewöhnlicher Fall ist, bei der eine starke elektronische Wechselwirkung durch van-der-Waals Kräfte aktiviert wird.

Im Fall der selbstorganisierten Monolage von Perfluoranthracenylaminoalkan-Thiolat war unser Hauptziel ein NEXAFS-Spektrum zu simulieren, um ein tieferes Verständnis der Experimente an diesem Systems zu erhalten. Dieser Teil der Arbeit war aufgrund der Einschränkungen der derzeit verfügbaren Methodik lediglich ein Teilerfolg. Wir konnten jedoch die Ursache des Problems identifizieren, was es erlaubt durch zukünftige Verbesserungen der Methodik das.

PUBLICATIONS

I contributed to the following journal articles during the course of my doctoral studies. The first entry in the list, for which I am an equally contributing main author, is reproduced in the thesis as Chapter 1. This reproduction is done here under the Creative Commons Attribution (CC-BY) License. The second and the third entries are not reproduced as my contributions to them were minor.

[1] N. Ilyas, S. S. Harivyasi, P. Zahl, R. Cortes, O. T. Hofmann, P. Sutter, E. Zojer, and O. L. A. Monti. "Sticking with the Pointy End? Molecular Configuration of Chloro Boron-Subphthalocyanine on Cu(111)." In: *The Journal of Physical Chemistry C* 120.13 (Apr. 7, 2016), pp. 7113–7121. DOI: 10.1021/acs.jpcc.5b11799.

[2] A. Ugolotti, S. S. Harivyasi, A. Baby, M. Dominguez, A. L. Pinardi, M. F. López, J. Á. Martín-Gago, G. Fratesi, L. Floreano, and G. P. Brivio. "Chemisorption of Pentacene on Pt(111) with a Little Molecular Distortion." In: *The Journal of Physical Chemistry C* 121.41 (Oct. 19, 2017), pp. 22797–22805. DOI: 10.1021/acs.jpcc.7b06555.

[3] C. Winkler, S. S. Harivyasi, and E. Zojer. "Controlling the electronic properties of van der Waals heterostructures by applying electrostatic design." In: *2D Materials* (2018). DOI: 10.1088/2053-1583/aabea6.

In addition, the following article has been submitted for publication in a peer-reviewed journal. It is reproduced here, in its preprint form, as Chapter 3. Written permission for this has been obtained from the Editor-in-Chief of the journal to which the article has been submitted.

> S. S. Harivyasi, O. T. Hofmann, N. Ilyas, O. L. A. Monti, and E. Zojer. "Van Der Waals Interaction Activated Strong Electronic Coupling at the Interface Between Chloro Boron-Subphthalocyanine and Cu(111)."

I thank all my co-authors for their support and cooperation.

ACKNOWLEDGMENTS

Teacher and Truth are both here
First salutation should go where?
Very many thanks to thee Teacher
For ye revealed Truth's very nature!
— Kabir

I express my heartfelt gratitude to *Egbert* for his excellent guidance and unlimited support from the day I first wrote to him; I owe the fruition of this endeavor to him. Beyond his vast knowledge, he possesses a kind heart and the highest of values.

The completion of this work was made possible with the help of many people and institutions. I would like to thank:

Prof. Brivio and Morten, for welcoming me into their groups and for providing me with an opportunity to explore and learn new techniques. Many thanks to Guido for leading, by example, towards fine workmanship.

Oliver and Karin, for their patience while bearing with my numerous doubts. Oliver, the real one, for being cool and fun to collaborate with!

The European Union Seventh Framework Programme for funding my employment and travels under the grant agreement n° 607232, ThinFace. Thanks Katharina, for managing the project and for your support for my activities as the representative of the ESRs.

The 'Physics and Chemistry of Advanced Materials' (PCAM) European Doctorate Programme for providing a network of like-minded colleagues.

The Vienna Scientific Cluster and the TU Graz Zentraler Informatikdienst for computing resources, on VSC3 and d-clsuter, and technical support.

I thank my superb colleagues with whom I had the pleasure to work, discuss ideas, share meals and have coffees:

The *Egbert(inn)en:* Alexander, Andreas, Antón, Aurelie, Berni, Christian, Eduardo, Elsi, Georgii, Gernot, Giulia, Hermann, Iris, Jimmy, Lisi, Lukas, Lukas, Markus, Michael, Natalia, Philipp, Simon, Thomas, Tomas and Veronika.

The Danskere, the Italiani and the ThinFace tribe: Abhilash, Aldo, André, Anu, Bernhard, Bhushan, Chloé, Golnaz, Laura, Mattia, Mehrad, Mina, Moritz, Myles, Paola, Vida and Weike.

I am grateful to my teachers, past and present: my education is as much a cumulative result of their efforts as mine. I am indebted to family and friends for their support and kindness through the journey.

Srishti, for being there with me.

CONTENTS

ACRONYMS

ClB-SubPc Chloro boron-subphthalocyanine

CLS core-level spectroscopy

DoS Density of States

DFT density functional theory

DOI digital object identifier

ELPA Eigenvalue SoLvers for Petaflop-Applications

xc exchange-correlation

HF Hartree-Fock

fcc face-centered cubic

FCH full core-hole

FHI-aims Fritz Haber Institute *ab-initio* molecular simulations

GGA Generalized Gradient Approximation

HCH half core-hole

hcp hexagonally close-packed

HOMO highest occupied molecular orbital

HOPG highly oriented pyrolytic graphite

KS Kohn-Sham

LUMO lowest unoccupied molecular orbital

MLE monolayer equivalent

NEXAFS near edge X-ray absorption fine structure

NAO numeric atom-centered orbitals

OVITO The Open Visualization Tool

PAH polycyclic aromatic hydrocarbon

PBE Perdew-Burke-Ernzerhof

PTCDA Perylenetetracarboxylic dianhydride

PW plane wave

QE Quantum Espresso

SCF self-consistent field

STM scanning tunneling microscopy

SAM self-assembled monolayer

TS Tkatchenko-Scheffler

UHV ultrahigh vacuum

UP ultraviolet photoelectron

vdW van der Waals

VASP Vienna *Ab-initio* Simulation Package

XPS X-ray photoelectron spectroscopy

Part I

INTRODUCTION

Maybe 'doing it' is the right way of learning [physics]...

— Gerd Binnig
from *Nobel Lectures, Physics 1981-1990*

INTRODUCTION

Silicon-based electronic devices are the workhorse of the information age we live in. However, these devices are limited in their scope of applicability (being bulky, inflexible and opaque) and are produced by energy and cost intensive methods. Therefore, the idea of augmenting them with a new class of materials has been explored to a great extent, with organic semiconductors, 2D materials and molecular frameworks being some strong (not necessarily competing) candidates. Of these, organic semiconductors have been very successful and are already being commercialized, especially in (organic) light emitting diodes which are now ubiquitous in hand-held devices with displays. Such electronic devices, that are based on organic semiconductors, form the basis of 'organic electronics'.

The aspect of an organic electronic device that determines its (opto)electronic properties to a large extent is the 'interface' that the organic semiconductor in the device forms with other active elements of the device circuitry. This makes it necessary to develop a comprehensive understanding of these interfaces, particularly organic semiconductor-metal interfaces, in order to improve the performance of organic electronic devices [69]. Two important aspects of the interface that have significant impact on the properties of the organic semiconductor-metal interface are (i) the (molecular) structure of the organic semiconductor in vicinity of the metal conductor, and (ii) the electronic structure at the interface between the metal and the molecules of the semiconductor [17, 76].

In this thesis we first explore both these aspects in context of the interface between non-planar subphthalocyanine molecules and Cu(111). In Chapter 1, we develop a new understanding of the molecule's geometry after it interacts with the metal. In Chapter 3, we follow this with an exploration of the resulting interfacial electronic structure and report on how, in this particular case, dispersive interactions lead to a fundamental alteration in the interfacial electronic structure. In both these chapters, our simulated *ab-initio* results build on a fruitful dialogue with experimental results, at times corroborating them and at times being validated by them. Particularly, the findings presented in Chapter 1 rest mainly on successful simulation of experimental scanning tunneling microscopy images. This, in itself, highlights the importance of being able to simulate various experimental techniques.

Therefore, in the second half of this thesis, we work on a strategy to simulate core-level spectroscopy techniques. Focusing on acenes and terphenyls, and their perfluorinated counterparts, we make an attempt at simulating X-ray photoelectron spectroscopy and near edge X-ray absorption fine structure (NEXAFS) spectroscopy of these molecules and of self-assembled monolayers (SAMs) that have them as their molecular backbone. In Chapter 5 we reproduce known results and then successfully replicate the experimental NEXAFS spectra for a SAM with terphenyl as its backbone. In Chapter 6, we discuss the problematic case of a SAM that sports a perfluorinated anthracene molecule as its molecular backbone and then detail a worked-around solution to successfully simulate its NEXAFS spectra.

Part II

SUBPHTHALOCYANINE ON COPPER

In this part of the thesis, we discuss the adsorption of subphthalocyanine molecules on copper. While these molecules are known to adsorb on coinage metals and exhibit interesting features, there are a number of open questions regarding their registry with the metal surface as well as the dynamics of the adsorption process. Focusing mainly on their adsorption on the Cu(111) surface, we explored both these issues using *ab-initio* methods and, aided by experimental results, built a comprehensive understanding for this system. The findings were split into two sets: The first one, answering the question of molecules' registry on Cu(111), was published in *The Journal of Physical Chemistry C* and is reproduced here as Chapter 1. The second set of results, pertaining adsorption dynamics, rests on a novel approach of studying adsorption which was developed during the course of this thesis. The results have been compiled in form a *manuscript* which has now been submitted for publication as an article in a peer-reviewed journal. The *manuscript* in its extant form, before submission, is the basis of Chapter 3.

1

MOLECULAR CONFIGURATION OF CHLORO BORON-SUBPHTHALOCYANINE ON Cu(111)

PREAMBLE

This chapter was published as a peer-reviewed journal article entitled "Sticking with the Pointy End? Molecular Configuration of Chloro Boron-Subphthalocyanine on Cu(111)" in *The Journal of Physical Chemistry C*. The original version can be accessed using the digital object identifier (DOI): 10.1021/acs.jpcc.5b11799. Supporting information which was published along with the journal article and a list of affiliations of its authors is given in the addendum, Chapter 2.

Several authors contributed to this article and the research it is based on. Nahid Ilyas did the experiments, wrote the first draft and placed all the experimental results in its context. The author of this thesis performed all the *ab-initio* simulations, added the results generated from them to the draft and, in the process, significantly rewrote the text to accommodate for the new insights that emerged from the simulations. Rocio Cortes assisted, Percy Zahl oversaw and Peter Sutter advised on the STM experiments. Oliver T. Hofmann helped with the DFT calculations, particularly those pertaining simulation of STM. Egbert Zojer and Oliver L.A. Monti steered the course of computational and experimental studies respectively, together developed a coherent interpretation for all the results and polished the manuscript. All authors contributed towards developing the scientific insights delivered in the article. Last, but not the least, the quality of the article in its published form was further improved by catering to the constructive comments received during the peer-review process.

ABSTRACT

In this combined low-temperature scanning tunneling microscopy (STM) and density functional theory (DFT) study, we investigate self-assembly of the dipolar nonplanar organic semiconductor Chloro boron-subphthalocyanine (ClB-SubPc) on Cu(111). We observe multiple distinct adsorption configurations and demonstrate that these can only be understood by taking surface-catalyzed dechlorination into account. A detailed investigation of possible adsorption configurations and the comparison of experimental and computational STM images demonstrates that the configurations correspond to "Cl-up" molecules with the B—Cl moiety pointing toward the vacuum side of the interface, and dechlorinated molecules. In contrast to the standard interpretation of adsorption of nonplanar molecules in the phthalocyanine family,

we find no evidence for "Cl-down" molecules where the B—Cl moiety would be pointing toward the Cu surface. We show computationally that such a configuration is unstable and thus is highly unlikely to occur for ClB-SubPc on Cu(111). Using these assignments, we discuss the different self-assembly motifs in the submonolayer coverage regime. The combination of DFT and STM is essential to gain a full atomistic understanding of the surface-molecule interactions, and our findings imply that phthalocyanines may undergo surface-catalyzed reactions hitherto not considered. Our results also indicate that care has to be taken when analyzing possible adsorption configurations of polar members of the phthalocyanine family, especially when they are adsorbed on comparably reactive surfaces like Cu(111).

1.1 INTRODUCTION

Well-defined structure-function relationships relating molecular structure to thin film structure and ultimately interfacial energy level alignment have been difficult to establish for many organic semiconductor/metal surface combinations due to the high structural diversity of the organic molecules of interest [22, 32, 33, 65, 91, 136, 155]. This is further compounded by frequent polymorphism and often complex phase diagrams for organic thin film growth [10, 104, 125]. The root cause lies likely in the fact that the important interactions, ranging from dipole repulsion and van der Waals interactions to charge-transfer related forces, occur on comparable energy scales. This makes predictive insight into the molecular adsorption and resulting thin film structure for arbitrary organic semiconductors still challenging [131, 145, 153].

Nonplanar members of the phthalocyanine family provide a step toward addressing such issues. Their shuttlecock shape results in a limited number of different adsorption configurations that have been widely interpreted as stemming from the polar axial group either facing vacuum ("up") or the supporting surface ("down") [1, 14, 45, 86, 107, 109, 131–133, 153, 160]. In principle, this offers an attractive opportunity for investigating the consequences of different adsorption configurations and surface-molecule coupling on energy level alignment and thin film structure for the same molecule.

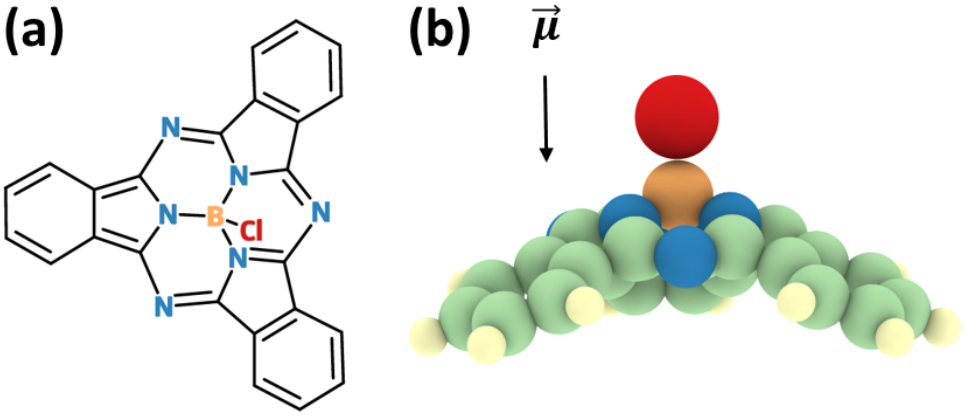

Figure 1.1: (a) Chemical structure and (b) shuttle-cock shaped geometry of a gas-phase ClB-SubPc molecule. The permanent dipole moment is also indicated. Color code of atoms: Cl, red; C, pale green; N, blue; B, orange; H, pale yellow.

The present paper reports on the detailed investigation of Chloro boron-subphthalocyanine (ClB-SubPc, Figure 1.1) on Cu(111). ClB-SubPc is an important member of the class of three-fold symmetric SubPc molecules, which displays distinctly different structures upon adsorption on (111) coinage metal surfaces [12, 68, 71, 96, 148]. On Cu(111), scanning tunneling microscopy (STM) reveals two adsorption configurations [68, 148], while on both Ag(111) and Au(111) only a single adsorption configuration for all ClB-SubPc molecules was found [12, 71, 96]. Still, the nature of the different adsorbate configurations and their consequences for self-assembly are not yet fully understood.

Here, we combine findings from low-temperature scanning tunneling microscopy (LT-STM) and dispersion-corrected density functional theory (DFT) to elucidate in detail the adsorption of ClB-SubPc on Cu(111) and its consequences for self-assembly in the submonolayer regime. We provide for the first time both experimental and theoretical evidence that the different adsorbate configurations on Cu(111) are in fact two distinct molecules, (i) intact ClB-SubPc and (ii) B-SubPc, the result of a surface-catalyzed dechlorination reaction. Our findings may apply more broadly to dipolar phthalocyanines on metal surfaces and highlight that surface-catalyzed reactions must be taken carefully into account when investigating such interfaces.

1.2 MATERIALS AND METHODS

1.2.1 *Scanning tunneling microscopy*

Cu(111) was cleaned by repeated cycles of Ar^+ sputtering (1.0 kV) and annealing at 830 K. ClB-SubPc was purchased from Sigma-Aldrich (85%) and was further purified by a single cycle of gradient sublimation in a custom-built furnace, where it formed large ($\geq$1 cm) crystal sheets of high purity. Prior to deposition, the purified ClB-SubPc was degassed overnight in a home-built water-cooled Knudsen cell under ultrahigh vacuum (UHV) conditions ($< 2 \times 10^{-9}$ Torr) slightly below its sublimation point at 433 K. The molecular film thickness on the substrate was monitored by a quartz crystal microbalance and calibrated against a statistical ensemble of STM images. The molecules were deposited at a slow rate corresponding to an average growth rate of one monolayer equivalent (MLE) in ~28 min. Here, a full MLE refers to a hypothetical layer formed with molecules in a high-density hexagonal-closed packing arrangement (see Section 1.3.2 for more detail). Following deposition at temperatures variously chosen between 150 and 255 K, the surface was quenched to 77 K and the sample was transferred immediately (< 5 min) to a cryogenic UHV scanning tunneling microscope (LT-STM) held at 5 K and equipped with GXSM custom control [161, 162]. All images were acquired with electrochemically etched tungsten tips in constant-current mode and were subsequently further processed using the WSxM software package [64].

1.2.2 *Computational*

All calculations of the ClB-SubPc | Cu(111) interface were carried out using the Fritz Haber Institute *ab-initio* molecular simulations (FHI-aims) package [13] with

"tight" settings, as shipped with the code, and employing the dispersion corrected PBE+vdW^{surf} functional [113, 120, 144]. The functional provides remarkable reliability for both the geometric [94] and electronic structure [61] of metal-organic interfaces. The repeated-slab approach was employed in an orthogonal $(7 \times 4\sqrt{3})$ unit cell with periodic replicas of the metal slab/adsorbate separated by at least 25 Å of vacuum. Each unit cell contained one molecule of ClB-SubPc (corresponding to a coverage of 0.54 MLE). This results in a distance of at least 5.14 Å between each molecule and its periodic image. The registry of the molecule with the Cu(111) surface and its orientation relative to the high-symmetry directions of the surface were deliberately varied prior to geometry optimization in order to scan multiple local minimum geometries (vide infra). The metal substrate in the unit cell was represented by six layers of Cu exposing the (111) surface. The bottom four layers were frozen at the bulk positions during geometry optimization. Dispersion correction for the Cu-Cu atom pairs of the substrate was disabled. The replicas were electrostatically decoupled using a self-consistently determined discontinuity of the electrostatic energy in the vacuum region [106]. A $2 \times 2 \times 1$ Monkhorst-Pack [100] k-point grid was used. The convergence criterion for the energy self-consistency cycle was 10^{-6} eV and the geometry was relaxed until the maximum residual force component per atom was below 0.01 eV/Å.

The adsorption energy, E_{ads}, for all cases was calculated as

$$E_{ads} = E_{inter} - (E_{Cu} + E_{ML}) \tag{1.1}$$

where E_{inter} refers to the energy of the interacting ClB-SubPc | Cu(111) system; E_{Cu} is the energy of a pristine Cu(111) slab with the top two layers relaxed, and E_{ML} is the energy of relaxed free-standing monolayer of ClB-SubPc molecules. Simulated STM images were obtained using the Tersoff-Hamann approximation [142] at a sample bias of -2 V and with an active tip radius of 1.5 Å, following the procedure described in reference [57]. All images showing 3D structures have been created using OVITO [135].

1.3 RESULTS AND DISCUSSION

1.3.1 *Overview*

In order to investigate the molecular self-assembly of ClB-SubPc on Cu(111), we prepared thin films in a wide range of conditions, varying surface coverage in particular. For all coverages and growth conditions, we find exclusively two markedly different STM contrasts for the molecular adsorbate in the first layer, as shown in a representative close-up constant-current STM image in Figure 1.2a. They are labeled **I** and **II** and are characteristic of the two STM contrasts obtained throughout all images. The overview at low coverage in Figure 1.2b indicates that type **I** and **II** molecules are the only species on the surface other than occasional small aggregates (labeled "cluster" in Figure 1.2b) whose structure is not resolved. The contrast of the type **I** and **II** molecular adsorbates is remarkably independent of the tip-surface voltage (reported here as sample bias V_s) at least over the investigated window from -2.5 V to $+0.5$ V. The salient difference between the two molecular types is that molecules of type **I** exhibit a bright center while for type **II**

the conductance increase in the molecular center is much less pronounced. Similar observations have been reported for various dipolar metal phthalocyanines on a range of different surfaces [1, 86, 107, 109, 153]. The two distinct contrasts in STM images of dipolar phthalocyanines are usually interpreted as originating from two molecular adsorption configurations that differ primarily in the spatial orientation of the axial ligand, either protruding into the vacuum side of the interface (**I**) or facing the surface (**II**). The microscopic detail of how the axial ClB ligand in type **II** faces the Cu(111) surface is however rather unclear. This is important, because the two configurations of ClB-SubPc on Cu(111) exhibit fundamentally different thin film formation propensities as shown below. The differences in the self-assembly behavior suggest that the surface-molecule interactions differ substantially for the two configurations.

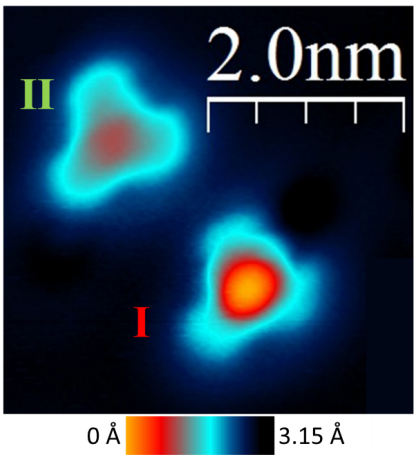

(a) Close-up ($V_s = 0.5$ V; $I_t = 150$ pA; $T = 5$ K).

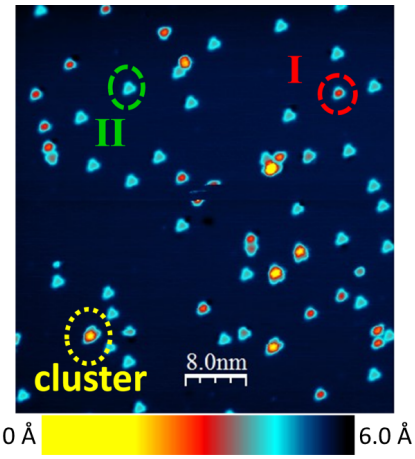

(b) Overview (0.04 MLE coverage; $V_s = -1.94$ V; $I_t = 50$ pA; $T = 5$ K). An example of the "cluster" feature is also marked.

Figure 1.2: Representative STM images showing two adsorbate species, classified as type **I** (high) and type **II** (low) depending on the conductance in the molecular center. Films grown at 205 K.

To investigate this issue in more detail, we used quantum-mechanical simulations to consider a broad range of possible adsorption configurations. These configurations are shown in Figure 1.3 in schematic and atomistic pictures where the latter are the result of DFT-based geometry optimizations.

First, we simulated the two most widely proposed configurations for similar systems: Molecules with chlorine atoms protruding toward vacuum (conventionally called the "Cl-up" system, Figure 1.3a), and molecules with chlorine atoms oriented toward the substrate (usually referred to as "Cl-down", Figure 1.3b). Out of all possibilities considered, the Cl-up configuration results in the most stable adsorbate geometry, with an adsorption energy of -3.6 eV and a simulated STM image that is remarkably similar to those observed for type **I** molecules. Our simulations reveal however that the proposed Cl-down configuration does not form readily on this surface; it can only be obtained when the molecular C_{3v}-symmetry axis is aligned exactly perpendicular to the substrate. It is also accompanied by

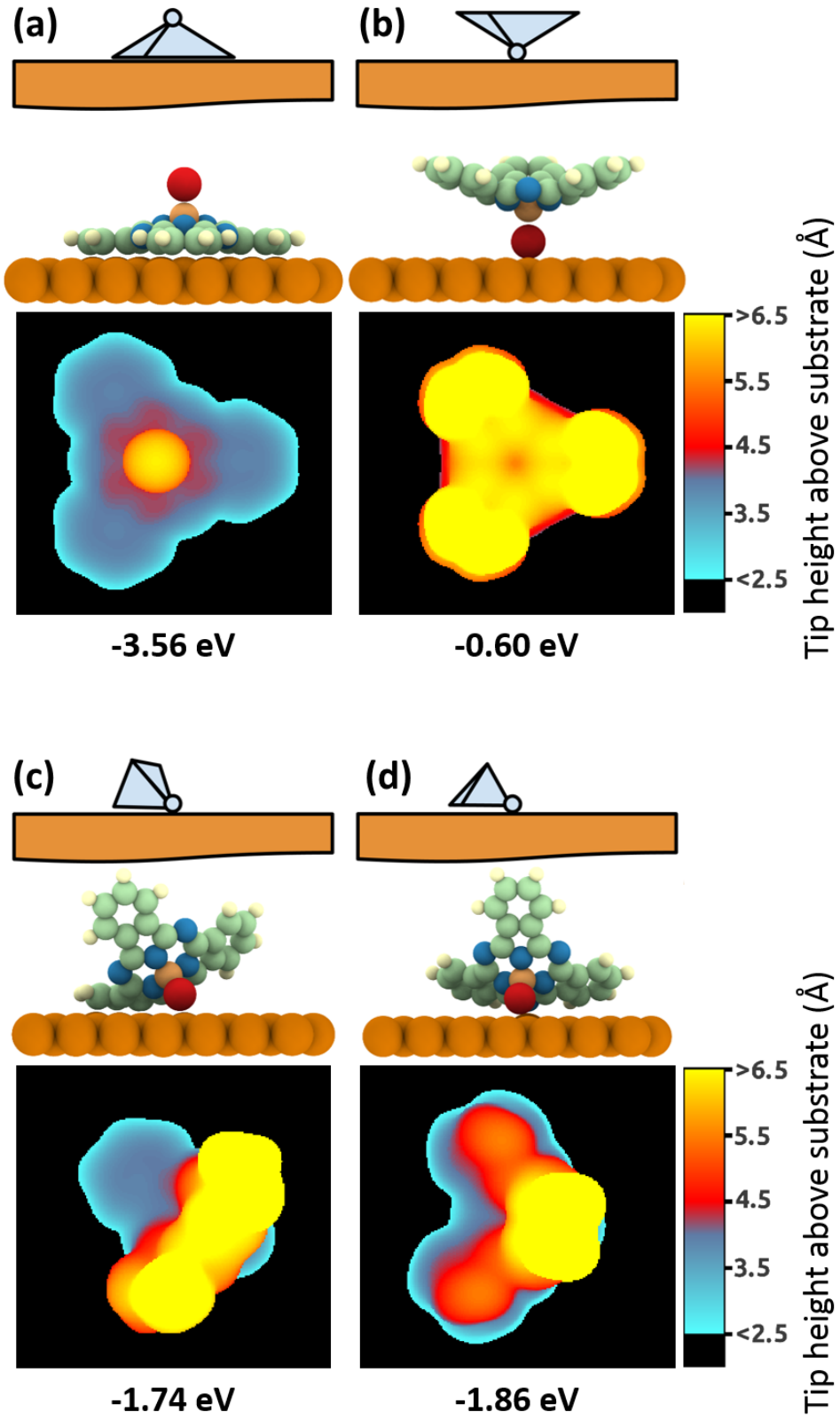

Figure 1.3: Adsorption configurations investigated by DFT: (a) Cl-up, (b) Cl-down, and "fallen" with (c) one or (d) two isoindole unit(s) in contact with the Cu(111) substrate. In every panel, top row: schematic; second row: atomistic picture based on DFT; third row: corresponding simulated STM image ($V_s = -2$ V); and bottom row: calculated adsorption energy for the configuration. Color code of atoms: Cl, red; C, pale green; N, blue; B, orange; H, pale yellow.

a comparatively small adsorption energy of only −0.60 eV. This surface-molecule geometry is thermodynamically not stable towards the formation of one of two possible "fallen" configurations, which have either a single isoindole (Figure 1.3c) or two isoindole groups in contact with the substrate (Figure 1.3d). Though not as strongly adsorbed as Cl-up, both "fallen" configurations are significantly more stable than the upright-standing Cl-down structure. Most strikingly, the simulated STM images in Figure 1.3 for Cl-down and "fallen" look profoundly different from either the type **I** or the type **II** molecules observed in the experimental images. Note that the brightest features in Figure 1.2b, labeled "cluster", have too large of an apparent height to be consistent with the "fallen" configurations. This suggests a different nature of the type **II** configuration. To clarify this finding, we investigate in the following sections each of the two adsorption types in more detail relating the atomistic structure of the adsorbate geometry to (sub)monolayer growth. We then explore the possibility of a surface-catalyzed chemical modification of the ClB-SubPc molecules as the origin for configuration **II**.

1.3.2 *Origin of adsorbate type I: Cl-up*

Among the four simulated configurations (Figure 1.3), the Cl-up system reproduces all the salient characteristics of adsorbate type **I** satisfactorily. Thus, the results of the corresponding calculations can be used to better understand the atomistic properties of the adsorbate: In the simulated Cl-up configuration, the molecule flattens considerably upon surface adsorption. When measuring the molecular height, defined as the distance between the Cl atom and the plane spanned by the six outermost C atoms (see Figure 2.1 in Chapter 2), one observes a decrease from 4.46 Å (gas phase) to 3.25 Å (adsorbed). During adsorption, the B—Cl bond length remains virtually unchanged at 1.86 Å, as the flattening almost exclusively affects the π-backbone of the molecule. Consequently, the Cl atom protrudes sharply from the backbone and results in a large contrast enhancement at the center of the molecule in the simulated STM image. This is indeed also the case for the measured images of the Cl-up system (Figure 1.2).

1.3.3 *Growth of adsorbate type I: Cl-up*

Beyond the very lowest coverages investigated, we observe a small number of disordered molecular clusters and bilayer structures (Figure 1.4, marked by green circles and discussed in more detail in Section 1.3.5) and the nucleation of ordered islands. For type **I** molecules, self-assembly manifests itself in the coexistence of two kinds of ordered islands with different packing densities, interspersed with randomly distributed isolated molecules. Most notable at this and similar coverages is the formation of large hexagonally close-packed (hcp) islands (Figure 1.4a and red square close-up) that consist predominantly of Cl-up (type **I** molecule). These islands are densely packed with measured unit cell dimensions of 13.7(10) Å × 14.7(10) Å, an acute angle of 60°, and an area of 174 Å² (see Figure 2.2 in Chapter 2 for a molecular model). Similar hcp structures have also been reported for ClB-SubPc islands on Ag(111) and Au(111) surfaces [12, 71], albeit for the suggested Cl-down adsorbate configuration. On Cu(111), after annealing to 350 K, a

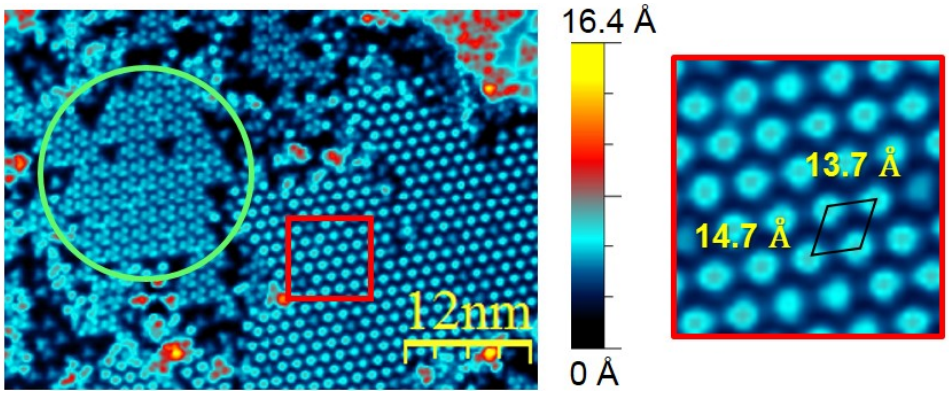

(a) Two-dimensional hcp islands of Cl-up molecules with detail and unit cell dimensions (close-up red box in right panel). Imaging conditions: $V_s = -2.5$ V; $I_t = 50$ pA; 5 K.

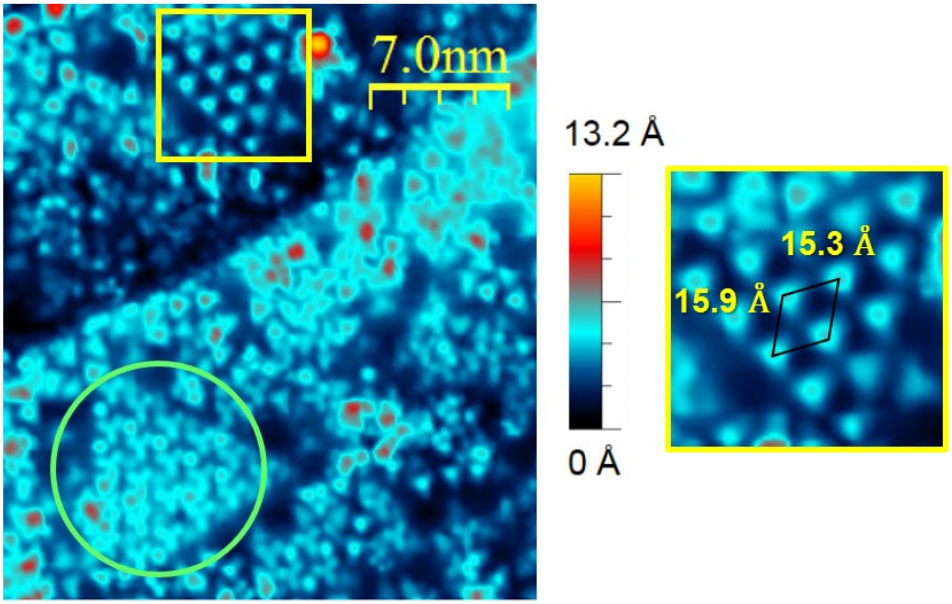

(b) Low-density hcp Cl-up islands with close-up detail and unit cell dimensions in right panel. Imaging conditions:$V_s = -2.0$ V; $I_t = 50$ pA; 5 K.

Figure 1.4: STM images of 0.50 MLE ClB-SubPc on Cu(111) prepared at 205 K showing the coexistence of different types of ordered islands.
Note that the height scale bar in both panels is different from the ones used in Figure 1.2 in order to accommodate the much wider range of heights in this image caused by step edges, terraces, and bilayer structures. Also, the contrast between panels (a) and (b) differs due to the presence of a step in (b). Green circles: bilayer structures, discussed in detail in Section 1.3.5. Red and yellow squares: close-up of the two observed hcp structures.

(9 × 9) honeycomb structure was reported instead [148]. We used these islands to define coverage in terms of MLE (cf. Section 1.2). Less frequent are low-density hcp islands (Figure 1.4b and yellow square close-up), which also consist predominantly of adsorbates of type **I** (Cl-up). The unit cell dimensions for these islands are 15.9(10) Å × 15.3(10) Å, and the acute angle of the unit cell is again ~60°, resulting in a unit cell area of 220 Å². This structure has not been previously reported. Although unit cell measurements are uncertain to within approximately 1 Å due to piezo hysteresis, low- and high-density hcp structures are clearly distinct and correspond to different molecular growth on the Cu(111) surface. The slightly different shape of the molecules in these two island kinds is likely due to finite STM tip-size effects, slightly different local DoS, and the z-dependence of the tunneling matrix element.

Close inspection of these islands shows that most molecules are oriented along the same surface direction although one might conclude that the six-fold symmetry of the top-layer of the surface together with the three-fold molecular symmetry should allow for two molecular orientations on the surface. Contrary to this, molecules rotated by 60° are found primarily at the edges of hcp islands (vide infra). A computational survey of different surface-molecule registries, summarized in Figure 1.5, shows that the most favorable adsorption geometry places the axial ClB ligand above one of the two hollow sites (hcp and face-centered cubic (fcc) hollow).

Atop (Figure 1.5a) and bridge (Figure 1.5b) sites are significantly less stable, and adsorption at hollow sites is thermodynamically preferred. The DFT simulations predict that the energy difference between different rotational orientations for molecules adsorbed at either hcp or fcc hollow site is at least 0.2 eV. Consequently, at those sites orientations with near-perfect registry between the isoindole N atoms and the Cu atoms in the top layer of the (111) surface are expected (Figures 1.5c and 1.5f). Strong Cu-N interactions have been reported to be favorable also, for example, for azobenzene on Cu(111) [156]. This alone would still allow for two orientations of the molecular adsorbates on the surface, but the calculations predict that a location of the B atom at the hcp-hollow site is energetically preferable by ~0.14 eV over the fcc-hollow site, hinting towards an interaction of the molecule also with the second layer of the substrate. Consequently, it is not sufficient to consider only the topmost substrate layer and the actual three-fold rotational symmetry of the substrate is crucial for explaining why only one orientation of the molecules is observed experimentally on the Cu(111) surface. This is in spite of the fact that calculated energy differences for different orientations are small compared to the total adsorption energy of −3.6 eV and potentially approach the limit of accuracy of the applied computational methodology. Experimentally, a definitive identification of surface registry has not been possible; however, a correlation of the isolated Cl-up molecule with an atomically resolved Cu(111) lattice is in tentative agreement with adsorption at a hollow site (see Figure 2.3 in Chapter 2). Defects in the sense of molecules rotated by 60° occur principally at boundaries of well-ordered islands (vide infra).

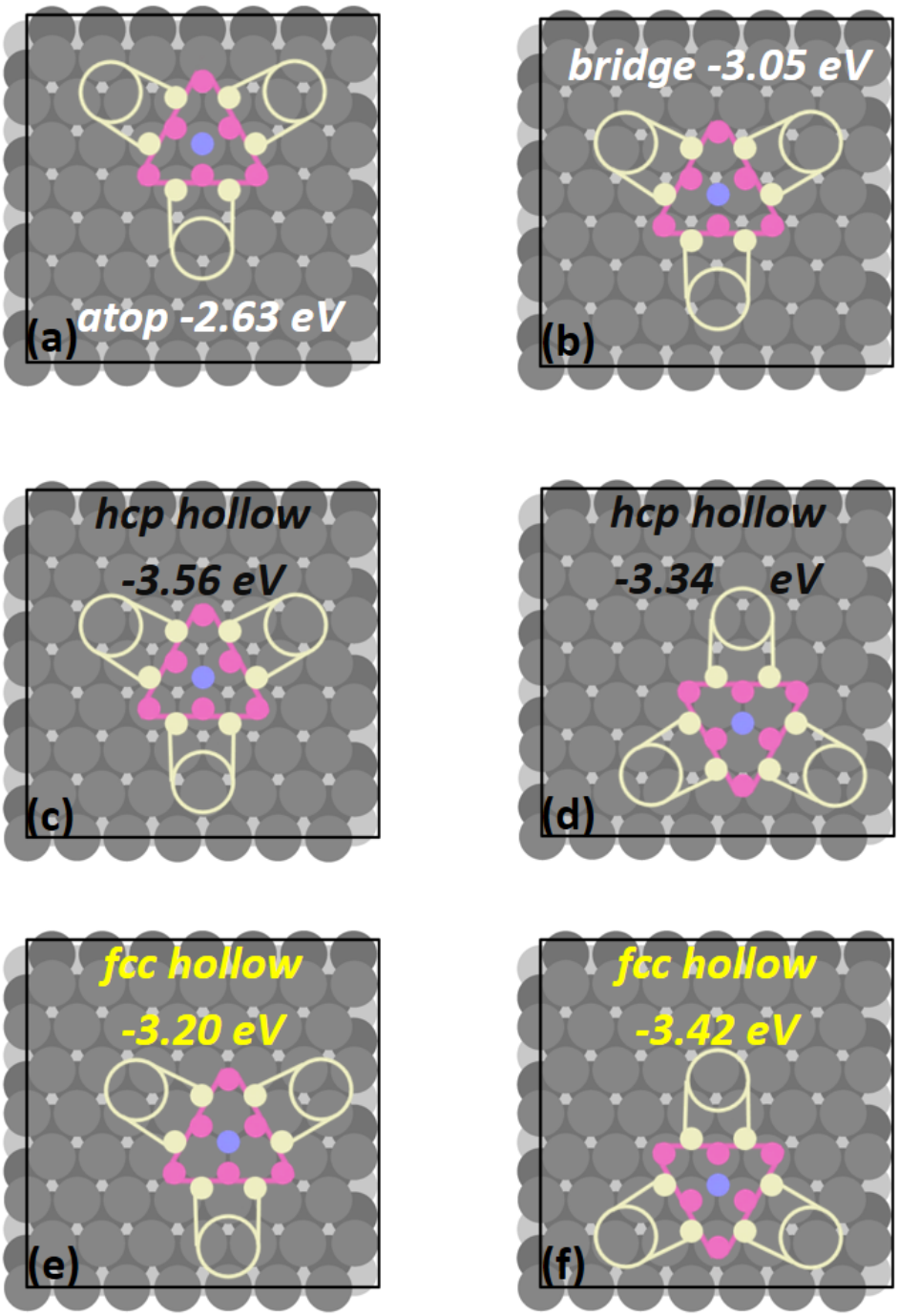

Figure 1.5: ClB-SubPc Cl-up on (a) atop site, (b) bridge site, (c) hcp hollow site with maximum N-Cu registry (referenced as 0°), (d) hcp hollow site with reduced registry (rotated by 60°), (e) fcc hollow site with reduced registry (0°), (f) fcc hollow site with maximum registry (rotated by 60°). Numbers in all schematics represent calculated adsorption energies. The top three layers of the copper slab are color coded in gray (top layer), dark gray (second layer) and light gray (third layer) respectively. N atoms are shown in magenta, the C frame is beige, and the B—Cl moiety is blue.

1.3.4 *Origin of adsorbate type II: Dechlorination*

The identification of the nature of the adsorbate type **II** turns out to be considerably more complex than for type **I**. As discussed above, "fallen" geometries would result in a symmetry reduction in the STM pictures, which is not observed experimentally. Thus, the fallen configurations can be immediately excluded as possible candidates for the adsorbate type **II**.

The upright Cl-down configuration with the ClB-SubPc molecule precariously balanced along its B—Cl bond axis indeed yields simulated STM images preserving the molecular C_{3v} symmetry (Figure 1.3b). However, contrary to the experimental STM images of type **II** molecules, in the simulated image the conductance is highest in the isoindole groups of the heterocycle with a contrasting depression in the molecular center. Moreover, for such a configuration the apparent height of the isoindole groups is larger than even that of the Cl atom in Cl-up molecules, again at variance with the experimental observations. The fact that this is not a configuration likely found on the Cu(111) surface is further emphasized by the rather low adsorption energy of -0.60 eV, dramatically smaller than all other adsorption configurations investigated thus far (vide supra). Additionally, such a configuration would likely entail a rather low rotational barrier around the C_3 axis bearing in mind the significant distance between the molecular backbone and the metal surface. Consequently, rotational motion is not expected to be frozen even at 5 K, resulting in random orientations of type **II** molecules and rotational blurring. Yet, none of the experimentally obtained STM images show any indication of rotational motion, and all type **II** ClB-SubPc molecules appear identically oriented on the Cu(111) surface. To summarize, by comparing atomistic simulations with experiments we find no stable Cl-down configuration that preserves the experimentally observed three-fold molecular symmetry while simultaneously leaving the B—Cl bond intact.

In light of these findings, we next consider surface-catalyzed dechlorination of ClB-SubPc. To this end, we removed the chlorine atom from the molecule in the fallen configuration with one isoindole group in contact with the substrate and proceeded to relax the resulting dechlorinated structure. Because of the sizable adsorption energy of Cl atoms on Cu(111) [112], the Cl atom is expected to remain on the substrate. In order to minimize residual interactions between the molecular fragment and the Cl atom, the Cl atom was moved in our calculations 6 Å away from the dechlorinated molecule (Figure 1.6). Consistent with the observations of dechlorination for porphyrin derivatives [59, 152], we investigated two likely configurations, referred to in the following as "DeCl-down" (with the Cl atom below the molecular backbone, cf. Figure 1.6a) and "DeCl-up" (with the Cl atom above the molecular backbone, cf. Figure 1.6b). Our calculations suggest that the DeCl-up configuration is considerably more stable than DeCl-down; the transition from DeCl-down to DeCl-up is thermodynamically favored by 0.6 eV (see Figure 2.4 in Chapter 2 for further discussion), and the net adsorption energy for the dechlorinated DeCl-up molecule plus a chlorine adatom is -3.44 eV. Remarkably, other than the Cl-up configuration this is the most stable configuration we were able to identify. It is also more favorable by 1.58 eV than the fallen configuration (with two isoindole in contact with the substrate), which is the energetically

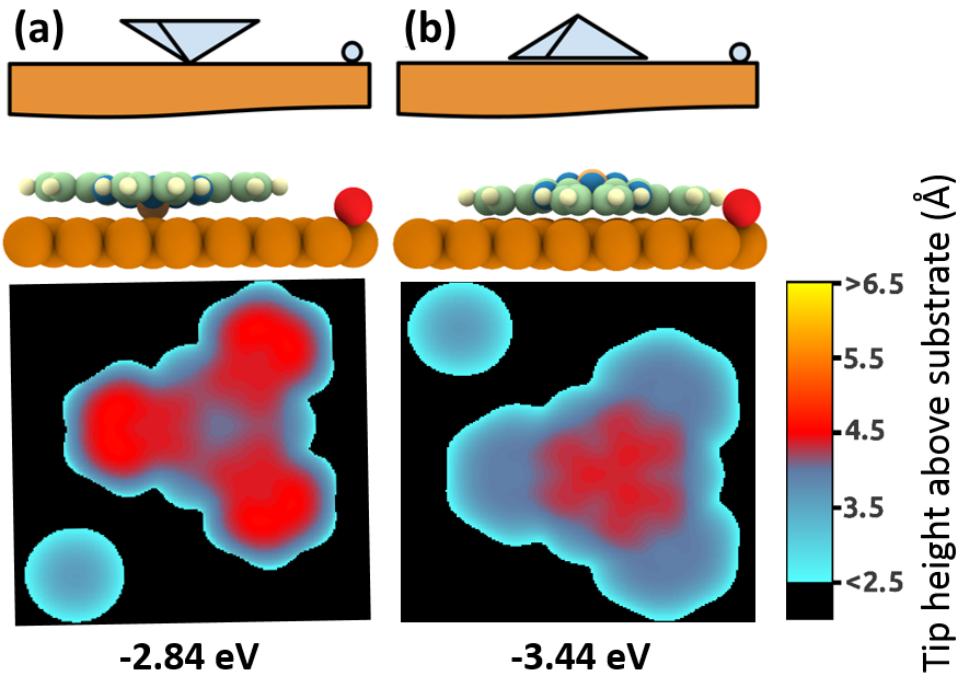

Figure 1.6: Dechlorinated configurations investigated by DFT: (a) DeCl-down and (b) DeCl-up. Top row: schematic; second row: atomistic picture; third row: simulated STM images ($V_s = -2$ V); and bottom row: calculated adsorption energies for each configuration. Color code of atoms: Cl, red; C, pale green; N, blue; B, orange; H, pale yellow.

closest configuration that preserves the molecule's chemical structure and has the molecule's Cl atom oriented toward the surface. On the basis of these thermodynamic considerations summarized in Table 1.1, we associate type **II** molecules observed experimentally in the adsorption of ClB-SubPc on Cu(111) with the DeCl-up configuration.

This association is further reinforced when comparing the simulated STM images for the two DeCl possibilities with experimental STM images. Simulated DeCl-up shows a moderate apparent height increase in the center of the molecule (Figure 1.6b), which agrees well with the experimentally determined constant current images for adsorbate type **II** (Figure 1.2). In contrast, simulated DeCl-down exhibits

configuration[1]	adsorption energy (eV)
Cl-up	−3.56
Cl-down	−0.60
fallen; one isoindole in contact with substrate	−1.74
fallen; two isoindole in contact with substrate	−1.86
DeCl-up	−3.44
DeCl-down	−2.84

Table 1.1: Adsorption energy for all considered configurations of (Cl)B-SubPc molecule on Cu(111)

a contrast depression in the molecular center (Figure 1.6a) at variance with experiments. Our interpretation of the nature of configuration **II** is further corroborated by the fact that Cl-up and DeCl-up are expected to orient the same way on the surface, driven by highly favorable registry of the isoindole N atoms and Cu atoms on the surface. This is indeed found to be the case both computationally and in the experimental data (see Table 2.1 and Figure 2.3 in Chapter 2).

The observation of dechlorinated molecules together with intact Cl-up molecules indicates that dechlorination is kinetically hindered. Though a detailed investigation of the mechanism for this reaction is beyond the scope of the present report, we suggest that this process is determined by the approach of the ClB-SubPc molecules toward the surface upon adsorption: When the molecule approaches with the B—Cl bond pointing away from the surface, an intact Cl-up configuration will result. Other relative orientations will lead to initial full or partial coordination of the Cl-group with the surface followed by dechlorination. In passing, we note that we found no evidence for dechlorination prior to adsorption. Rather, large crystals grow during purification, a clear indication of high molecular purity. Further, we observed an essentially constant ratio of DeCl/Cl-up molecules even after many molecular adsorption cycles from the same crucible. This indicates that the ClB-SubPc molecules remain intact during the deposition process, consistent also with a bond-breaking enthalpy of 5.6 eV for the B—Cl bond in the gas phase [12].

Comparing these findings to literature, we note that a number of nonplanar phthalocyanines and in particular axially substituted chloro-(sub)phthalocyanines have been investigated by STM on a range of surfaces already [12, 68, 71, 96, 148]. In many of these systems, adsorbate configurations resembling our type **I**, that is, with a bright center, are found. These are indeed typically interpreted as Cl-up, which is in agreement with our findings. In some STM studies [65, 68, 86, 107, 108, 153], adsorbates that resemble our type **II**, that is, configurations that lack the enhanced apparent height along the central symmetry axis, are also reported. They are commonly interpreted as resulting from a configuration akin to the Cl-down situation in our work. In some instances, such an interpretation has also been developed based on photoelectron spectroscopy [12, 15, 68] and X-ray standing wave data [45]. In passing, we note that for the system studied in reference [45] dechlorination has, in fact, recently been discussed as a possible scenario [158].

The possibility that Cl-down adsorbates are in fact the result of dechlorination on the surface has been mostly disregarded. When discussed at all, the following arguments against dechlorination are commonly made:

A. There is no direct evidence of dechlorination of (sub)phthalocyanines on surfaces of coinage metals, such as the formation of Cl adatom clusters on the surface. Even small quantities of chlorine are known to form clusters on Cu(111) at room temperature that form incommensurate hexagonal structures [2]. Such adatom clusters are absent also in our STM pictures. This could, however, be a consequence of the aggregation of Cl atoms at defects and steps on Cu(111), which would make their direct observation difficult.

B. Cl adatoms on Cu(111) increase the work function even at rather small coverages [112, 118], in direct conflict with photoemission spectroscopy results for the present system [68], For example, for ClB-SubPc on Cu(111) a work

function decrease in excess of 800 meV was reported at 1 MLE [68]. This is however not necessarily conclusive evidence against dechlorination because photoemission is an area-averaged measurement, where the net change in the work function may easily be dominated by the organic adsorbate even in the presence of significant amounts of chlorine adatoms. The latter would be particularly true for the case of Fermi-level pinning, where the electron affinity of the organic adsorbate layer determines the work function [62]. We have recently observed for gallium chloride phthalocyanine on Cu(111) that the work function upon dechlorination is indeed determined by the energetics of the pinned phthalocyanine orbital [158].

c. Dechlorination is considered to be a thermodynamically costly process requiring 5.6 eV in the gas phase [12], making it unlikely to occur. The above number is, however, based on gas phase calculations and thus fails to acknowledge the important role of the surface. It is in fact known that the axial boron-chloride bond is labile already in the presence of moderate nucleophiles in solution [114]. Also, dechlorination is a known process for instance in the case of iron octaethylporphyrin chloride (FeCl-OEP) on Cu(111) [152] and Au(III)-tetraphenylporphyrin chloride ($[Au^{III}TPP]^{+}Cl^{-}$) on Au (111) [59]. Note that at least in the case of FeCl-OEP on Cu(111) chlorine adatoms were not clearly visible either.

The impact of the surroundings on the dechlorination process was recently reported by Guilleme *et al*. [54], who investigated the kinetics of dechlorination and hydrolysis of ClB-SubPc in solution. They observed an elevated rate of dechlorination when the solvent stabilizes partial charges formed during the reaction, further accelerated by increasing the strength of electron-donating groups substituted at the periphery of the subphthalocyanine heterocycle. Although solvents are quite different from surfaces, we propose that the dechlorination of the ClB-SubPc molecule is mediated in a somewhat similar fashion by the Cu(111) surface, which can readily stabilize partial charges and act as an electron donating pool. Guilleme *et al*. proposed that dechlorination involves significant stretching and deviation of the B—Cl bond away from the molecular symmetry axis. This is similar to the putative precursor to dechlorination apparent in our computational treatment: In the fallen configurations, the B—Cl bond is at least 1.94 Å long (compared to 1.84 Å in the gas phase) and deviates by 7.3° from the gas phase symmetry axis.

1.3.5 *Growth of adsorbate type II: DeCl-up*

In striking contrast to type **I** molecules, molecules of adsorbate type **II** do not form monolayer hcp islands readily; instead, they are generally found in isolation (Figure 1.7). We interpret this fundamentally different thin film formation behavior as a direct consequence of their different chemical nature. The energetic cost for rotation by 60° is small enough (see Figure 1.5) such that type **II** molecules are occasionally also found at the edges of Cl-up islands, reminiscent of stacking faults on crystal surfaces.

At higher coverages, DeCl-up molecules do start to form aggregates that in some cases become part of ordered structures (green circles in Figure 1.4). The latter have

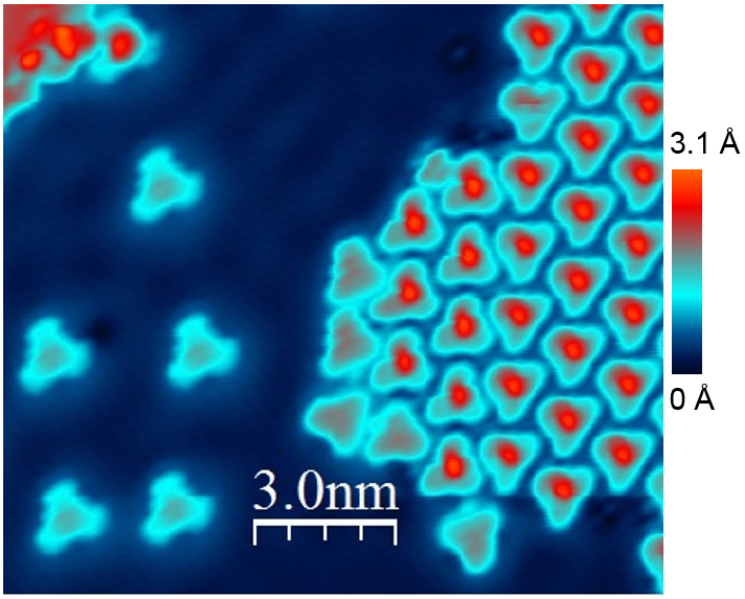

Figure 1.7: STM image of 0.14 MLE ClB-SubPc on Cu(111) for a film prepared at 223 K (V_s = 0.1 V; I_t = 50 pA; 5 K), contrasting film growth for Cl-up/type **I** molecules and DeCl-up/type **II** molecules.

a noticeably greater apparent height than monolayer islands. A close-up of such an ordered structure is shown in Figure 1.8 and reveals that they consist principally of two separate components of different heights: A wetting layer of molecules residing directly on the Cu(111) surface (see red dashed line in Figure 1.8a, connecting one row of these molecules); and more prominently an intercalated set of trefoil-shaped molecules with much enhanced apparent height. A small number of Cl-up molecules, identifiable by the bright central feature of the Cl-atom, are interspersed throughout the island as well (e.g., right half of red dashed line in Figure 1.8a), and may be considered "defects" in the island. Molecules in the wetting layer other than Cl-up defects resemble in appearance the isolated DeCl-up molecules. This assignment is further supported by comparing height changes across the island, measured along the red dashed line in Figure 1.8a and shown in Figure 1.8b. This lineout shows tall features that correspond to the Cl atom in the Cl-up molecules (height difference >1 Å), medium height features that correspond to one wing of the intercalated trefoil molecules (height difference ~0.7 Å) and a low feature (height difference below 0.5 Å) corresponding to the center of the molecules that primarily form the wetting layer. Comparing the general appearance of the STM images in Figure 1.8 with the simulations from Figures 1.3 and 1.6 and considering the differences in apparent height, a wetting layer of largely DeCl-up is most consistent with the experimental data. Interspersed in this wetting layer is also a limited number of intact Cl-up molecules. An alternative assignment associating the bright protrusions between the trefoil-shaped molecules with Cl atoms which would originate from dechlorination of ClB-SubPc molecules appears unlikely, since these atoms would exhibit a significantly lower apparent height.

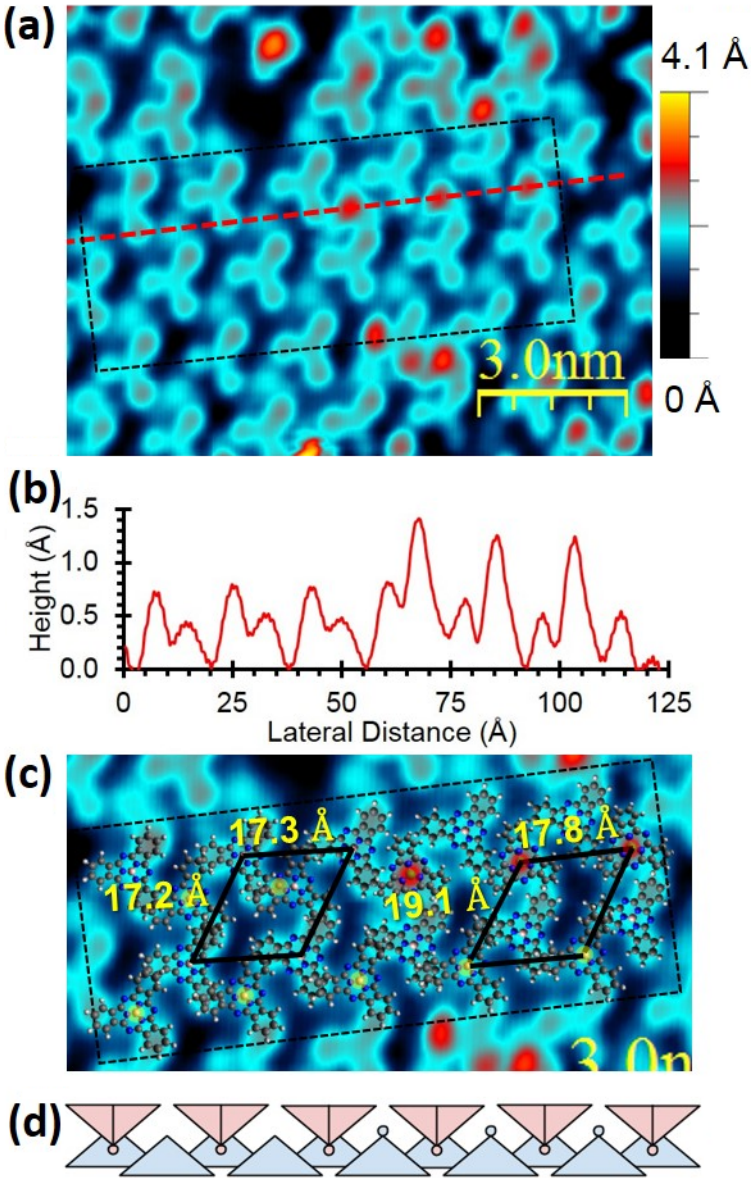

Figure 1.8: (a) STM image of 0.50 MLE ClB-SubPc on Cu(111) for a film prepared at 205 K ($V_s = -2$ V; $I_t = 50$ pA; 5 K) showing the bilayer structure in detail. (b) Profile of height difference along dashed red line in part (a). (c) Unit cells of wetting layer DeCl-up and second layer Cl-down molecules. (d) Side-on cartoon view of bilayer structure.

The trefoil molecules intercalated between lattice sites of the wetting layer are different from all other observed molecules adsorbed directly on the Cu(111) surface. They strongly resemble the simulated DeCl-down molecules shown in Figure 1.6a, or possibly the Cl-down molecules shown in Figure 1.3b. The structure of these islands is therefore interpreted as a bilayer composed of a wetting layer of DeCl-up molecules (interspersed with Cl-up defects) and an intercalated second layer of either DeCl-down or Cl-down molecules. This suggests that formation of DeCl-up islands may require stabilization by a second layer. The wetting layer of DeCl-up molecules is not packed as densely in this bilayer structure as the hcp Cl-up islands (cf. Figures 1.8c and 1.4a). The molecular arrangement is overlaid in Figure

1.8c and a side-on cartoon view is shown in Figure 1.8d. Similar bilayer structures have also been reported for iron(II) phthalocyanine on Cu(111) [123] and vanadyl phthalocyanine on Cu(111) [107], and Trelka *et al*. observed a similar structure for the ClB-SubPc | Cu(111) interface [148].

1.4 CONCLUSION

We investigated the adsorbate structure and self-assembly at submonolayer coverages of ClB-SubPc on Cu(111) for a range of temperatures and coverages by LT-STM and density functional theory calculations. Although similar shuttlecock shaped polar molecules have been reported to adsorb either with the polar group pointing toward or away from the surface, we find that this is not the case for ClB-SubPc on Cu(111). Instead, we observe both computationally and by STM that these molecules adsorb either as Cl-up with the Cl-atom pointing toward the vacuum side of the interface or they dechlorinate. The latter we ascribe to a reaction catalyzed at the surface even at low temperatures, which yields dechlorinated DeCl-up molecules. Both species adsorb preferentially at hcp hollow sites where maximum interaction between the N atoms of the subphthalocyanine ligand and the Cu atoms in the first surface layer is obtained. The Cl-up molecules self-assemble on the surface to form two different types of hcp islands, while the DeCl-up molecules remain isolated unless stabilized in a bilayer structure with Cl-down or DeCl-down molecules. Our results highlight that caution must be used when interpreting STM contrast for complex interfaces. Dissociation of halogenated polar groups in molecules belonging to the phthalocyanine class may be more general, requiring a full atomistic understanding of molecular adsorption at the surface. As a consequence, the use of halogen-based dipolar groups to tailor the interfacial electronic structure is not necessarily as straightforward as typically assumed, at least not on some coinage metal surfaces. Consequently, other approaches for a controlled work-function tuning have to be sought.

2

ADDENDUM TO CHAPTER 1

2.1 SUPPORTING INFORMATION TO CHAPTER 1

This section was published as supporting information for the journal article entitled "Sticking with the Pointy End? Molecular Configuration of Chloro Boron-Subphthalocyanine on Cu(111)" in *The Journal of Physical Chemistry C*. The original version can be accessed at the DOI: 10.1021/acs.jpcc.5b11799.

2.1.1 *Molecular height*

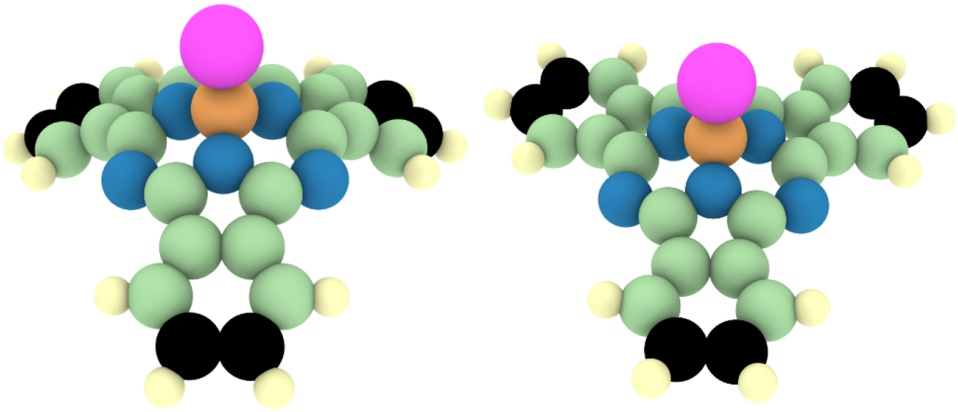

Figure 2.1: The gas-phase (left) and adsorbed (right) geometry of the ClB-SubPc molecule in "Cl-up" conformation. The molecule's height decreases from 4.46 Å to 3.25 Å as it gets adsorbed on copper (not shown). Color code of atoms: Cl purple, N blue, B orange, C light green and black, H pale yellow.

The height of the molecule is defined as the difference in the z-coordinate of the chlorine atom (colored pink in Figure 2.1) and the averaged z-coordinate of the six peripheral carbon atoms (colored black). The gas-phase molecule (left panel) is thus 4.46 Å high while the adsorbed molecule (right panel) is 3.25 Å high. However, this definition of molecular height holds true only for the "Cl-up" conformation as it is the only chlorinated case where all six peripheral C atoms are in the same xy plane.

2.1.2 *Molecular arrangement in dense hcp islands*

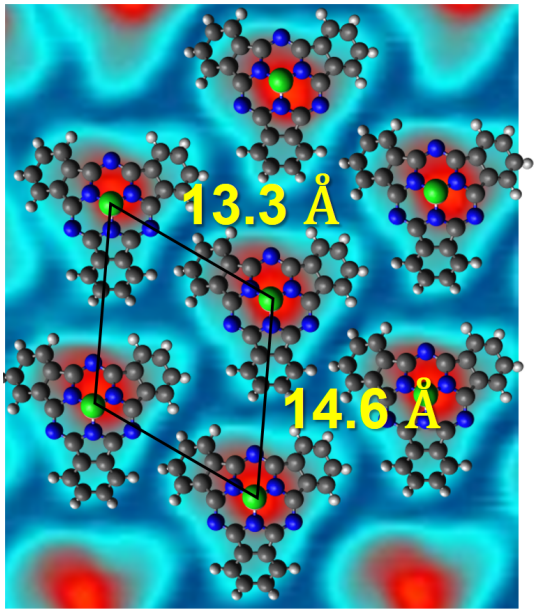

Figure 2.2: STM image ($V_s = 0.1$ V; $I_t = 50$ pA; $T = 5$ K), molecular arrangement and measured unit cell dimensions of "Cl-up" molecules in high-density hcp islands. 0.14 MLE coverage, growth at 223 K. Color code of atoms: Cl green, N blue, C grey, H white.

A cartoon of the molecular arrangement of "Cl-up" molecules and the measured associated unit cell dimensions overlaid on a close-up STM image of a high-density hcp islands is shown in Figure 2.2.

2.1.3 *Molecular registry with surface*

Atomically resolved images of the substrate were obtained in a few instances in the vicinity of a ClB-SubPc molecule, making a tentative assignment of the molecular registry with the surface possible. In Figure 2.3, this is shown for both the "Cl-up" (Figures 2.3a and 2.3c) and the "DeCl-up" (Figures 2.3b and 2.3d) molecules. In both cases, the Cu lattice is visible only for part of the image (lower third of Figure 2.3a and middle third for Figure 2.3b), sufficient to overlay the Cu(111) atomic lattice. Some uncertainty regarding the precise position of the molecules on the lattice, however, persists.

2.1.4 *Adsorption site of "DeCl-up"*

A comparison of the different calculated adsorption energies of "DeCl-up" molecules vis-à-vis the "Cl-up" molecule is contained in Table 2.1. hcp hollow sites are thermodynamically most stable also for DeCl-up, and again a maximum overlap of the isoindole N atoms with the Cu lattice is energetically preferrable.

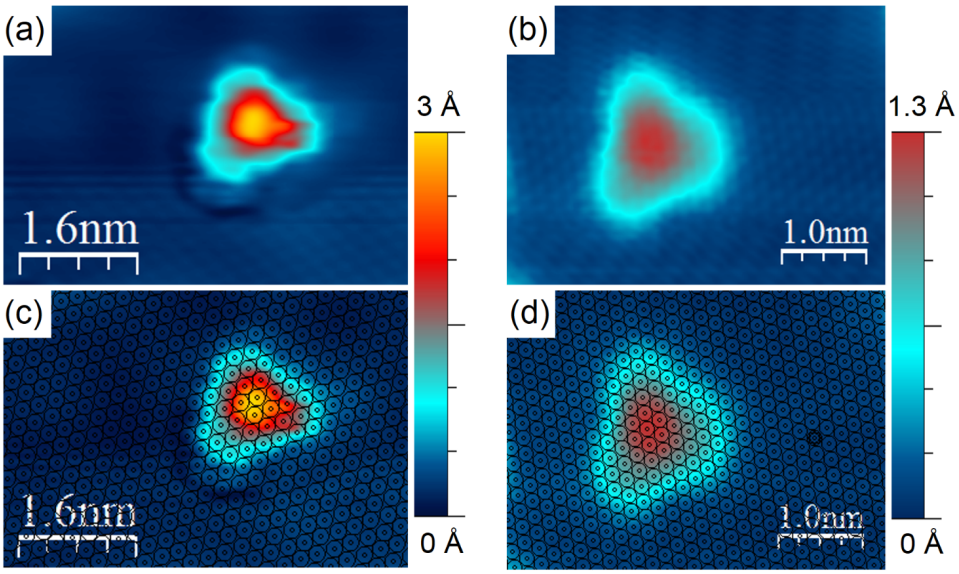

Figure 2.3: (a) STM image of isolated "Cl-up" molecule with atomically resolved Cu(111) lattice in lower third of image ($V_t = 0.06$ V; $I_t = 200$ pA; $T = 5$ K). (b) STM image of isolated "DeCl-up" molecule with atomically resolved Cu(111) lattice in middle third of image ($V_t = -1.7$ V; $I_t = 50$ pA; $T = 5$ K). (c) and (d) are same as (a) and (b) respectively, but with overlay of Cu lattice

adsorption site	adsorption energy (eV) for Cl-up	adsorption energy (eV) for DeCl-up
bridge	−3.05	−2.96
atop	−2.63	−2.53
hcp hollow (maximum N/Cu registry)	−3.56	−3.44
hcp hollow (reduced N/Cu registry)	−3.34	−3.35
fcc hollow (maximum N/Cu registry)	−3.42	−3.31
fcc hollow (reduced N/Cu registry)	−3.20	−3.23

Table 2.1: Adsorption energy for "Cl-up" and "DeCl-up" conformations of the (Cl)B-SubPc molecule at different adsorption sites of Cu(111) surface. Reduced N/Cu was obtained by rotating the molecule (in its maximum registry orientation) by 60° along the C_3 symmetry axis.

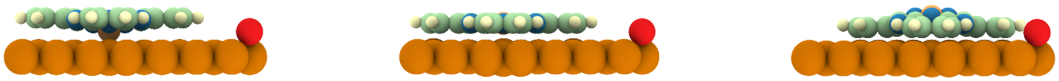

(a) DeCl-down; −2.84 eV (b) Transition; −2.88 eV (c) DeCl-up; −3.44 eV

Figure 2.4: Molecule in "DeCl-down" conformation (left) that forms when the molecule lands on copper substrate chlorine-first. An artificial intermediate state (middle) that may form while transiting from "DeCl-down" to "DeCl-up"conformation (right). Numbers below the images are the adsorption energies for their respective systems. Color code of atoms: Cl red, C pale green, N blue, B orange, H pale yellow.

2.1.5 *Energy barrier for flipping from "DeCl-down" to "DeCl-up"*

To determine an approximate barrier for flipping of the molecule from "DeCl-down" to "DeCl-up" orientation while it is adsorbed on the substrate, we calculated the adsorption energy of an approximated intermediate state (see Figure 2.4). This state was *constructed* by moving all atoms of the dechlorinated molecule to a fixed height. This height, in turn, was determined by averaging the height of the boron atoms from the relaxed geometries of the DeCl-up and DeCl-down systems.

While relaxing this approximated geometry, the vertical positions of all atoms of the molecule except hydrogen were kept fixed. Though this method of estimating a flipping barrier is somewhat crude, it gives nevertheless a meaningful insight into the energetics involved: The adsorption energy for the intermediate state is −2.88 eV, i.e., this state is already more favorable than the "DeCl-down" configuration, which implies that the actual transition state representing the barrier for conversion between the two conformations is somewhere between the fully planar molecule and the "DeCl-down" configuration. It also suggests that the overall barrier is very small. Similar flipping has, in fact, been reported for the central atom in Tin-Pc.[154]

2.2 AUTHORS WHO CONTRIBUTED TO CHAPTER 1

This section lists the authors who contributed to the journal article that formed the basis of Chapter 1. Their affiliation for the time period during which they contributed to the underlying research is also listed. Nahid and I (Shashank) contributed equally to the work. Egbert Zojer and Oliver L. A. Monti were the corresponding authors.

• Nahid Ilyas
Department of Chemistry and Biochemistry, University of Arizona, Tucson, 1306 E. University Boulevard, Tucson, Arizona 85721, United States

• Shashank S. Harivyasi
Institute of Solid State Physics, NAWI Graz, Graz University of Technology, Petersgasse 16, 8010 Graz, Austria

• Percy Zahl
Center for Functional Nanomaterials, Brookhaven National Laboratory, Upton, New York 11973, United States

• Rocio Cortes
Center for Functional Nanomaterials, Brookhaven National Laboratory, Upton, New York 11973, United States

• Oliver T. Hofmann
Institute of Solid State Physics, NAWI Graz, Graz University of Technology, Petersgasse 16, 8010 Graz, Austria

• Peter Sutter
Center for Functional Nanomaterials, Brookhaven National Laboratory, Upton, New York 11973, United States
Department of Electrical and Computer Engineering, University of Nebraska-Lincoln, Lincoln, Nebraska 68588, United States

• Egbert Zojer
Institute of Solid State Physics, NAWI Graz, Graz University of Technology, Petersgasse 16, 8010 Graz, Austria

• Oliver L. A. Monti
Department of Chemistry and Biochemistry, University of Arizona, Tucson, 1306 E. University Boulevard, Tucson, Arizona 85721, United States
Department of Physics, University of Arizona, Tucson, 1118 E 4th Street, Tucson, Arizona 85721, United States

3

VAN DER WAALS INTERACTION ACTIVATED STRONG ELECTRONIC COUPLING AT THE INTERFACE BETWEEN CHLORO BORON-SUBPHTHALOCYANINE AND Cu(111)

PREAMBLE

This chapter has been submitted for consideration and publication as a peer-reviewed article entitled "Van Der Waals Interaction Activated Strong Electronic Coupling at the Interface Between Chloro Boron-Subphthalocyanine and Cu(111)". Supporting information for this manuscript and a list of affiliations of its authors is given in Addendum 4.

As is the nature of such work, multiple authors contributed to this manuscript and the underlying research. The author of this thesis performed all the *ab-initio* simulations, wrote the first draft of this article and prepared all its figures. Oliver T. Hofmann helped with the DFT calculations, particularly aiding the implementation of some programming technicalities that were necessitated during the course of this work. Nahid Ilyas did the photoelectron spectroscopy experiments and provided us with its results. From early on, Oliver L.A. Monti highlighted the significance of strong hybridization at this interface and, thus, instigated us to look in this direction. He then helped us place the experimental facts in light of our findings from simulations. Egbert Zojer directed the computational research, rewrote parts of the text and suggested inputs that eventually made the results more lucid. All authors approved of this version of the manuscript and contributed to the scientific insights presented in it.

ABSTRACT

In this article, we investigate the interface between shuttlecock-shaped Chloro boron-subphthalocyanine (ClB-SubPc) molecules and the Cu(111) surface. We highlight, how molecular planarization induced by van der Waals forces can fundamentally alter the interface properties, and how it can enable a particularly strong hybridization between molecular and metal states. In our simulations, we start from a situation in which we disregard van der Waals forces and then introduce them gradually by rescaling the interaction parameter, thereby "pulling" the molecule towards the surface. This reveals two adsorption regimes with significantly different adsorption distances, molecular conformations, and adsorbate-induced changes of the work function. Notably, the above-mentioned massive hybridization of electronic states, also observed in photoelectron spectroscopy, is obtained solely for

one of the regimes. We show that this regime is accessible only as a consequence of the planarization of the molecular backbone resulting from the van der Waals attraction between the molecule and the surface. The results of this study indicate that for certain metal-molecule combinations unusually strong interfacial electronic interactions can be triggered by van der Waals forces creating a situation that goes beyond the usually described cases of physisorptive and chemisorptive interactions.

3.1 INTRODUCTION

In organic (opto)electronic devices, molecules are often in direct contact with metal electrodes. This makes a comprehensive understanding of metal-organic interfaces a prerequisite for improving device performance. A key factor that dominates the properties of such interfaces is the strength of the interaction between the metal and the molecules. Together with the electronic structure of these interfaces, the interactions have been explained by invoking a number of phenomena such as exchange interaction, dipole interaction, charge transfer, and covalent bonding [5, 17, 69, 76, 93, 101, 119, 139, 146, 147].

The present study focuses on understanding peculiarities of the interfacial interactions and the electronic structure that may arise from adsorption-induced geometry changes in certain non-planar molecules. In particular, we present a detailed computational study of the adsorption of Chloro boron-subphthalocyanine (ClB-SubPc) on Cu(111) and corroborate it with an assessment of the interfacial electronic structure via photoelectron spectroscopy. The system serves as a prototypical example for the hitherto rarely discussed scenario in which the electronic structure of an interface is fundamentally altered by changes of molecular conformation that are, in turn, enabled by the van der Waals (vdW) forces between the molecule and the substrate.

Beyond the fundamental character of the present study, it is also motivated by the increasing technological relevance of subphthalocyanines (SubPcs), which calls for an improved understanding of their properties. SubPcs are optically active dyes that exhibit fluorescence and a high second-order linear response [116, 121]. They have been used in organic photovoltaic cells [102], in light-harvesting systems [74], and for blending-driven band gap engineering [126]. Consequently, film formation of the archetypical subphthalocyanine, ClB-SubPc, on different metal surfaces has been the focus of numerous studies [12, 67, 68, 71, 96, 148], all revealing feature-rich thin films. The latter is, at least in part, a consequence of the molecule's peculiar geometry: A ClB-SubPc molecule has three-fold rotational symmetry, combined with a conical 'shuttlecock-shaped' non-planar geometry (Figure 3.1).

Consequently, depending on the molecular orientation with respect to the substrate upon adsorption, multiple plausible adsorption situations can be envisaged [67]. This results, for example, in charge transfer from the surface to the chlorine atom on Ag(111) [12], in the formation of bi-layer nanocrystals on Cu(111) [148], or in surface-catalyzed dechlorination of (a fraction of) the molecules on Cu(111) [67]. In the last case, one observes the formation of chemically different ClB-SubPc domains consisting of either dechlorinated or intact molecules [67]. Here, we focus on molecules that remain intact while adsorbing on Cu(111), while the most

relevant data for dechlorinated molecules are compiled in Chapter 4. The case of intact molecules is particularly insightful for understanding the peculiarities that can arise from the interaction between a non-planar π-electron system and a coinage metal substrate: By tuning the magnitude of vdW forces when simulating the ClB-SubPc/Cu(111) interface, we are able to show how the van der Waals-induced planarization of (significant parts of) the molecular backbone upon adsorption gives rise to two distinct adsorption regimes. Moreover, the planarization enables a particularly strong electronic coupling between substrate and adsorbate. This, in turn, fundamentally changes interface properties like the adsorbate-induced work function modification, local densities of states, and interfacial charge rearrangements.

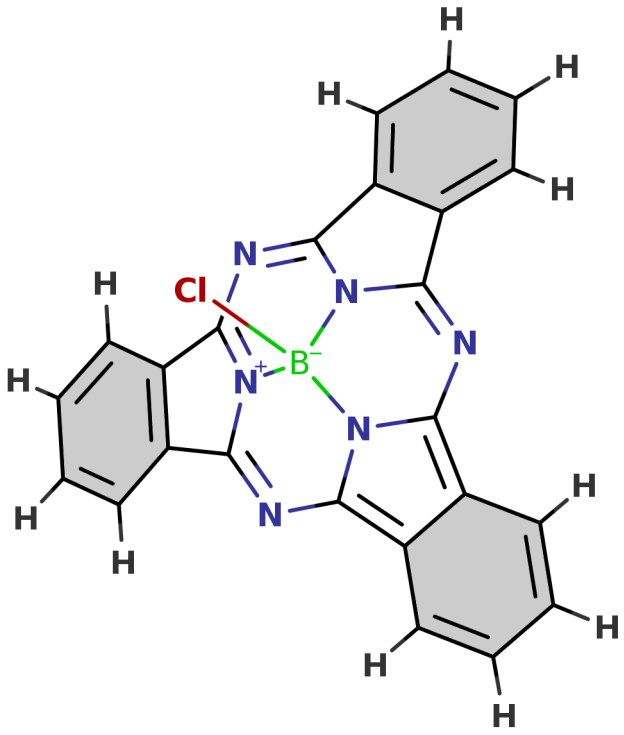

Figure 3.1: Chemical structure of Chloro boron-subphthalocyanine (ClB-SubPc). Upon adsorption, the eighteen carbon atoms of the three benzene subunits of the molecule (shaded grey here) are found closest to the Cu substrate. They are collectively referred to as C18 in this chapter.

3.2 METHODOLOGY

3.2.1 *Computational*

For our simulations, we relied on density functional theory (DFT) as implemented in the Fritz Haber Institute *ab-initio* molecular simulations (FHI-aims) package [13], employing the default 'tight' settings. We used the Perdew-Burke-Ernzerhof (PBE) functional [113] complemented by a surface-screening corrected van der Waals energy term [120], a scheme commonly designated as PBE+vdW$^{\text{surf}}$. Employing the repeated-slab approach [124], we studied the adsorption process at a moderate

packing density [67] with just one molecule in every $7 \times 4\sqrt{3}$ orthogonal surface unit cell. This represents the smallest orthogonal cell in which the energy contribution from intermolecular interactions has decayed to less than 0.1 eV. The Cu(111) surface was represented by a slab with a thickness of six atomic layers, of which only the top two were allowed to relax in geometry optimizations. In the direction perpendicular to the surface, a vacuum gap of at least 25 Å was introduced together with a self-consistently determined discontinuity in the electrostatic energy to decouple periodic replicas of the slab [106]. The convergence criterion for the self-consistent field cycles was set to 10^{-6} eV for the total energy and the geometry was relaxed until the maximum residual force component per atom was less than 0.01 eV/Å. The states were broadened using a Gaussian function and also a Gaussian occupation scheme [42] was used. For both, σ was set to 0.2 eV. A $4 \times 4 \times 1$ Γ-centered k-point grid was used for all periodic calculations and van der Waals corrections were not included for Cu-Cu atom pairs in calculations having the Cu slab. The lattice constant for Cu, thus obtained, is 3.637 Å.

3.2.2 *Experimental*

ClB-SubPc was purchased from Sigma-Aldrich and was purified by repeated gradient sublimation in a custom-built furnace. It was degassed overnight in a home-built Knudsen cell under ultrahigh vacuum conditions and at temperatures slightly below the sublimation point. A polished Cu(111) crystal of 99.999% purity (Princeton Scientific) was cleaned by repeated cycles of Ar^+ sputtering and annealing, while highly oriented pyrolytic graphite (HOPG) was freshly cleaved and annealed at 450 °C in vacuum. Molecular deposition occurred at room temperature on both substrates, at a rate of 0.1 Å per minute. Photoelectron spectroscopy was carried out using a He(I) UV source (SPECS UVS 10/35) incident at a 30° angle in a VG EscaLab MK II photoelectron spectrometer. Spectra were acquired with an energy resolution of 89(8) meV.

3.3 RESULTS AND DISCUSSION

3.3.1 *Planarization and hybridization of ClB-SubPc upon adsorption on Cu(111)*

The shuttlecock-shaped geometry of the ClB-SubPc molecule (Figure 3.2a) is lost once it adsorbs on Cu(111). The molecule then resembles a planarized disk with only a trigonal pyramidal feature (composed of the chlorine, the boron, and the three pyrrolic nitrogen atoms) preserved in its center (Figure 3.2b). The eighteen carbon atoms closest to the substrate (collectively termed as C18; see shaded rings in Figure 3.1) end up lying approximately in the same plane, with the standard deviation in their z-coordinates $\sigma = \sqrt{\frac{1}{18}\Sigma_i^{18}(z_i - \overline{z_i})^2}$ as low as 0.03 Å. As a more accessible quantification, in the following we define the planarity, Π, of any given ClB-SubPc conformation via the standard deviation in the heights of the C18 atoms as

$$\Pi = \frac{\sigma_{\text{C18, gas-phase}} - \sigma_{\text{C18, given-geometry}}}{\sigma_{\text{C18, gas-phase}}} \times 100\%. \tag{3.1}$$

This definition implies that the molecule in its gas-phase geometry has a planarity, Π, of 0%, while Π is 100% when all C18 atoms are in the same plane. For the relaxed ClB-SubPc/Cu(111) interface, a planarity of 94% is obtained for the adsorbed molecule. Concomitantly, the molecule's "shuttlecock angle" — the obtuse angle between the central symmetry axis and any of the six peripheral carbon atoms in the benzene subunits — decreases by 13° (from 116° to 103°, Figures 3.2a and 3.2b).

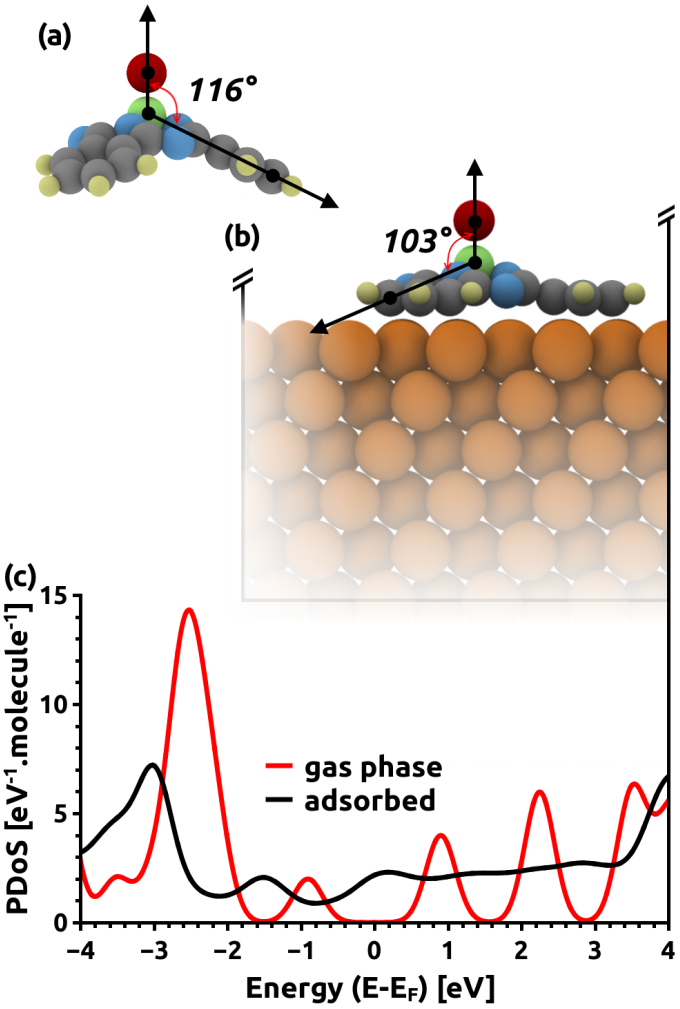

Figure 3.2: Structure of the ClB-SubPc molecule (a) before and (b) after adsorption on Cu(111). (c) The molecule-projected density of states (PDoS) of the ClB-SubPc molecule adsorbed on the Cu(111) substrate (black curve) and in the gas phase (red). The DoS of the gas phase molecule has been Gaussian-broadened and shifted to align the centre of its HOMO-LUMO gap with the Fermi level. Panel (b) also indicates the unit cell used in all calculations employing periodic boundary conditions. The coloring scheme is: chlorine: red, boron: green, nitrogen: blue, carbon: grey, hydrogen: yellow and copper: brown.

Putting the planarization of the ClB-SubPc π-system into the context of similar molecules is difficult. With three instead of four isoindole units and meso N atoms, boron-subphthalocyanines are, so far, the only known lower homologues of phthalocyanine (Pc) molecules. While the adsorption of numerous non-planar Pcs has been studied extensively [3, 8, 9, 19, 27, 43, 73, 99, 109, 127, 158], most have comparably smaller shuttlecock angles, and thus, do not lend themselves to direct

comparison. For instance, the nearest comparable study, of SnPc on Ag(111), also employing dispersion-corrected DFT reports that adsorption results in a change of 5°, from 105° to 100°, in the molecule's shuttlecock angle when its adsorbs in similar orientation [9]. On the other extreme, there are spherical and bowl-shaped molecules like C_{60} and corannulene ($C_{20}H_{10}$) that appear not to flatten on Cu(111), and for which the overall geometry remains largely unchanged upon adsorption [103, 164].

Besides planarization, the other significant consequence of adsorption of ClB-SubPc molecules on Cu(111) is the change in their electronic structure (Figure 3.2c). Notably, adsorption leads to a substantial "smearing" of the molecule-projected DoS (PDoS) around the Fermi level of the metal-molecule system, to the extent that different molecular states are difficult to identify both in the PDoS and in the spectrum from ultraviolet photoelectron (UP) spectroscopy (see below). The particularly strong smearing of the PDoS is caused by the hybridization of occupied as well as unoccupied molecular states with the *d*-band and the *sp*-band of copper. Similar observations have actually been made on Cu substrates for other conjugated molecules, which are flat in the gas phase. The relevant interfaces include, for example, pentacene on Cu(111) [128, 146], Cu(100) [34] and Cu(110) [105, 151], as well as for Perylenetetracarboxylic dianhydride (PTCDA) on Cu(111) [30, 119].

Additionally, the ClB-SubPc monolayer is rendered metallic since the Fermi level lies in a region of significant PDoS. Metallization of the interface due to strong hybridization is a commonly observed feature for planar molecules adsorbed on metal surfaces [4, 30, 34, 95, 105, 119, 128, 146, 150, 151]. In fact, a previous investigation of ClB-SubPc on Cu(111) using two-photon photoemission spectroscopy also suggested hybridization and charge-transfer to the molecular orbitals from metal surface states [68].

The strong broadening of the PDoS found in the computational results is also present in the experimental data. In Figure 3.3 we show a comparison of the UP-spectra of 0.7 monolayer equivalents (as defined in Ref. [67]) of ClB-SubPc on both Cu(111) and on HOPG. On HOPG, a distinct feature representing the ClB-SubPc HOMO centered at a binding energy (E_B) of -1.7 eV is clearly resolved on top of the rather weak background originating from the HOPG π-band. This is consistent with a UP spectroscopy report on a 7.5 nm thick ClB-SubPc film on Si [31]. Further peaks are observed at higher binding energies. In contrast, on Cu(111) only weak and broad features are visible between 0 and -2 eV. These stem primarily from the Cu *d*-band He $(I)_\beta$ satellite features at -0.8 eV. Additional contributions from the remainder of the Cu(111) Shockley surface state (-0.2 to -0.4 eV) and from a partially filled LUMO near the Fermi edge are expected at the positions indicated in Figure 3.3 following the two-photon photoemission data in Ref. [68]. Below -2 eV, the Cu *d*-bands manifest as the strongest features in the ClB-SubPc/Cu(111) UP-spectrum. Their broad structure is indicative of scattering in the organic adlayer and interfacial hybridization. There is no clear evidence of the HOMO or other molecular features in the UP-spectrum, though a contribution from the HOMO to the shoulder at $E_B = -2.2$ eV or the *d*-band region cannot be excluded (we do not necessarily expect the HOMO feature on Cu(111) to be at the same energy as on HOPG). In summary, the distinctly different contributions of ClB-SubPc to the UP-spectra when adsorbed on HOPG and Cu(111) support the notion of a strong

smearing of the molecular states at the ClB-SubPc/Cu(111) interface that has been observed in the simulations.

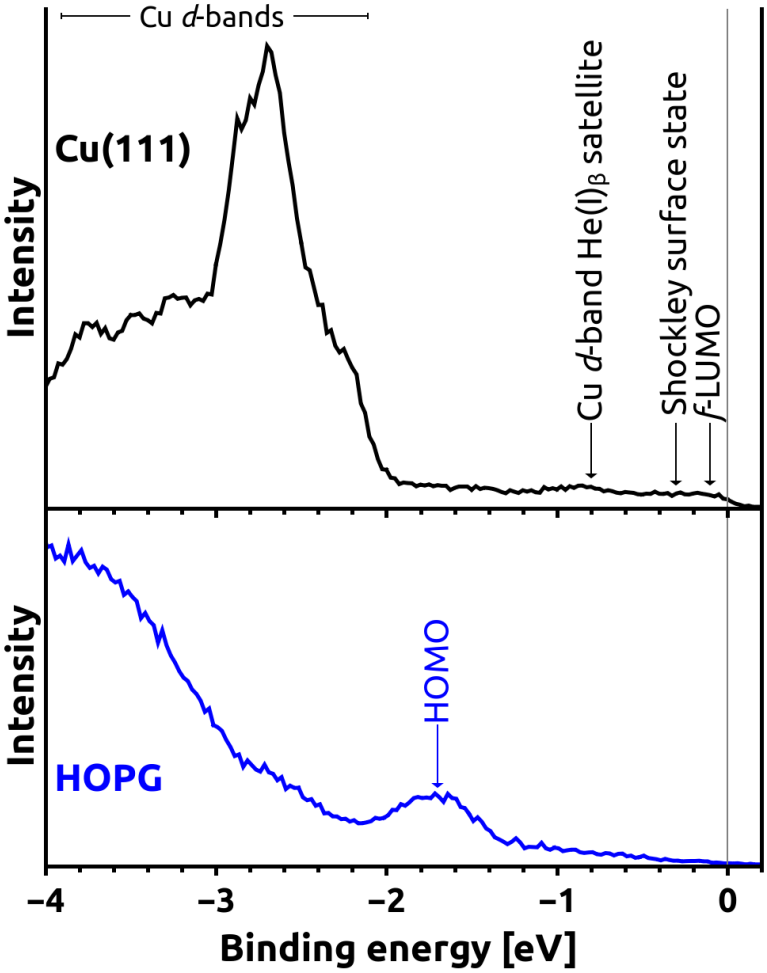

Figure 3.3: Ultraviolet photoelectron spectra of a ClB-SubPc monolayer on Cu(111) (top panel, black, strong hybridization) and HOPG (bottom panel, blue, weak hybridization). The binding energy is referenced to the Fermi level.

The above observations raise the question to what extent the particularly strong coupling between substrate and adsorbate and the interaction-induced planarization of most of the molecular backbone are interrelated. To address this issue and as a first step, we calculated the adsorption energy E_{ads} as a function of the adsorption height h_{ads}. We define E_{ads} as

$$E_{ads} = E_{inter} - (E_{Cu} + E_{mol}), \tag{3.2}$$

where E_{inter} is the energy of the interacting metal-molecule system, E_{Cu} is the energy of a pristine Cu(111) slab (again, with only the top two layers relaxed) and E_{mol} is the energy of a single relaxed ClB-SubPc molecule in the gas phase. In addition, the methodology applied to treat van der Waals interactions allows us to compute separately the contribution of these energies to E_{ads}, which we term as E_{vdW} (see section 4.1.4 for details).

The adsorption height, h_{ads}, is defined as the difference between the average heights of the C18 atoms and that of the metal atoms in the topmost layer of the

reconstructed substrate. At equilibrium, this height is 2.23 Å which appears low at first glance, but it is comparable to adsorption distances measured for planar π-conjugated systems in similar situations, such as 2.34 Å found for pentacene on Cu(111) [77].

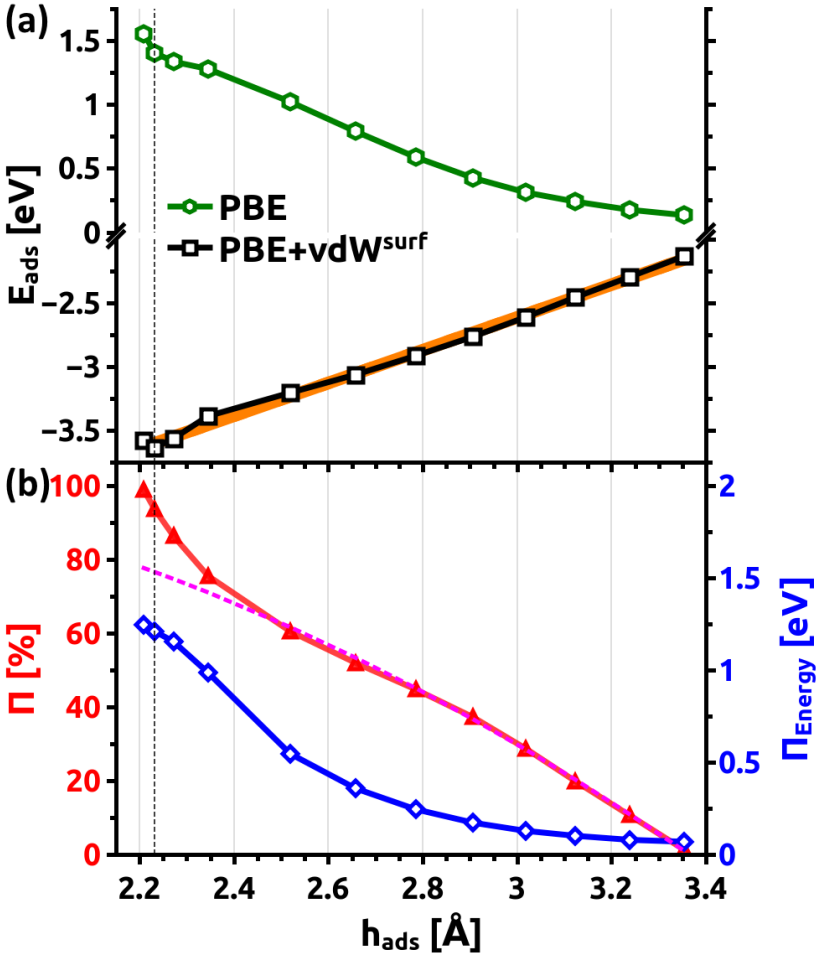

Figure 3.4: (a) Adsorption energy (E_{ads}) per ClB-SubPc molecule as a function of adsorption distance (h_{ads}) including (black curve) and neglecting (green curve) long-range van der Waals interactions (E_{vdW}). The orange line in the background is a linear fit to the E_{ads} (PBE+vdW^{surf}) curve highlighting the unusual shape of the adsorption potential. (b) The planarity (Π) of the molecule as a function of its adsorption h_{ads} (red triangles). The pink dashed-curve indicates the "expected" trend extrapolated from quadratic fitting of the data points with h_{ads}>2.7 Å. The blue curve and right axis refer to the energetic cost of planarizing the molecule (Π_{Energy}), i.e., of changing the molecular geometry from that obtained for the gas phase to that found at a specific adsorption distance.

In practice, to trace E_{ads} vs. h_{ads}, we gradually vertically moved the molecule from its equilibrium position in steps of 0.2 Å, fixed the position of the Cl atom and then optimized the geometry of the rest of the molecule as well as the top two atomic layers of the Cu substrate. The resulting curve, shown in Figure 3.4a, displays a few peculiarities:

1. The PBE contribution to the adsorption energy (green curve) is positive for all distances. This hints at a distinctly repulsive interaction between the

ClB-SubPc molecules and the Cu(111) surface in the absence of long-range vdW interactions. In fact, we observe a detachment of the molecule from the surface, if vdW interactions are turned off and the system geometry is allowed to optimize again.

2. The dependence of the adsorption energy on adsorption distance (when including vdW attraction), displays an unusual, essentially linear shape between the equilibrium distance of 2.23 Å and the largest considered distance of 3.35 Å ($r^2 = 0.996$ for a linear fit plotted in orange). There is also no indication of multiple minima, as are observed for systems displaying physisorbed as well as chemisorbed structures [20, 93].

Further insight can be gained by tracing the planarity of the adsorbed molecules as a function of h_{ads} as shown in Figure 3.4b: First, Π increases smoothly, as the molecule approaches the surface. However, at ca. 0.2 Å above the equilibrium distance, an increased planarization sets in, as is particularly evident when comparing the actual behavior at short distances with an extrapolation from larger adsorption heights (i.e., for $h_{ads} \in [2.79\ \text{Å}, 3.35\ \text{Å}]$, pink dashed-curve). This means that the molecule undergoes a disproportionately large planarization within a very small range (~0.2 Å) above the equilibrium height in spite of the significantly increased energetic cost to do so, as is evidenced by the calculated planarization energy in Figure 3.4b (blue curve).

3.3.2 *Uncovering the interplay between adsorption and planarization*

Given the unusual behavior of the ClB-SubPc/Cu(111) interface (massive molecular distortion, strong hybridization and unusual shape of the adsorption potential), we focus next on the role of the vdW forces. Here, we started from the repulsive situation, i.e., using solely the PBE functional (in absence of long-range vdW interactions). Then, we introduced and gradually increased the long-range van der Waals attraction, in this way pulling the molecule towards the surface. This scaling of the vdW forces allowed us to follow the gradual transition from an essentially non-interacting metal-molecule system to a situation characterized by a significant distortion of the adsorbate geometry and a strong hybridization between the molecular and metal states.

Technically, the rescaling is achieved by calculating the energy contribution due to long-range vdW interactions, analogous to the original Tkatchenko-Scheffler scheme [144], while introducing a scaling prefactor S that varies between 0 and 1. S scales the $C_{6,AB}$ coefficients that govern the pairwise inter-atomic interactions between two atoms A and B. This yields

$$E_{vdW}[\rho(\mathbf{r})] = -\frac{1}{2}\sum_{AB} S C_{6,AB}[\rho(\mathbf{r})] R_{AB}^{-6} f_{AB}. \tag{3.3}$$

Here, R_{AB} is the inter-atomic distance and f_{AB} is a Fermi-type damping function that subdues the correction at short-range. Notably, the Tkatchenko-Scheffler (TS) approach like Grimme's D3 scheme [52], the Becke-Johnson scheme [11], and the scheme from Sato and Nakai [122] aims to include the influence of the atom-pair's local chemical environment into the C_6 coefficients. In TS, this is done by making

the C_6 coefficient dependent on the charge density around the atoms to account for the dependence of vdW interactions on the system's local polarizability [21]. This makes the TS approach particularly useful in the present case, as in the course of changing S the charge distribution at the interface undergoes pronounced changes (vide infra).

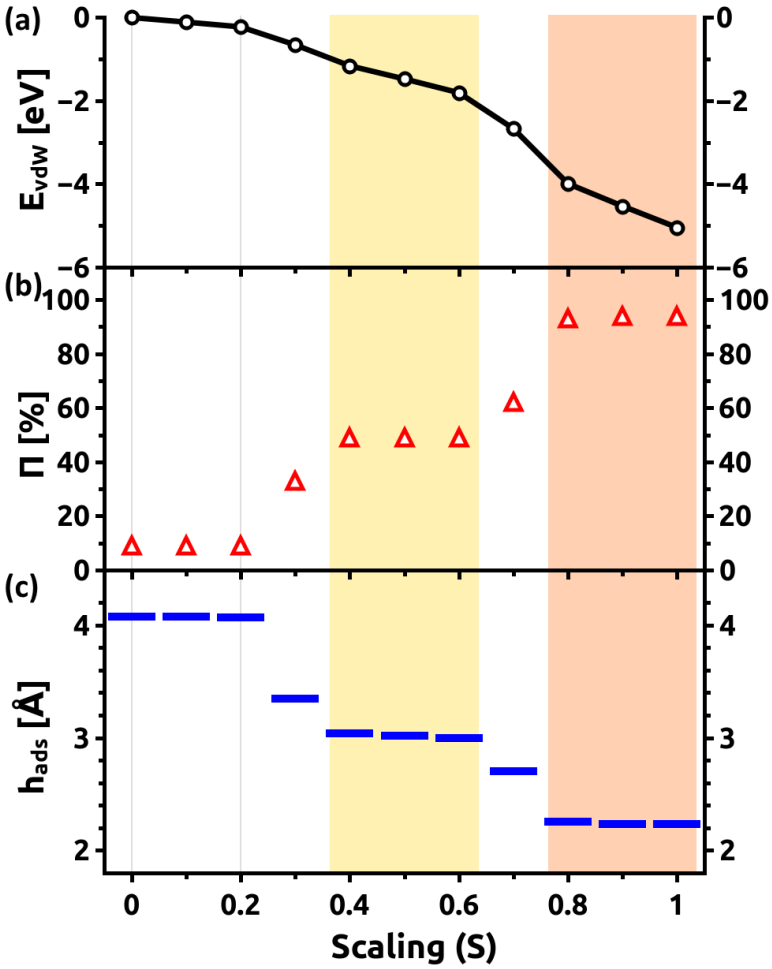

Figure 3.5: Evolution of the properties of the ClB-SubPc/Cu(111) interface with increasing the C_6 scaling prefactor S. (a) Non-linear increase in E_{vdW} (the contribution of the long-range vdW interaction to the adsorption energy) as a function of the van der Waals scaling prefactor S. (b) Molecular distortion quantified by the planarity of the adsorbed molecule (Π), as defined above. (c) Calculated adsorption height, h_{ads}. There are two distinct regimes with unchanging planarity and adsorption height ($S = 0.2$ to 0.6 and $S = 0.8$ to 1.0), shaded in yellow and orange respectively.

The resulting vdW contribution to the adsorption energy E_{vdW} as a function of S is shown in Figure 3.5a. Interestingly, the curve does not increase linearly with S. Rather, there are more pronounced drops between $0.2 \leq S \leq 0.4$ and between $0.6 \leq S \leq 0.8$. These more abrupt changes in energy are accompanied by step-wise increases in the planarity of the ClB-SubPc molecules (Figure 3.5b) and by step-wise decreases in the adsorption heights (Figure 3.5c). Consequently, when scaling the vdW interactions and in this way pulling the molecule towards the surface, one observes two clearly distinct adsorption regimes: Between $S = 0.4$

and $S = 0.6$ the molecule adsorbs in a somewhat planarized geometry ($\Pi \approx 49\%$) at a comparably large distance of around ~3.0 Å. Conversely, for $S \geq 0.8$, the C18 atoms of ClB-SubPc become essentially planar ($\Pi \approx 94\%$) and the adsorption height reduces to 2.2 Å. The transition between these regimes coincides with massive modifications of the electronic structure of the interface, as discussed in the following section.

3.3.3 *Interfacial electronic structure*

A first impression of modifications to the electronic structure of the ClB-SubPc/Cu(111) interface caused by increasing the van der Waals attraction can be obtained from the adsorption-induced changes in the work function, $\Delta\Phi$. For the sake of analysis, this quantity can be separated into a contribution from the monolayer due to molecular dipoles, $\Delta\Phi_{ML}$, and a contribution from the so called "bond-dipole" resulting from the interaction between substrate and adsorbate, dominated by the adsorption-induced charge rearrangements, $\Delta\Phi_{BD}$ [58]. This yields

$$\Delta\Phi = \Delta\Phi_{BD} + \Delta\Phi_{ML}. \tag{3.4}$$

In practice, $\Delta\Phi$ and $\Delta\Phi_{ML}$ are calculated explicitly and $\Delta\Phi_{BD}$ is obtained as the difference between these two numbers. Note that the above quantities for the subsystems are calculated in the optimized geometries they adopt upon adsorption.

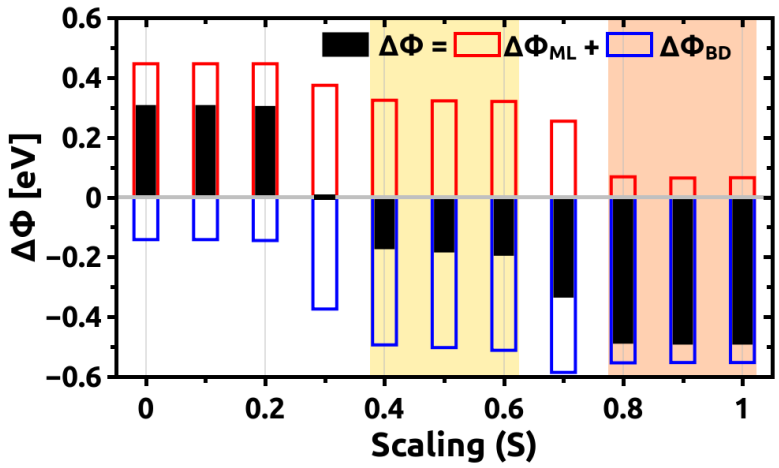

Figure 3.6: Evolution of the change in work function, $\Delta\Phi$ (black) and the contributions due to the molecular layer, $\Delta\Phi_{ML}$ (red), and the interfacial charge rearrangements, $\Delta\Phi_{BD}$ (blue), with increasing C_6 scaling prefactor S. The work function of the pristine Cu(111) surface is calculated to be 4.8 eV.

As shown in Figure 3.6, for small S, $\Delta\Phi$ is positive. This is a consequence of the significant molecular dipole moment pointing towards the surface, which results in a large positive value of $\Delta\Phi_{ML}$. As the adsorption distance for small S is large, the change in work function due the interaction-induced charge rearrangements, $\Delta\Phi_{BD}$, has only a minor impact. This changes in the first adsorption regime (for $0.4 \leq S \leq 0.6$), where the absolute value of $\Delta\Phi_{BD}$ rises by 0.5 eV. Simultaneously, the increasing planarity of the adsorbed molecules results in a decreasing molecular dipole and, thus, a smaller $\Delta\Phi_{ML}$. (The values for the molecular dipoles of

the different geometries obtained when varying S can be found in Chapter 4.) As both trends act in the same direction, the overall effect is a change in the sign of the work function modification and a resulting $\Delta\Phi$ of -0.2 eV. Notably, this value remains constant over the first adsorption regime.

Upon approaching the second adsorption regime, another step in the work function modification is observed and $\Delta\Phi$ drops to ~ -0.5 eV (for $0.8 \leq S \leq 1.0$). This is primarily a consequence of the further planarization of the adsorbate molecules resulting in a further reduced molecular dipole (see Chapter 4), such that $\Delta\Phi_{ML}$ becomes ≈ 0.06 eV. Notably, the contribution to the work function modification arising from the molecule-metal interaction adjusts much less, and $\Delta\Phi_{BD}$ saturates at -0.55 eV. This is quite surprising, considering the massive change in the adsorption distance and the fundamentally different shapes of the interfacial charge rearrangements between the first and second adsorption regimes (vide infra).

A direct comparison of the calculated $\Delta\Phi$ to experiments is difficult, as the experimentally accessible interface contains multiple species [67], including dechlorinated molecules (for which we calculate a $\Delta\Phi$ of -0.8 eV). Nevertheless, it is interesting to point out that the experimentally determined work function modification at a nominal coverage of 0.5 monolayer equivalents (corresponding to the coverage in the simulations) amounts to -0.5 eV.

The evolution of $\Delta\Phi_{BD}$ from Figure 3.6 is expected to map directly onto the evolution of the level alignment between the electronic states in the metal, characterized by the position of the Fermi level, and the states in the adsorbate layer; as demonstrated for a variety of organic molecules on Ag(111) [61]. This is shown in Figure 3.7. Indeed, up to $S = 0.4$, one sees a pronounced shift in the states of the ClB-SubPc monolayer towards higher binding energies (by ca. 0.7 eV). This can be explained by Pauli pushback [7] reducing the surface dipole of the metal [69] and, thus, its work function. Consistent with a constant adsorption height and adsorbate shape, there is no further change in the PDoS up to $S = 0.6$. Notably, there is virtually no difference in the shape of the PDoS compared to the effectively non-interacting situation ($S = 0$). Upon further increasing S (i.e. upon pulling the molecule further towards the surface), one again observes a shift of the PDoS towards higher binding energies by 0.4 eV. However, like in the above-discussed evolution for $\Delta\Phi_{BD}$, the net effect is weaker than what is expected based on the strongly decreasing adsorption distance and the resulting massively amplified Pauli pushback. The reason for that is that here one enters the regime of Fermi-level pinning: the formerly unoccupied PDoS of the adsorbate layer is shifted into resonance with the Fermi level, resulting in electron transfer from the metal to the molecules such that the resulting dipole counteracts the effect of Pauli pushback and the overall interfacial dipole remains constant [62].

Based on these observations, one can denote the first adsorption regime ($0.4 \leq S \leq 0.6$) as the "weak coupling regime" with only negligible charge transfer between molecular states and the metal, as is usually observed for physisorption. Here it should be stressed that this regime is not merely a curiosity resulting from the scaling of the van der Waals attraction. In fact, it is representative of the situation of ClB-SubPc adsorbing on less reactive metals, as is shown in section 4.1.10 for ClB-SubPc/Ag(111) interface or other even more inert substrates like HOPG (see Figure 3.3).

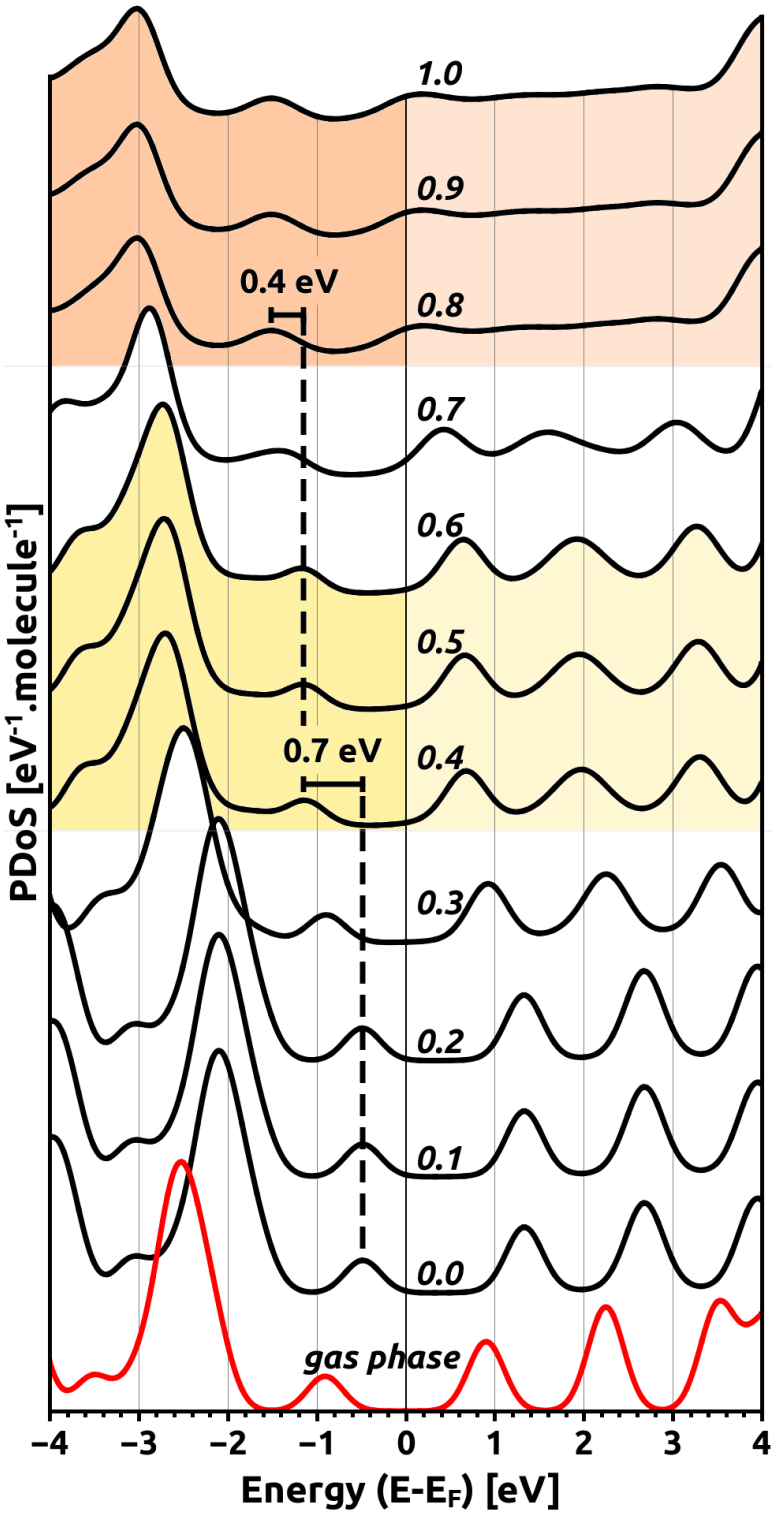

Figure 3.7: Density of states projected onto the molecular region (PDoS) for the ClB-SubPc/Cu(111) interface as a function of the van der Waals scaling prefactor S. The DoS of the gas-phase molecule has been Gaussian broadened and shifted to align the center of the HOMO-LUMO gap with the Fermi level, E_F. The shading denotes the different adsorption regimes (cf., Figures 3.5 and **3.6**).

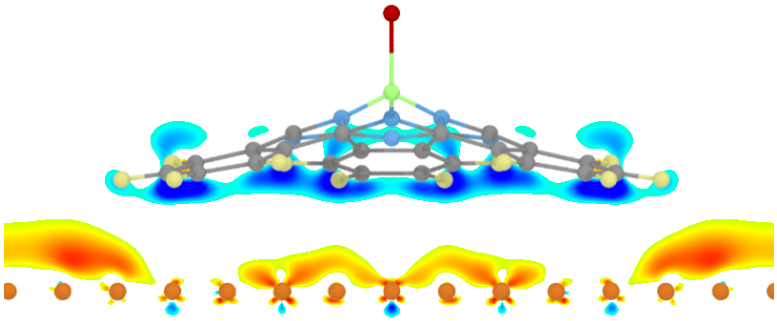

(a) $S = 0.4$

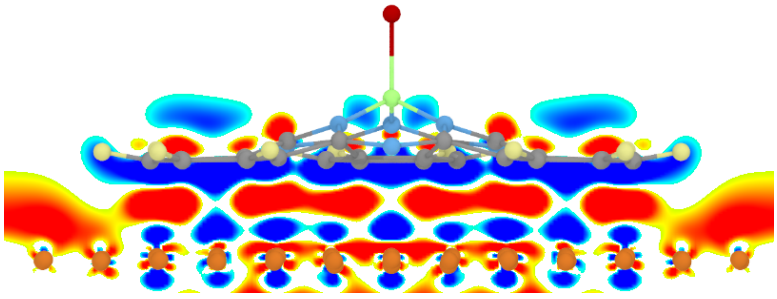

(b) $S = 1.0$

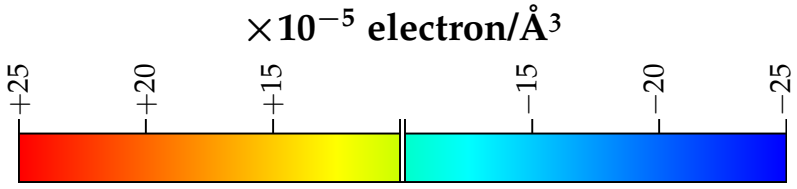

Figure 3.8: Side-view of the interfacial charge rearrangements for (a) $S = 0.4$ and (b) $S = 1.0$ averaged over the unit cell along the direction perpendicular to the plane of projection.

The second regime ($0.8 \leq S \leq 1.0$) is then denoted as the "strong coupling regime", as there we see the partial filling of the molecular PDoS suggesting that electrons have been transferred from the Cu substrate into previously unoccupied orbitals of the molecular layer. Moreover, a massive broadening of all molecule-derived features in the PDoS occurs. As mentioned earlier, the latter is indicative of a particularly strong hybridization between molecular and metal states. Notably, we refrain from associating it with chemisorption, as in spite of the significant interaction between the ClB-SubPc molecules and the Cu(111) substrate, Figure 3.4a suggests that there would be no bonding in the absence of vdW attraction. That is, we face a situation of strong electronic coupling between substrate and adsorbate that by itself would, however, not be sufficient to trigger adsorption.

To further distinguish between the two adsorption regimes and to trace the strong hybridization between substrate and adsorbate states, it is useful to consider the adsorption-induced interfacial charge rearrangements, $\Delta\rho$. These are obtained via

$$\Delta\rho = \Delta\rho_{inter} - (\Delta\rho_{slab} + \Delta\rho_{mol}), \tag{3.5}$$

where $\Delta\rho_{inter}$ is the charge density of the interacting metal-molecule system, $\Delta\rho_{slab}$ is the charge density of only the metal slab, and $\Delta\rho_{mol}$ is charge density of an isolated molecule (again, all in the geometry obtained for the interacting system). $\Delta\rho$ can be further averaged/integrated along one or two spatial directions to obtain 2D or 1D charge rearrangement plots respectively.

The situation for the weak coupling regime ($S = 0.4$) is shown in Figure 3.8a. The charge rearrangements indicate the prevalence of Pauli pushback with a pronounced electron-density depletion in the region of the overlap between the tailing electron cloud of the metal and the π-states of the molecules. The effect is stronger below the plane of the molecule, as there the tailing states from the metal are more prevalent than above. The "pushed-back" electrons are accumulated directly above the metal surface (see also plot of plane-integrated 1D charge rearrangements contained in Chapter 4).

The situation changes qualitatively in the strong coupling regime, shown for $S = 1.0$ in Figure 3.8b. There, in addition to the electron density depletion immediately below the molecular backbone, one observes accumulation directly above the molecule and, even more pronounced, in the region about half way between the C18 atoms and the topmost layer of the Cu(111) substrate. Especially the latter deserves attention: As shown in Figure 3.9a, electron accumulation occurs in those regions where the C18 atoms and the Cu atoms of the topmost metal layer are particularly close, while there is depletion above the bridge- and hollow-sites of the substrate. The assessment that the driving force for electron accumulation in specific regions is the local proximity between the molecular π-system and on-top metal sites is confirmed by the very different shape of the charge rearrangement pattern for ClB-SubPc on the four-fold symmetric Cu(100) surface shown in Figure 3.9b.

We also find that that the H atoms are located 0.2 Å above the C18 plane and that the carbon-carbon bond lengths within the rings constituting the C18 system increase on average by ~3 pm. These are further indications for a minor disruption of the molecular π-system caused by the hybridization of the molecular and metal states.

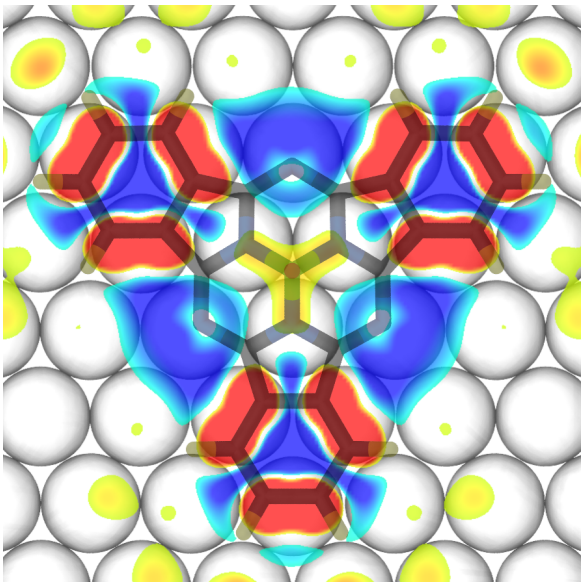

(a) Charge rearrangements on **Cu (111)**

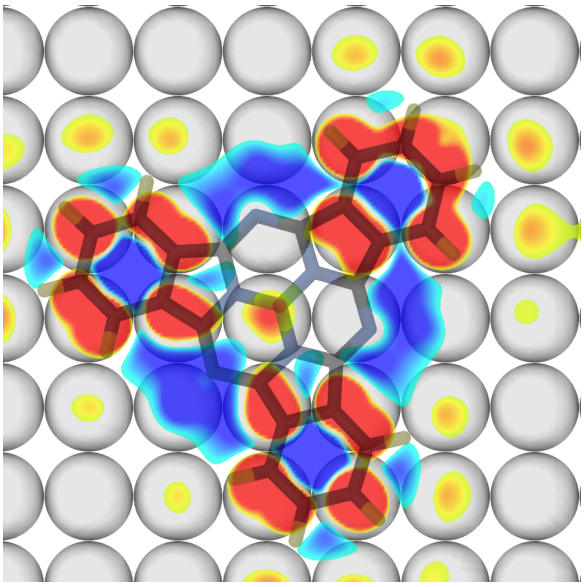

(b) Charge rearrangements on **Cu (100)**

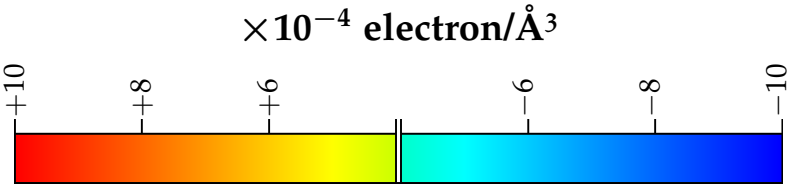

Figure 3.9: : Top view of the charge rearrangements induced by ClB-SubPc on (a) Cu (111) and (b) Cu(100). The graphs show a 2D slice of the charge rearrangements calculated for the plane half-way between the molecule and the metal.

3.3.4 *Role of molecular planarity in its ability to hybridize*

Even though the above results provide evidence that the planarization of the ClB-SubPc molecule is an integral aspect of the adsorption process, the data presented thus far do not fully clarify how crucial planarization actually is for the electronic structure of the interface and especially for the strong hybridization of molecular and metal states. To address this question, we simulated the adsorption of a *rigidified* ClB-SubPc molecule. For this we fixed the lateral positions of the carbon atoms in the gas-phase geometry of the molecule, thereby reducing the degrees of freedom during geometry relaxation. In other words, the C atoms

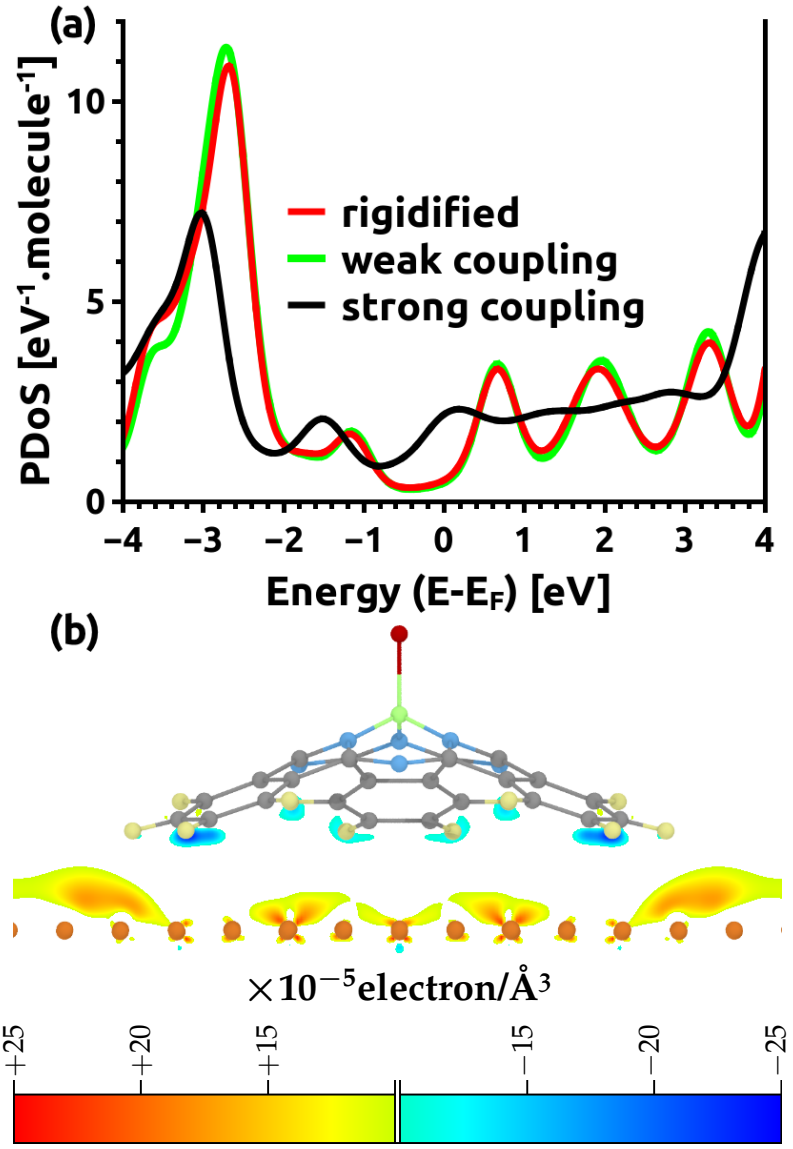

Figure 3.10: (a) Comparison of the molecule-projected densities of states for the artificially *rigidified* molecule ($S = 1.0$), and the fully relaxed structures in the weak ($S = 0.4$) and strong ($S = 1.0$) coupling regimes. (b) Side-view of the interfacial charge rearrangements for the rigidified molecule averaged over the unit cell along the direction perpendicular to the plane of projection.

could relax solely along the direction perpendicular to the surface thereby largely preventing a planarization of the molecule. Care was taken to align the rigidified molecule such that its registry with the Cu(111) surface is identical to that of the fully relaxed case. The optimum adsorption height for the rigidified molecule rose to 3.0 Å, 0.77 Å more than the fully relaxed structure (vide supra). Interestingly, this adsorption height is almost identical to that obtained for the fully optimized interface molecule in the weak coupling regime (calculated in the full optimizations for $0.4 \leq S \leq 0.6$). Therefore, in Figure 3.10a, we compare the PDoS of the fully optimized and rigidified structures (both calculated at $S = 1.0$) with the situation obtained for the weak coupling case ($S = 0.4$, fully optimized).

Intriguingly, we find an almost perfect correspondence between the latter two cases in the PDoSes as well as in the work function modifications ($\Delta\Phi = -0.14$ eV for the rigidified molecule and -0.17 eV for weak coupling regime). Likewise, the charge rearrangements for the rigidified system show no indication of strong hybridization (Figure 3.10b). Rather, one solely observes Pauli pushback, as displayed already in Figure 3.8a for the weak coupling regime. This clearly shows that the ability of the non-planar ClB-SubPc to strongly couple to the metal substrate crucially depends on its ability to planarize, which occurs only when vdW attractions pull the molecule towards the surface.

3.4 SUMMARY AND CONCLUSIONS

The ClB-SubPc/Cu(111) interface provides valuable insight into how changes in an adsorbate geometry induced by the van der Waals attraction to a substrate can change the electronic coupling between substrate and adsorbate, pushing the interface into a significantly different coupling regime. To better understand the peculiarities of this interface, we adopted a strategy that allowed us to scale the vdW interactions, in order to gradually pull the molecule towards the substrate. This revealed two adsorption regimes, which we identified to be cases of weak and strong interfacial coupling. In the former, the originally shuttlecock-shaped molecules are planarized to a lesser degree and the electronic interaction with the substrate is dominated by Pauli pushback, which together with the molecular dipoles then determines the adsorbate-induced work function modification. In the second regime, the molecule is pulled very close to the surface, it is largely planarized, and a particularly strong hybridization between molecular and metal states occurs in conjunction with electron transfer from the substrate to adsorbate. In that case, the adsorbate layer becomes metallic and the system work function is determined by Fermi-level pinning. Notably, we show that this regime cannot be characterized as conventional chemisorption, as in spite of the sizable electronic interactions between substrate and adsorbate, the molecule would not attach to the surface in the absence of vdW attraction. In fact, the strong coupling regime can be reached only provided that the molecule significantly changes its shape, which is shown to be a consequence of vdW forces pulling it towards the surface. Thus, the present system can be regarded as an intriguing example for a vdW enabled strong electronic coupling between a metal surface and an organic adsorbate molecule.

4

ADDENDUM TO CHAPTER 3

4.1 SUPPORTING INFORMATION TO CHAPTER 3

4.1.1 *Registry of chlorinated and dechlorinated (Cl)B-SubPc on Cu(111)*

Dechlorination results in formation of two distinct species of the subphthalocyanine molecule on Cu(111) surface. Interestingly, both have the same orientation and registry with respect to the underlying copper atoms: They sit on an hcp hollow site such that there is maximum overlap between their six nitrogen atoms and the copper atoms, as shown in Figure 4.1. This finding has been discussed in more detail in a previous study [67], reprinted in this thesis as Chapter 1.

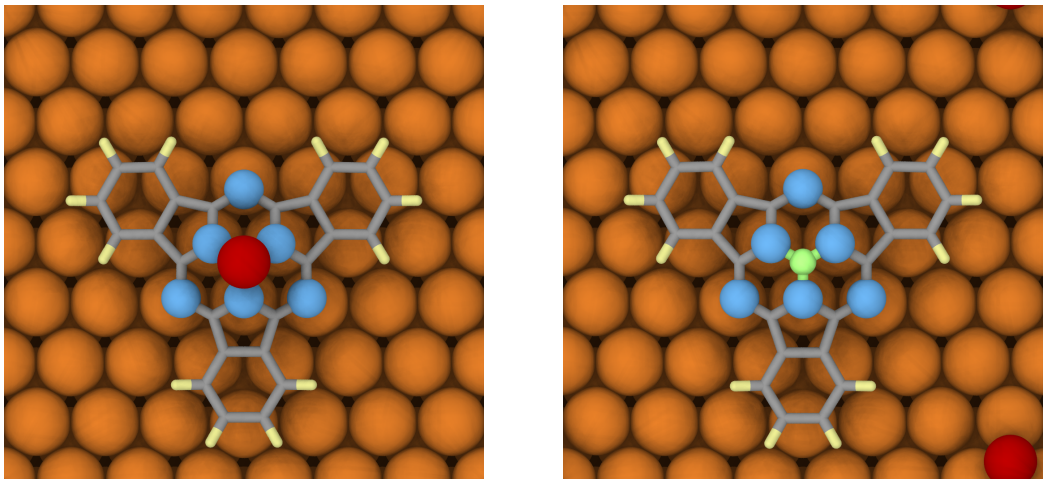

(a) ClB-SubPc molecule and Cu(111) surface after intact adsorption

(b) B-SubPc molecule and Cu(111) surface after surface-mediated dechlorination and adsorption.

Figure 4.1: Registry between (Cl)B-SubPc molecule and Cu(111) surface (a) after intact adsorption and (b) after surface-mediated dechlorination and adsorption. The six nitrogen atoms (blue) align vertically with underlying Cu atoms of the topmost layer, while the molecule's central axis aligns with an hcp hollow site. The chlorine atom (red) has been removed to the periphery of the periodic unit cell in panel (b).

4.1.2 *Results for the dechlorinated system*

Property	ClB-SubPc adsorbed on Cu(111)	Adsorbed B-SubPc with Cl atom moved to periphery of the unit cell
Planarity	94%	90%
Adsorption energy	−3.64 eV	−3.58 eV
Adsorption height	2.23 Å	2.26 Å
Change in work function	0.49 eV	0.79 eV

Table 4.1: Comparison of the main properties of intact ClB-SubPc on Cu(111) system and its dechlorinated version, B-SubPc, on Cu(111). In the latter case, whether the Cl atom is put in the periphery of the unit cell or entirely removed from the system makes only a minor difference (for example, in the latter case the work-function change amounts to 0.82 eV).

4.1.3 *Effect of dechlorination on the interfacial electronic structure*

Dechlorination affects the interfacial electronic structure minimally. Figure 4.2 presents the molecule projected DoS of the dechlorinated system (shown in Figure 4.1b), superimposed on Figure 3.2c of Chapter 3. The only significant change is between −4 eV and −2.5 eV, where the dechlorinated molecule is missing a feature that originates from the chlorine atom.

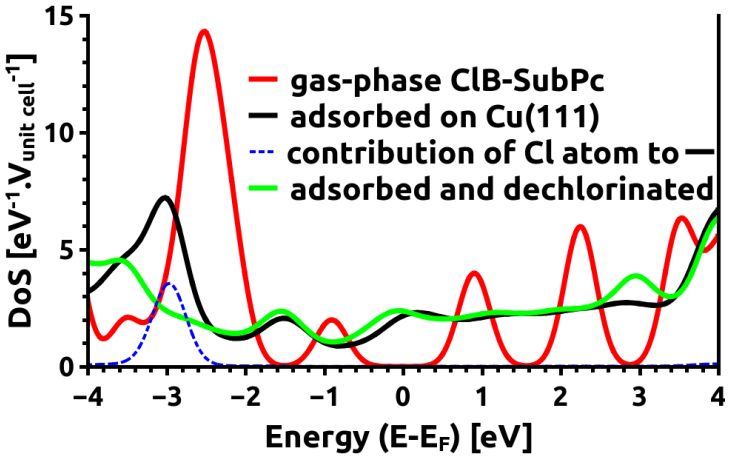

Figure 4.2: Density of states projected onto the ClB-SubPc molecule for the molecule is in gas-phase (red), when it is adsorbed intact on on Cu(111) (black) and when adsorbed after surface mediated dechlorination (green). The noticeable difference between the latter two, between −4 eV and −2.5 eV, is due to the contribution from the chlorine atom (dashed-blue curve) in the periphery of the monolayer.

Further evidence for the fact that dechlorination does not fundamentally alter the interfacial electronic structure can be gathered from plane-integrated charge redistribution for the two systems shown in Figure 4.3. Other than slight deviations around 0.5 Å and 3.5 Å there is no noticeable difference between the two.

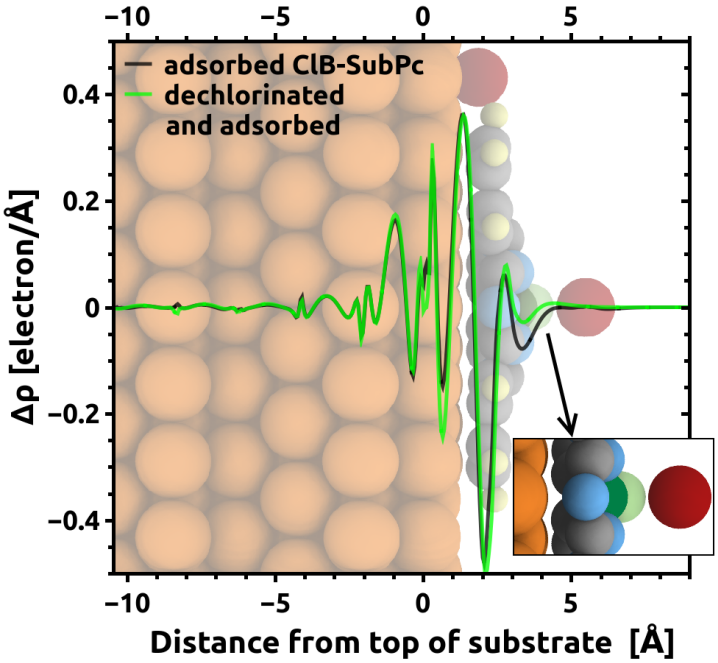

Figure 4.3: Density of states projected onto the ClB-SubPc molecule for the molecule is in gas-phase (red), when it is adsorbed intact on on Cu(111)(black) and when adsorbed after surface mediated dechlorination (green). The noticeable difference between the latter two, between -4 eV and -2.5 eV, is due to the contribution from the chlorine atom (dashed-blue curve) in the periphery of the monolayer.

4.1.4 *Calculation of E_{vdW}*

Because we calculate the van der Waals energy as an *a posteriori* correction, we can separate the total energy of any given system into

$$E_{given\text{-}system} = E_{given\text{-}system_{PBE}} + E_{given\text{-}system_{vdW}} \tag{4.1}$$

where $E_{given\text{-}system}$ is the contribution of van der Waals (vdW) interactions to the total energy of this system.

Using equation 4.1, for the three systems considered in Equation 3.2 of Chapter 3 (to calculate adsorption energy), one can write the following equations

$$E_{inter} = E_{inter_{PBE}} + E_{inter_{vdW}} \tag{4.2}$$
$$E_{Cu} = E_{Cu_{PBE}} + E_{Cu_{vdW}} \tag{4.3}$$
$$E_{mol} = E_{mol_{PBE}} + E_{mol_{vdW}} \tag{4.4}$$

where, E_{inter} is the energy of the interacting metal-molecule system, E_{Cu} is the energy of a pristine Cu(111) slab (with only the top two layers relaxed) and E_{mol} is the energy of a single relaxed ClB-SubPc molecule in vacuum (treated non-periodically).

Hence, when calculating adsorption energy, one ends up with the following equation

$$E_{ads} = E_{inter_{PBE}} + E_{inter_{vdW}} - (E_{Cu_{PBE}} + E_{Cu_{vdW}} + E_{mol_{PBE}} + E_{mol_{vdW}}). \tag{4.5}$$

Consequently, E_{ads} can also be separated into two components by defining

$$E_{ads_{PBE}} \overset{\text{def}}{=} E_{inter_{PBE}} - (E_{Cu_{PBE}} + E_{mol_{PBE}}) \text{ and} \tag{4.6}$$

$$E_{ads_{vdW}} \overset{\text{def}}{=} E_{inter_{vdW}} - (E_{Cu_{vdW}} + E_{mol_{vdW}}). \tag{4.7}$$

This results in

$$E_{ads} = E_{ads_{PBE}} + E_{ads_{vdW}} \tag{4.8}$$

where $E_{ads_{PBE}}$ comprises the contributions to the adsorption energy result from the PBE functional, whereas and $E_{ads_{vdW}}$ contains the van der Waals contribution. The latter energy can be further written as

$$E_{ads_{vdW}} = E_{inter_{vdW}} - E_{mol_{vdW}} \tag{4.9}$$

because $E_{Cu_{vdW}}$ in Equation 4.7 is 0 eV by definition, since we neglect of vdW interactions between Cu atom-pairs in all calculations (see Section 3.2.1). Here, $E_{inter_{vdW}}$ can be termed as the contribution of vdW interactions between the metal and the molecule to the adsorption energy, a quantity simply referred to as E_{vdw} in Chapter 3, i.e.,

$$E_{inter_{vdW}} \equiv E_{vdw}. \tag{4.10}$$

Calculating this quantity is necessary, because scaling the C_6 coefficient influences both factors from Equation 4.9, while we are interested only in $E_{inter_{vdW}}$, i.e., the influence of scaling on the interactions that originate from the adsorption of the molecule on the metal.

4.1.5 *Effect of planarization on DoS of the molecule*

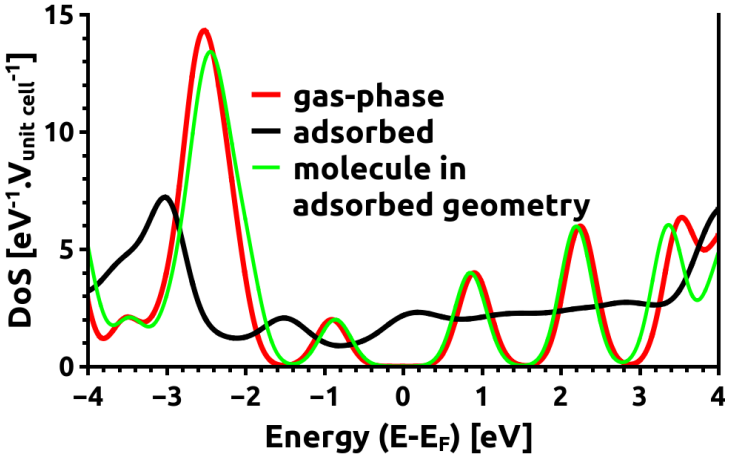

Figure 4.4: Density of States (DoS) of the molecule when it is in the geometry that it acquires upon adsorption i.e. planarized (green), overlaid on Figure 3.2c of Chapter 3. As evident by comparing the green and red curves, the change in geometry has little consequence on the DoS of the molecule.

4.1.6 *Energy spent on planarizing the molecule*

See Table 4.2.

Adsorption height [Å]	Height of Cl atom above Cu substrate [Å]	Contribution of vdW forces, E_{vdW} [eV]	Molecule reconstruction energy [eV]	Adsorption energy [eV]	Percentage of E_{vdW} used for molecule reconstruction or released as adsorption energy
2.209	5.25	−5.132	1.247	−3.576	94%
2.232	5.45	−5.041	1.210	−3.636	96%
2.272	5.65	−4.899	1.154	−3.564	96%
2.345	5.85	−4.667	0.986	−3.389	94%
2.519	6.05	−4.227	0.546	−3.206	89%
2.658	6.25	−3.852	0.358	−3.064	89%
2.785	6.45	−3.504	0.245	−2.917	90%
2.907	6.65	−3.190	0.172	−2.766	92%
3.000	6.85	−2.925	0.128	−2.614	94%
3.123	7.05	−2.697	0.101	−2.459	95%
3.238	7.25	−2.474	0.079	−2.299	96%
3.353	7.45	−2.271	0.069	−2.137	97%

Table 4.2: This table tabulates how E_{vdW} (3rd column), i.e. the energy earned from van der Waals interactions at the interface is spent: it is either used for planarizing the molecule (molecule reconstruction energy, 4th column) or released as free-energy (adsorption energy, 5th column). These two components account for at least ~90% of E_{vdW} (6^{th} column).
This table also illustrates that, given its non-planar geometry, adjusting the adsorption height for ClB-SubPc is not so straightforward; for instance, when calculating E_{ads} as a function of h_{ads}. For doing that, we fixed the height of the chlorine atom (see 2nd column) while allowing rest of the molecule to relax. This results in an increasing planarity as the molecule moves towards the substrate because of which 'adsorption height', as we define it, does not change in steps of 0.2 Å (compare 1st column with 2nd).

4.1.7 *Dipole moment and planarity of the molecule*

Table 4.3 testifies to a massive reduction of the molecular dipole moment as a consequence of planarization. This is mostly attributed to a reduction of the axial component of the electrostatic moments from the three isoindole groups.

scaling factor (S)	Planarity(Π) [%]	Dipole moment (μ) [debye]
0	9	4.14
0.1	9	4.14
0.2	9	4.14
0.3	33	3.45
0.4	49	2.99
0.5	49	2.97
0.6	49	2.95
0.7	62	2.34
0.8	93	0.64
0.9	94	0.61
1	94	0.62

Table 4.3: Planarity and dipole moment of an isolated ClB-SubPc in the geometry it adopts on the Cu(111) surface for various degrees of van der Waals interaction.

4.1.8 *1D charge redistributions for* $S = 0, 0.4$ *and* 1

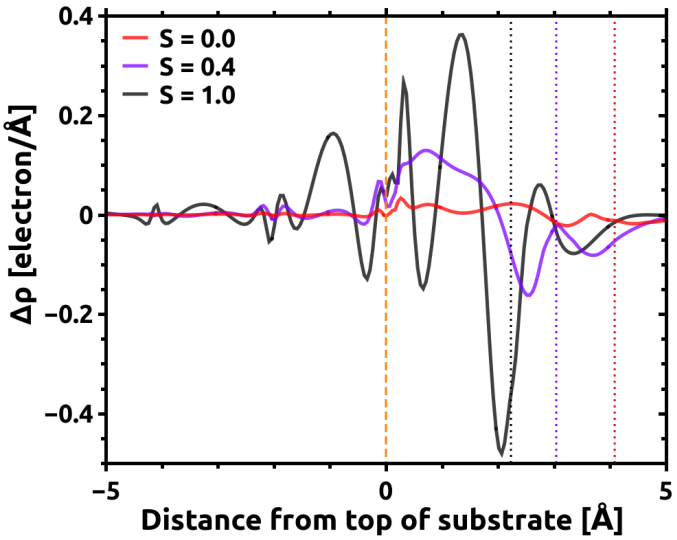

Figure 4.5: xy-plane integrated charge density redistribution for the ClB-SubPc on Cu(111) system for various degrees of vdW interaction with the surface, realized by changing the scaling factor S. The yellow vertical dashed-line represents the top layer of Cu atoms. The red, violet and black vertical dotted-lines represent the adsorption height of the molecule for $S = 0.0$ (4.08 Å), $S = 0.4$ (3.04 Å) and S = 1.0 (2.23 Å).

4.1.9 *2D charge redistributions for* $S = 0, 0.4$ *and* 1

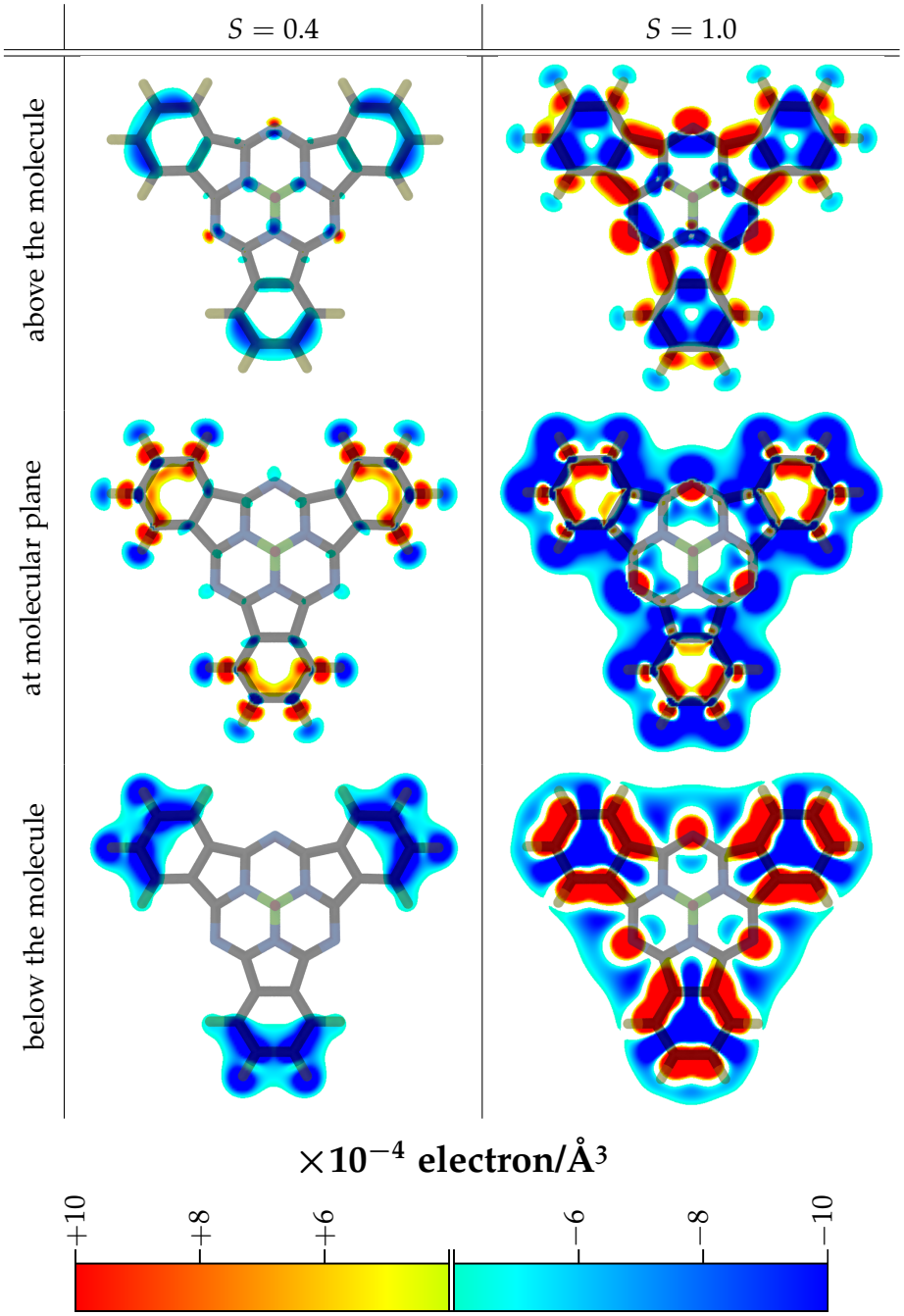

Figure 4.6: Charge redistribution associated with $S = 0.4$ (left) and $S = 1.0$ (right). These images present a 2D slice from 3D charge redistribution at different planes with respect to the C18 atoms. The average height of these atoms in the system is used to determine the plane of the molecule. The top panels shows charge redistributions 0.76 Å above the molecular plane, the central panels depict them in the molecular plane and the bottom panels show the results at a position 0.76 Å below the molecular plane. Steps of 0.76 Å are chosen because this corresponds to the covalent radius for a carbon atom.

4.1.10 *Comparison with adsorption on Ag(111)*

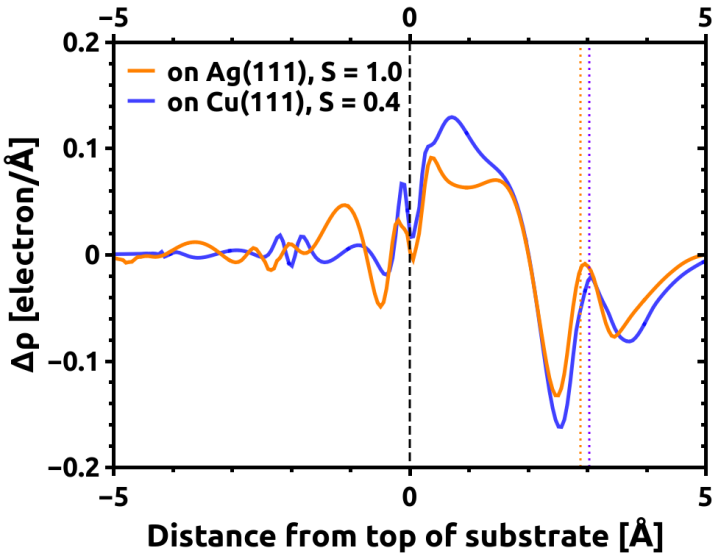

Figure 4.7: Charge redistribution associated with $S = 0.4$ (violet) when ClB-SubPc molecule adsorbs on Cu(111) and when it adsorbs with $S = 1.0$ on Ag(111); both show formation of the Pauli pushback 'cushion' immediately above the metal surface (represented by the black dashed line). The adsorption heights of the molecule are marked by orange vertical dotted-line (at 3.04 Å for Cu, when$S = 0.4$) and by violet vertical dotted line (at 2.88 Å for Ag, when $S = 1.0$). Further, the planarity of the two systems is comparable, with $\Pi = 67\%$ for Ag and $\Pi = 49\%$ for this stage of adsorption on Cu.

4.1.11 *Coordinates for gas phase geometry of the molecule*

FHI-aims [13] is capable of calculating systems with and without periodic boundary condition i.e. doing cluster calculations as well as supercell calculations. Therefore, to calculate the 'gas phase' geometry, one can simply relax the molecule while treating it non-periodically. Guassiano9 [41] is another widely used DFT package that is popular for molecular and cluster calculations. To obtain the gas phase geometry of ClB-SubPc molecule, we followed a two-step procedure. First, we relaxed the molecule in Gaussiano9 using 'tight' setting for SCF and default convergence criteria for geometry optimization (maximum force <~0.02 eV/Å). The standard PBE functional was used. Then we moved this geometry into FHI-aims and relaxed it again using PBE+vdW^{surf}. The resulting geometry, with the following coordinates is defined as the gas phase geometry:

```
Cl        4.86370186        6.28072167        4.91471928
B         4.86370336        6.28053374        3.05002553
N         6.21371560        6.48122928        2.44753002
N         4.36257808        5.01090059        2.44769954
N         4.01481691        7.34921586        2.44740241
N         5.84383904        8.76337550        1.88299264
N         6.52402810        4.18997423        1.88392974
```

```
N         2.22331367        5.88767271        1.88331417
C         2.73196687        7.12193069        2.02030976
C         4.52647733        8.54733782        2.02015487
C         6.65841502        7.70574141        2.02020309
C         6.99553395        5.43892658        2.02077685
C         5.20078853        4.01340569        2.02085663
C         3.06916568        4.85491014        2.02049602
C         8.19982183        6.05218780        1.48280415
C         7.98910511        7.46914810        1.48237870
C         2.99831002        3.50528575        1.48261342
C         4.33074197        2.97921688        1.48291250
C         2.27137625        8.39239527        1.48220764
C         3.39304265        9.28346091        1.48217780
C         4.59771973        1.72348934        0.93517195
C         3.53201201        0.99036510        0.41838967
C         2.22324701        1.50715848        0.41799373
C         1.94569120        2.77069650        0.93442720
C         9.36245804        5.50765812        0.93518096
C        10.31791363        6.37954484        0.41829001
C        10.11092155        7.77134838        0.41777832
C         8.94311657        8.32794942        0.93419968
C         3.28289394       10.56242102        0.93418458
C         2.04989684       10.95351597        0.41741517
C         0.94821174       10.07816461        0.41730226
C         1.05046944        8.78868680        0.93405584
H         5.61449315        1.33348586        0.91921448
H         3.71326086        0.00000000        0.00154625
H         1.41449447        0.90777303        0.00075651
H         0.93679457        3.18062380        0.91787975
H         9.51197833        4.42896354        0.91938302
H        11.24148178        5.97866682        0.00146214
H        10.87791114        8.42330661        0.00051587
H         8.77243108        9.40348434        0.91755913
H         4.14212169       11.23148699        0.91798818
H         1.93502782       11.95363505        0.00028974
H         0.00000000       10.41607592        0.00000000
H         0.20457725        8.10283686        0.91776482
```

4.1.12 *Using Grimme's D2 dispersion correction*

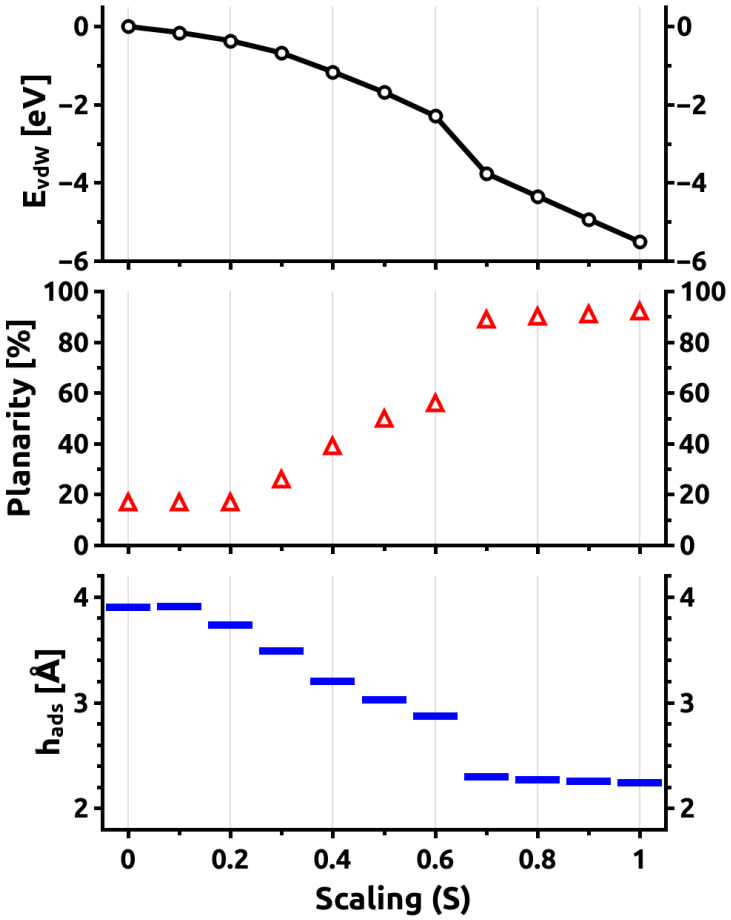

Figure 4.8: Figure analogous to Figure 3.4 of Chapter 3, but derived by employing scaling on the old version of Grimme's dispersion correction [51] scheme, referred to in literature as D2. The scheme does not 'dynamically' take into account the chemical environment of the atoms and is thus not as effective in delineating the two regimes of adsorption. The newer version, Grimme's D3 [52], does take into account the account the chemical environment of the atoms by using their coordination number an input parameter.

4.2 AUTHORS WHO CONTRIBUTED TO CHAPTER 3

This section lists the authors who contributed to Chapter 3. Their affiliation for the time period during which they contributed to the underlying research is also listed.

• Shashank S. Harivyasi
Institute of Solid State Physics, NAWI Graz, Graz University of Technology, Petersgasse 16, 8010 Graz, Austria

• Oliver T. Hofmann
Institute of Solid State Physics, NAWI Graz, Graz University of Technology, Petersgasse 16, 8010 Graz, Austria

• Nahid Ilyas
Department of Chemistry and Biochemistry, University of Arizona, Tucson, 1306 E. University Boulevard, Tucson, Arizona 85721, United States

• Oliver L. A. Monti
Department of Chemistry and Biochemistry, University of Arizona, Tucson, 1306 E. University Boulevard, Tucson, Arizona 85721, United States
Department of Physics, University of Arizona, Tucson, 1118 E 4th Street, Tucson, Arizona 85721, United States

• Egbert Zojer
Institute of Solid State Physics, NAWI Graz, Graz University of Technology, Petersgasse 16, 8010 Graz, Austria

Part III

CORE-LEVEL SPECTROSCOPY OF OLIGOMERS

In this part of the thesis we cover our study pertaining core-level spectroscopy of two types of oligomers, (perfluorinated) terphenyl and (perfluorinated) acenes, done with the motivation to develop a reliable methodology for supporting experimental studies with *ab-initio* ones. To this end, our experimentalist collaborator, Professor Michael Zharnikov of the Heidelberg University suggested that we begin by focusing on the molecules that form the molecular backbone in two well-studied self-assembled monolayers (SAMs) — perfluoroterphenyl-substituted alkanethiols on Au(111) and perfluoroanthracenylaminoalkane thiolates on Au(111) — namely perfluorinated terphenyl and perfluorinated anthracene respectively.

In our venture, we found that the experimental spectra for many systems can be reasonably simulated with ease when using the current state-of-the-art methodology. However, simulated spectra for perfluorinated systems such as that of perfluorinated acenes tends to compare poorly with experiments. In Chapter 5 we briefly discuss the simple case of acenes in order to develop a general background of concepts involved and then move on to discuss the results for the (perfluorinated) terphenyl molecules. In Chapter 6 we discuss the problems related to simulation of fluorinated systems and present a workable solution of this problem.

5

CORE-LEVEL SPECTROSCOPY OF TERPHENYL, PERFLUORINATED TERPHENYL AND ACENES

5.1 ACENES

5.1.1 *Geometry of the molecules*

For our first use-case scenario, mainly to understand and benchmark (vide infra) the simulation of core-level spectroscopy (CLS) techniques, we chose to work on the family of acene molecules. Acenes are polycyclic aromatic hydrocarbons (PAHs) made up of linearly fused benzene rings. Depending on the number of constituent benzene rings, the five chemically stable acenes are benzene (1 ring), naphthalene (2 rings), anthracene (3), tetracene (4) and pentacene (5); all having the (generalized) molecular formula $C_{4n+2}H_{2n+4}$ where n is the number of constituent rings. In this work, we discuss only four of the five acenes (Figure 5.1): (a) benzene, (b) naphthalene, (c) anthracene and (d) pentacene.

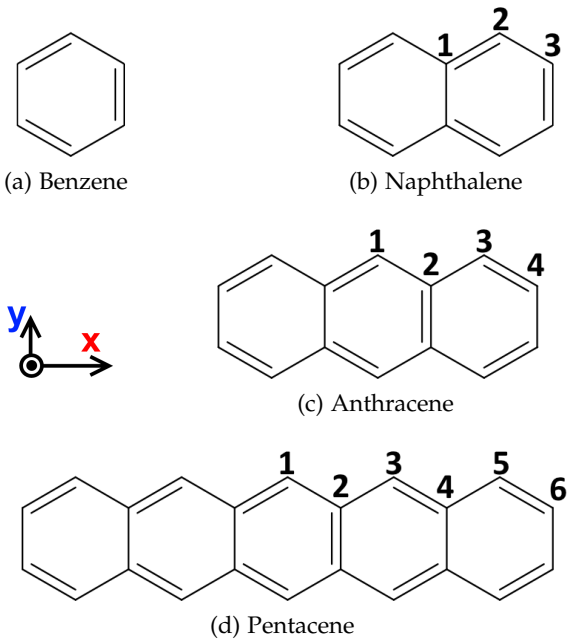

(a) Benzene (b) Naphthalene

(c) Anthracene

(d) Pentacene

Figure 5.1: The four acene molecules discussed in this work and the inequivalent carbon atoms in them. The axes define the directions we refer to in the accompanying text: the long molecular axis is along the **x** direction and while the shorter one is along **y**.

5.1.2 *Core-level spectroscopy*

We simulated the spectra for X-ray photoelectron spectroscopy (XPS) and near edge X-ray absorption fine structure (NEXAFS) spectroscopy for cases in which the excited photoelectron originates at the 1*s* core-level of a carbon atom. Also, we limited our scope to the first excitation process i.e. only *one* C atom[1] in the entire system is considered to be in the excited state when calculating the energy of the excited state. Further, it must be noted that in an experiment, any of the carbon atoms in the system might get excited and therefore it is necessary to calculate the spectra of every single C atom that can possibly be excited and then average all such spectra. Fortunately, in case of molecules, one can reduce the overall number of individual spectrum required by taking molecular symmetry into account and the only simulating the *inequivalent* C atoms of a given molecule (see also page 98).

In benzene, taking into account its C6 symmetry, all its carbon atoms are equivalent as far as simulating CLS techniques is concerned. Therefore, for simulations, any one of the six C atoms can be considered to be in an excited state while the others are considered to be in their ground state. Likewise, with their C_4 symmetry, naphthalene, anthracene and pentacene have 3, 4 and 6 six inequivalent carbon atoms respectively. These can be labeled 1 through 3/4/6 as shown in Figure 5.1 and are hereafter referred to as C1, C2 and so on.

Simulated XPS

Figure 5.2 shows the shift in core-level energy for the inequivalent C atoms in naphthalene, anthracene and pentacene molecules (vertical lines[2]); when broadened[3] and added, they generate a pseudo-Voigt profile resulting in a simulated XPS spectra[4]. Since the shifts are all aligned to their own average, it is not very meaningful to consider them individually. Instead, one must compare the shift of core-level energy of a given C atom with that of another.

On doing so, we see that the shifts for atoms C2 and C3 in naphthalene, atoms C3 and C4 in anthracene, and atoms C5 and C6 in pentacene are every close to each other; an indication that they are in similar chemical situation. Upon inspection of the molecular geometries (Figure 5.1) we see that this is indeed the case as all these atoms are peripheral C atoms, each bonded to two sp^2 C atoms and a hydrogen atom. The equal shift (by ~0.3 eV) of core-level energies for atom C2 in anthracene and atoms C2[5] and C4 in pentacene can be similarly explained by the fact they are all, also, in similar chemical situation: bonded with three sp^2 C atoms and *no* hydrogen atom. Carbon, being slightly more electronegative than hydrogen, leads to the greater shift observed for these atoms when compared to the previous case in which the atoms are bonded to two sp^2 C atoms and a hydrogen atom. Further,

1 It is this atom that is represented in a given calculation of the NEXAFS (XPS) simulation procedure by the half core-hole (HCH) (full core-hole (FCH)) pseudopotential file as discussed in Section 7.4.

2 Their length represents the 'weight' of the corresponding atom (given symmetry considerations) when averaging their spectra to form a consolidated the XPS (and later, NEXAFS) spectra.

3 Using 50% Gaussian broadening (standard deviation 0.5 eV) plus 50% Lorentzian broadening (width 0.5 eV). The same scheme is used for broadening all simulated XPS spectra presented in this thesis.

4 Note the inverted X-axis: this in keeping with convention used for experimental spectra plots.

5 The vertical line and the pseudo-Voigt profile for C2 of pentacene is unfortunately not visible in Figure 5.2 as it is immediately below the line/profile for C4.

atom C1 in anthracene and atoms C1 and C3 in pentacene have similar chemical situation (and similar energy shifts): located inwards in the molecule and bonded to two sp^2 C atoms and a hydrogen atom. Last, the atom C1 in pentacene shows an even further shift towards lower binding energy when compared to atom C3. This can be reasoned by its unique central position: with conjugated benzene rings on both ends, the central ring carries a high valence electron density, and thus, harbors a low binding energy.

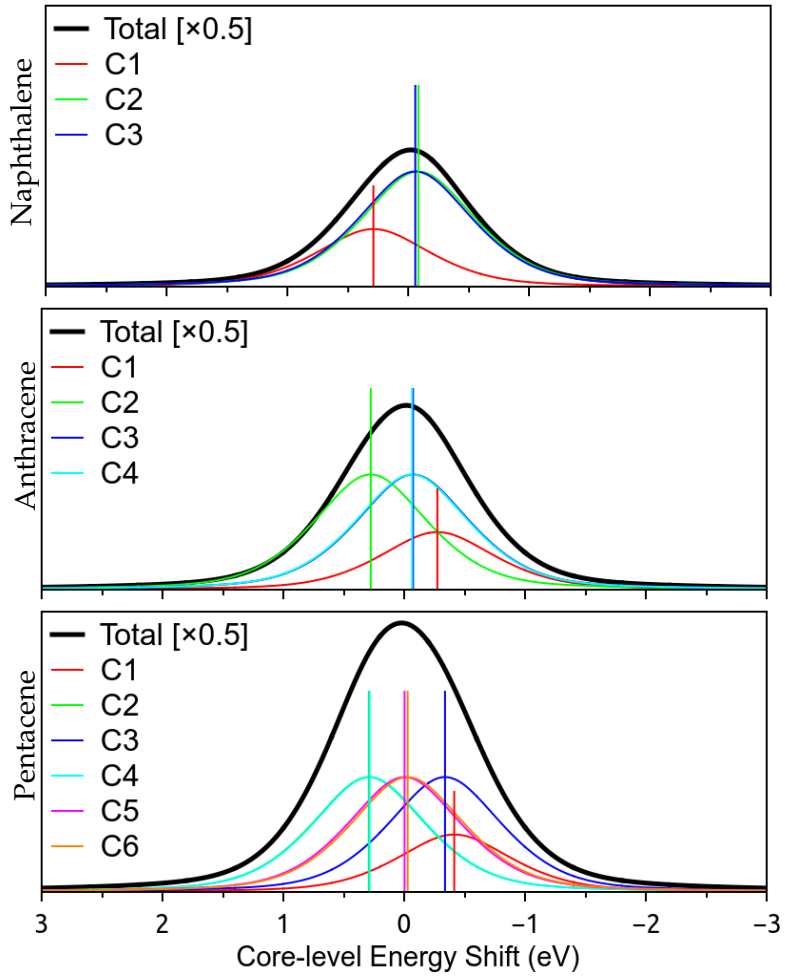

Figure 5.2: Simulated XPS spectra of three acenes: naphthalene, anthracene and pentacene.

Simulated NEXAFS

In order to explain the details associated with a (simulated) NEXAFS spectra, we discuss the example of anthracene. We chose this particularly because it is the hydrogenated cousin of the molecule that forms the backbone in the perfluoroanthracenylaminoalkane thiolate SAM, the case of which we consider in the next chapter.

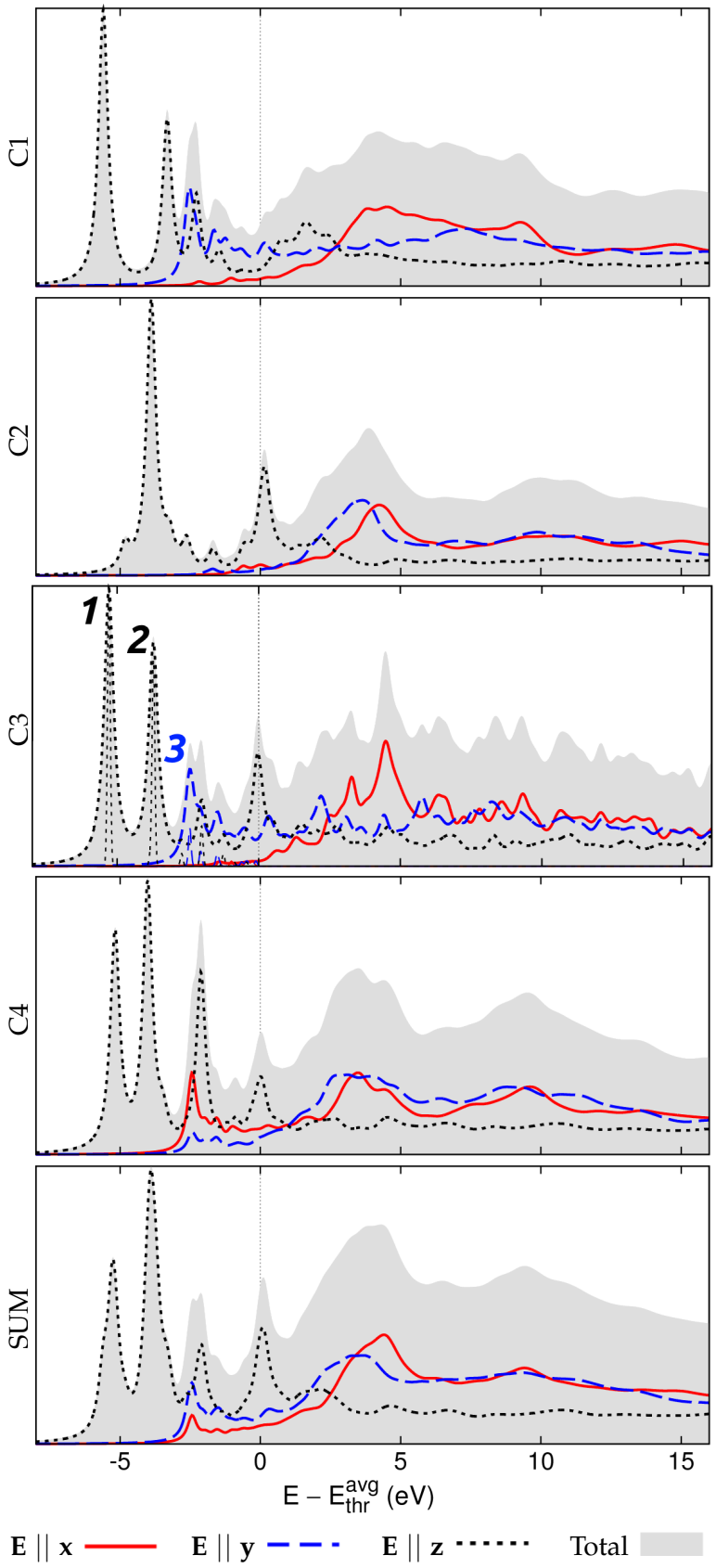

Figure 5.3: Simulated NEXAFS spectra of every inequivalent C atom in anthracene as well their weighted sum.

There are two necessary conditions for significant absorption[6] of an excited (core-level) photoelectron: First, the unoccupied energy level that receives the photoelectron must reside (i.e. have a significant density of state) on the atom which is being excited. Second, the photoexcitation process must follow selection rules (for electric dipole transitions); see Section 7.4.2 for more. Hence, if the incident radiation has its electric field **E** parallel to the x axis or y axis of the system (see Figure 5.1 for definition of the axes), i.e. it has *s* polarization,[7] the absorption probability is high for the $\sigma*$-orbitals while if **E** is parallel to the z axis (*p* polarization) then $s \rightarrow \pi*$ transitions have high probability (see also Table 7.1).

In experiments, the general tactic is to incident radiation at an angle of 55° with respect to the sample so that there is an equal absorption probability for $\pi*$ as well as for $\sigma*$ states and an 'averaged' spectra, that is characteristic of the sample, can be obtained.[8] In simulations, this replicated by totaling[9] the spectra for all three directions, which we show as 'Total' (gray shaded) in all plots (e.g. see Figure 5.3). The spectra for *p* polarization is marked as $\mathbf{E} \parallel \mathbf{z}$ (black-dotted curve) and shows strongest resonances for $s \rightarrow \pi*$ transitions while spectra for *s* polarization is separated into $\mathbf{E} \parallel \mathbf{x}$ (red-solid curve) and an $\mathbf{E} \parallel \mathbf{y}$ (blue-dashed curve).

Figure 5.3 shows the atom-wise (top four panels) as well as the consolidated[10] (bottom panel) NEXAFS spectra of anthracene. As an illustrative example for discussing the spectra associated with excitation of a particular inequivalent atom, we discuss the case of C3 atom.[11] The resonances in its spectra (middle panel in Figure 5.3) reveals that the two lowest lying unoccupied states (LUMO and LUMO+1) that reside on the C3 atom are of $\pi*$ kind (marked as *1* and *2*) while the third state is clearly of $\sigma*$ kind (*3*). These findings can be confirmed by overlaying the spectra with an orbital angular momenta resolved density of states plot, as done for C3. Further, since the composition of each molecular orbital can be discerned in simulations, it possible to do a compositional analysis for each resonance i.e. it is possible to tell which unoccupied molecular orbital(s) of the sample contribute to a given resonance as well as the composition of those molecular orbitals — details that are not always apparent in experiments but are necessary for accurately determining a molecule's geometry from its NEXAFS spectra — bringing forth the need and advantage of doing these simulations.

5.1.3 *Comparison to existing results*

The simulation of spectra of acenes was performed mainly to understand as well as replicate the strategy used in Ref. [38]. Figure 5.4 shows the simulated NEXAFS spectra of benzene, naphthalene, anthracene and pentacene. They are all successful

6 Since absorption is defined in terms of absorption *probability*, what constitutes 'significant' is inherently subjective. Generally this implies an observable resonance in the NEXAFS spectra.

7 Because we *always* define our unit cells such that the plane of the molecule (defined by the plane of its benzene rings) is along the x-y direction, we use can use a consistent notation throughout.

8 The angle is then changed to ~20° as well as 90° to also measure maximum absorption probabilities i.e. the spectra for absorption into account both kinds of states separately; but we do not discuss these cases here.

9 In principle, this should be an average but the absorption probability is in arbitrary units anyway.

10 Similar to the XPS spectra, the simulated NEXAFS spectra for a system is also weighted average obtained by simulating the photoexcitation process of every inequivalent carbon atom.

11 Chosen for no particular reason.

reproductions[12] of the results published in Ref. [38, 39]; in effect, also benchmarking author's compilation of the Quantum Espresso (QE) package.[13]

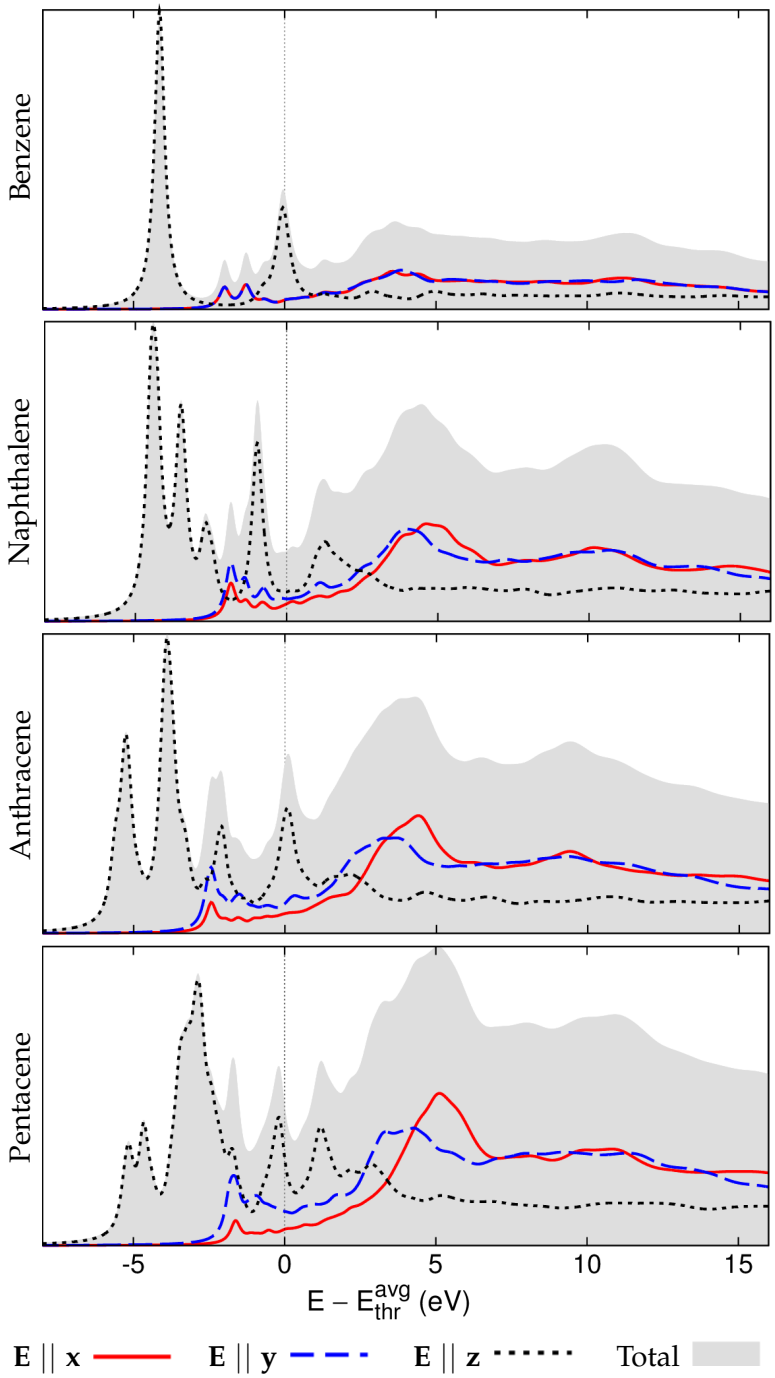

Figure 5.4: Simulated NEXAFS spectra of four acenes: benzene, naphthalene, anthracene and pentacene.

12 Independently generated by the author of this thesis when working with Dr. Guido Fratesi.
13 Version 5.4.0, compiled on Vienna Scientific Cluster 3.

5.2 TERPHENYL AND PERFLUORINATED TERPHENYL

5.2.1 *Geometry of the molecules*

A terphenyl molecule is composed of a central benzene ring that is substituted with two phenyl groups. Depending on the site of substitution of the third phenyl group, three isomers can be readily anticipated: *ortho*-terphenyl, *meta*-terphenyl and *para*-terphenyl (Figure 5.5).

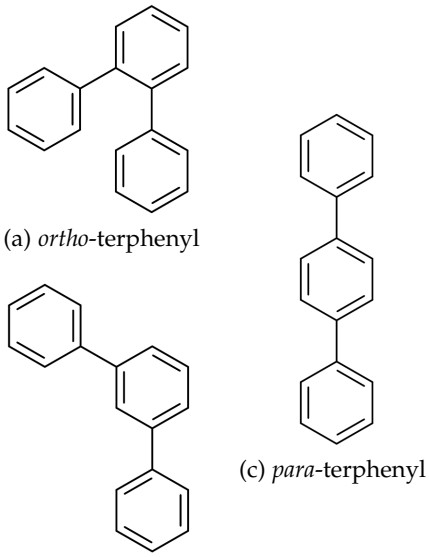

(a) *ortho*-terphenyl

(c) *para*-terphenyl

(b) *meta*-terphenyl

Figure 5.5: Substitutional isomers of terphenyl.

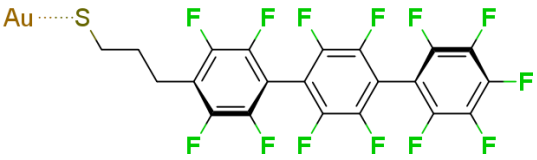

Figure 5.6: Perfluoroterphenyl-substituted alkanethiol that forms a self-assembled monolayer (SAM) on a Au(111) surface, represented here by the gold atom. In our simulations we greatly simplify our target system by replacing the linker (CH_2—CH_2—CH_2—S) with a F atom while removing the metal slab. Doing so makes the remaining portion of the molecule — the 'perfluorinated terphenyl' backbone — C_4 symmetric thus reducing the computational cost significantly.

Our motivation to simulate the core-level spectroscopy of the terphenyl and of the perfluorinated terphenyl molecules stems from their role as the molecular backbone (of the adsorbate) in the SAM we are interested in: *densely-packed* perfluoroterphenyl-substituted alkanethiol SAM on Au(111) (Figure 5.6), as discussed in reference [25]. This helps us severely limit the scope of our further discussion without sacrificing on merit of subsequent results. First, we can focus solely on (perfluorinated) *para*-terphenyl (*p*-terphenyl) isomer as it is the one that forms the backbone. Second, given the possibility of free-rotation of the benzene subunits

(they are held together by sp^3 bonds), infinitely many rotational conformations for a perfluorinated *p*-terphenyl molecule can be envisaged. But because a densely packed SAM implies minimization of intermolecular distances, and buttressed by the fact that there would be significant *intermolecular* fluorine-fluorine repulsion, we can expect the rotational degree of freedom in the adsorbed molecules to be significantly reduced. Third, the adsorbed molecules would also have to accommodate for a rotational barrier originating from *intramolecular* fluorine-fluorine repulsion that would work against complete planarization of the molecule.[14] Therefore, given these restrictions on molecular geometry when it is in the aforementioned SAM, we only study two rotational conformations of the (perfluorinated) terphenyl molecule: one each for the two extremes at which the *intramolecular* fluorine-fluorine repulsion in the SAM is minimized. Both were obtained by relaxing the (perfluorinated) molecule in its gas-phase[15] and are named on the basis of the relative orientation between the planes formed by the peripheral phenyl rings (Figure 5.7). We refer to them as periplanar or *pl* (planes form a torsional angle of 1°) and clinical or *cl* (torsional angle is 79°). Both these conformations are (almost) equally stable in their gas-phase geometry[16], and so we simulated the core-level spectroscopy for both of them.

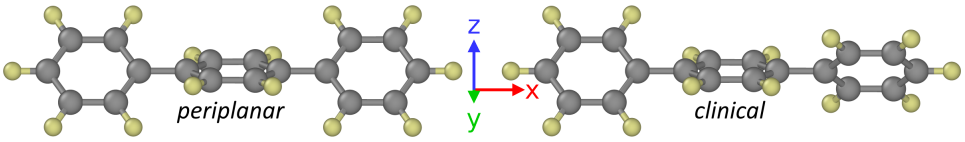

Figure 5.7: The two conformational isomers of *p*-terphenyl that were studied. For instance, the conformation represented in Figure 5.6 is of the *clinical* kind.

5.2.2 *Core-level spectroscopy*

In both the conformations of both the simulated molecules, after accounting for the C_4 symmetry in the molecular geometry, there are six inequivalent carbon atoms. They can be labeled 1 through 6 as shown in Figure 5.8.

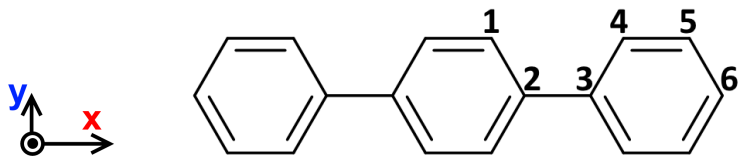

Figure 5.8: The six inequivalent carbon atoms in a (perfluorinated) terphenyl molecule. Hydrogen (fluorine) atoms are not shown. The axes define the directions we refer to in the accompanying text: the long molecular axis is along the **x** direction and while the shorter one is along **y**.

14 Henceforth, the point that we are limiting our discussion to *p*-terphenyl and *p*-F_{14}-terphenyl molecules (while excluding the other two substitutional isomers) is considered implicit in our discussion as well as nomenclature.

15 Starting from different initial geometries, two each for the hydrogenated and the perfluorinated molecule.

16 The hydrogenated terphenyls are 0.001 eV apart in energy while the perfluorinated ones are 0.153 eV apart.

Following the procedure outlined in the methodology chapter (see Sections 7.4.1 and 7.4.2), we simulated X-ray photoelectron spectroscopy (XPS) spectra and near edge X-ray absorption fine structure (NEXAFS) spectra for the *pl*-terphenyl and the *cl*-terphenyl molecules as well as for the *pl*-F_{14}-terphenyl and the *cl*-F_{14}-terphenyl molecules.

Simulated XPS

Figure 5.9 shows the shift in the core-level energies of every inequivalent carbon atom in the *pl*-terphenyl and the *cl*-terphenyl molecules as well as the summed-up simulated XPS spectra. The same for *pl*-F_{14}-terphenyl and the *cl*-F_{14}-terphenyl molecules is shown in Figure 5.10.For the hydrogenated (Figure 5.9) as well as the perfluorinated molecule (Figure 5.10), there are no apparent differences between the simulated spectra of the *periplanar* and the *clinical* conformations. This is well justified because, in spite of the geometric differences, the carbon atoms in both the conformations experience almost identical local-chemical environment.

The same, of course, cannot be said when comparing the XPS spectra of the hydrogenated and the perfluorinated molecules against each other. While the spectra from the hydrogenated conformations sports a single peak, the spectra from the perfluorinated molecules has two peaks. The origin of this difference lies in the high electronegativity of the fluorine atoms (that are bonded with the carbon atoms): Fluorine being strongly electronegative pulls onto the valence electrons that are shared between it and the carbon atom and, therefore, increases the effective nuclear charge on the carbon atom it is bonded to. This makes the process of exciting a core-level 1*s* electron more expensive in case of a fluorine bonded carbon atom than in case of a hydrogen bonded carbon atom. Because, in perfluorinated terphenyl molecules, two inequivalent atoms (here labeled as C2 and C3) are not bonded to a fluorine atom while the others are, there is an overall splitting (of ca. 1.5 eV) in its summed-up XPS spectra.

Simulated NEXAFS

In keeping with what we saw for the XPS spectra, we see that NEXAFS spectra for both the conformational isomers of the terphenyl molecule is essentially the same (Figure 5.11). However, unlike the XPS spectra, the NEXAFS spectra of the perfluorinated terphenyl molecule *does* differ slightly for each of the two conformations (Figure 5.12). The highest resonance in the spectra from *pl*-F_{14}-terphenyl (at ~ -6 eV) is split into two peaks while the spectra from the *cl*-F_{14}-terphenyl molecule is not, albeit it is equally broad. The split, and its lack thereof, in the spectra of the two conformational isomers is, in fact, a perfect example of the sensitivity of NEXAFS as a technique towards the geometry of the analyte; a feature that becomes even more apparent when studying the experiment spectrum in light of simulated ones.

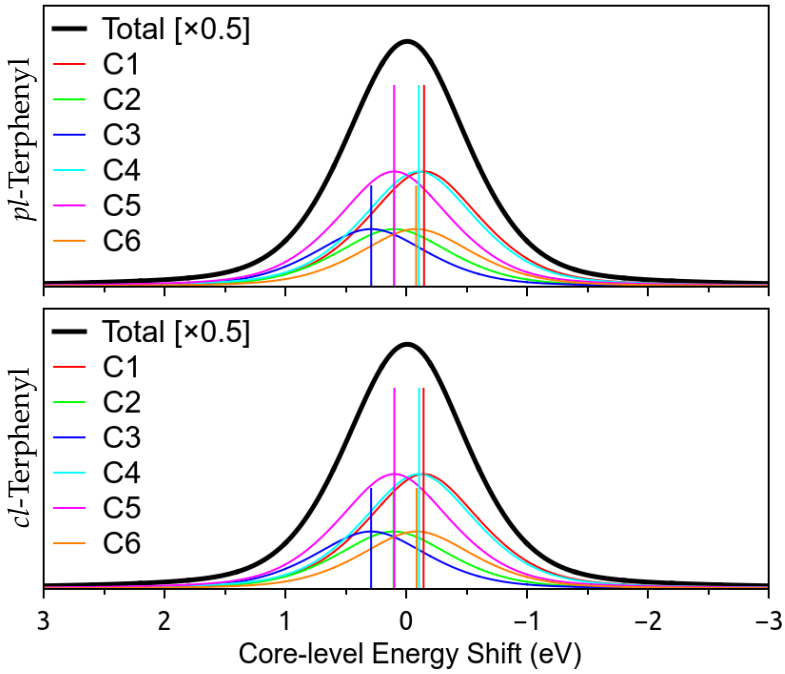

Figure 5.9: Simulated XPS spectra of the two conformations of terphenyl.

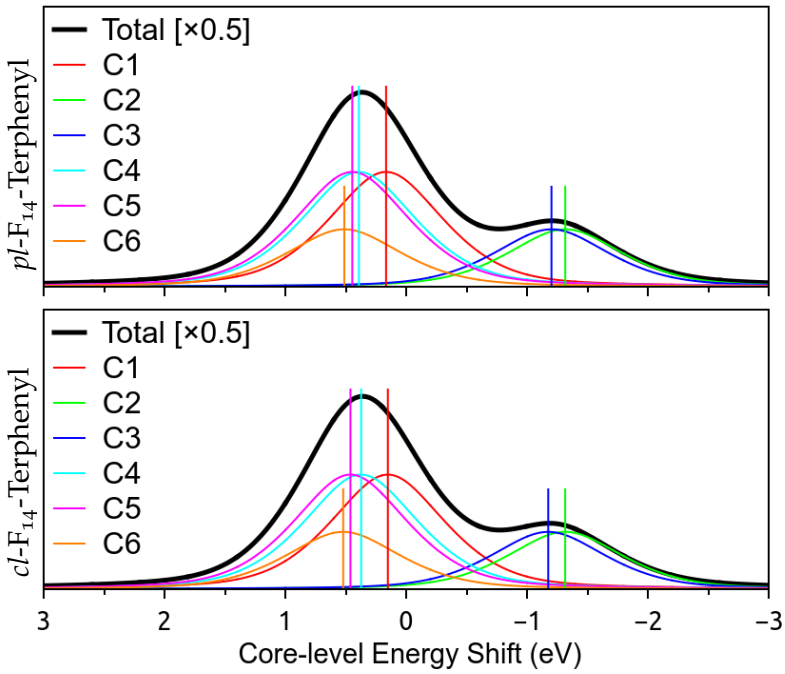

Figure 5.10: Simulated XPS spectra of the two conformations of perfluorinated terphenyl.

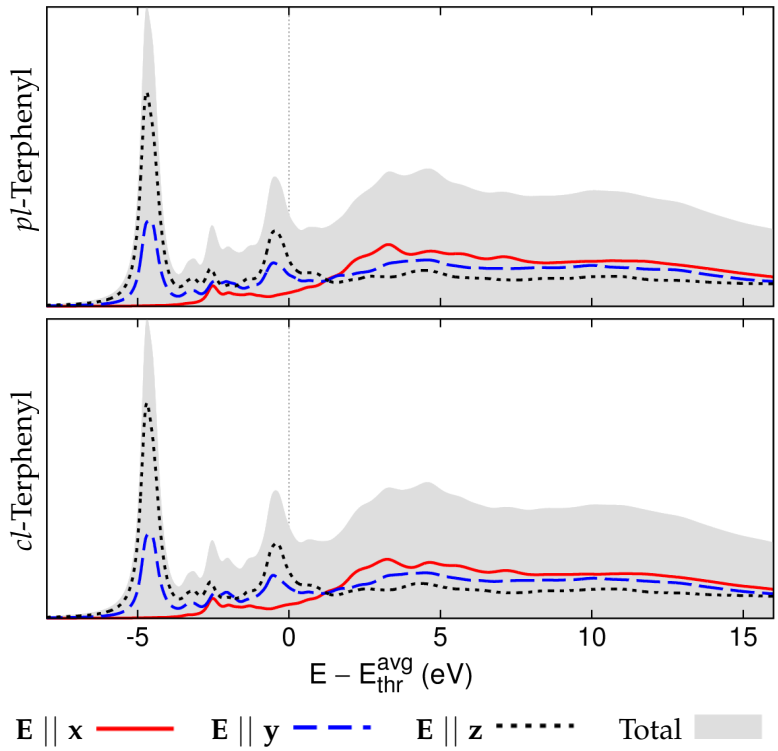

Figure 5.11: Simulated NEXAFS spectra of the two conformations of terphenyl.

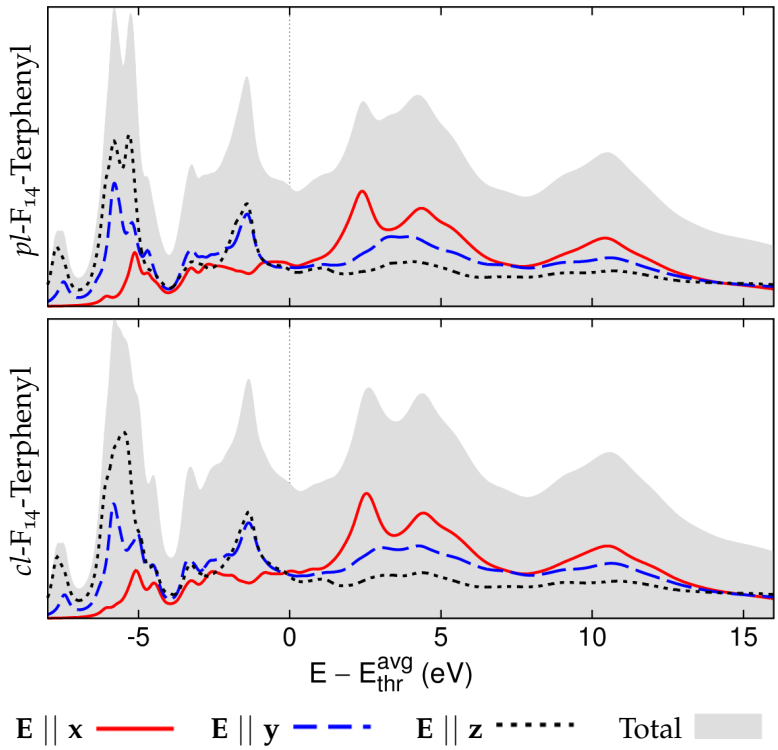

Figure 5.12: Simulated NEXAFS spectra of the two conformations of perfluorinated terphenyl.

5.2.3 *Comparability with experiments*

Figure 5.13 shows the simulated NEXAFS spectra of a terphenyl molecule and the experimental NEXAFS spectra [40] of a *p*-thioterphenyl molecule[17] *adsorbed* on Au(111) as a self-assembled monolayer (SAM). The x-axis (photon energy) of the simulated spectra had to been scaled down to 90% of the original in order to achieve the relatively good agreement that we observe here. With this correction, all the major resonances of the experimental spectra are all recovered in the simulated one.

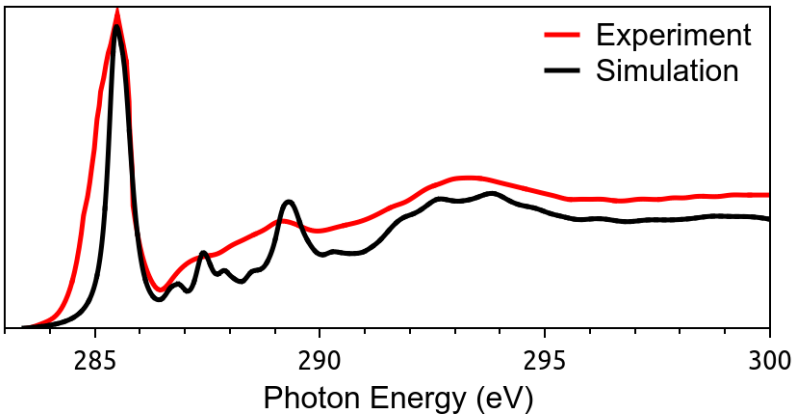

Figure 5.13: Simulated NEXAFS spectrum of *cl*-terphenyl and experimental NEXAFS spectrum of *para*-thioterphenyl SAM on Au(111) [40].

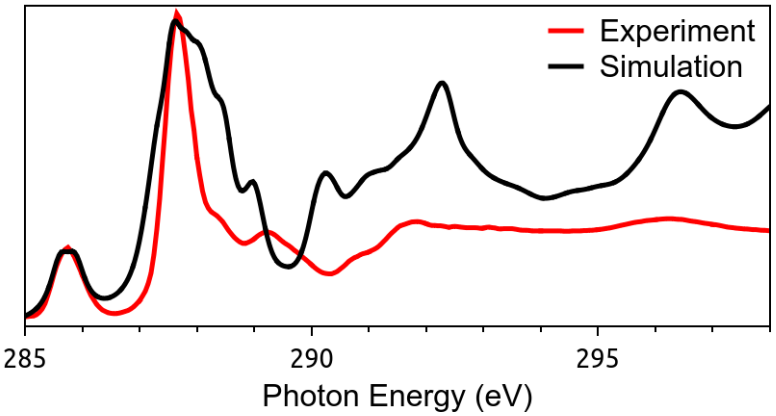

Figure 5.14: Simulated NEXAFS spectrum of *cl*-F_{14}-terphenyl and experimental NEXAFS spectrum of perfluoroterphenyl-substituted alkanethiol SAM on Au(111) [25].

Figure 5.14 shows the simulated NEXAFS spectra of a *cl*-F_{14}-terphenyl molecule in comparison with the experimental NEXAFS spectra [25] of a perfluoroterphenyl-substituted alkanethiol SAM on Au(111). The lack of a split in the highest resonance, against what was observed for the *pl*-F_{14}-terphenyl conformation, gives credence to the fact that the experimentally investigated SAM was formed of molecules

17 Note that in this case there is no alkyl chain (linker) between the sulfur atom (anchor) and the terphenyl molecule (backbone).

in the *clinical* conformation. This is, in fact, also the conclusion that was reached in the experimental study [25] where they suggest torsional angles of $\pm 58°$ for the densely packed SAM against the theoretical value of $\pm 40°$ that we calculated (for a gas phase molecule). In spite of this, the agreement between the simulated and experimental spectra is visibly worse (with exception of the resonance at ~285.8 eV). As it turns out, all perfluorinated systems have a generally poor correspondence when simulated with the strategy that we use here. We address this issue in the next chapter.

6

CORE-LEVEL SPECTROSCOPY OF FLUORINATED SYSTEMS

6.1 PERFLUORINATED ACENES

6.1.1 *Core-level spectroscopy*

Analogous to our simulation of core-level spectroscopy techniques for the acene family, we simulated the XPS and NEXAFS spectra of their perfluorinated acenes. For record, we have presented the XPS spectra at the end of this chapter, on page 82. Similar to the case of fluorination of the terphenyl molecule (page 72), fluorination of the acenes also leads to increased shifts in their core-level energies which, again, is attributable to the higher electronegativity of the fluorine atom.

While a thorough case-by-case analysis of NEXAFS spectra of all the perfluorinated acenes is beyond the scope of this work, we have presented also their simulated spectra at the end of this chapter (page 83). We note that for the case of perfluorinated naphthalene, there is relatively good correspondence of the simulated spectra (especially for the unoccupied levels that lie below the vacuum level), with an experimental study [117] *if* only the spectra from p polarized incident radiation is considered. The same is true for pentacene but there also the energy separation of the eigenvalues of the (simulated) unoccupied $\pi*$ levels is somewhat 'off', leading to a poor correspondence with the experiment [75]. To understand their origin better, we now discuss probable reasons for these incongruities in light of a specific system.

6.2 POSSIBLE REASONS FOR INCONGRUITIES

As the main motivation (since it was this result that triggered all subsequent investigations) we present the spectra of the perfluorinated anthracene molecule which shows (Figure 6.1) a rather poor congruence with the spectra of our target SAM (perfluoroanthracenylaminoalkane thiolate on Au(111) [163]), especially at higher photon energies.

On analysis, and by comparing to the detailed simulated spectra in Figure 6.2, the following points become immediately apparent:

1. The resonance *2* ($\pi*$) in the simulated spectra is reduced to a shoulder in the experiment.

2. The shoulder *1* ($\pi*$) and the resonance *3* ($\pi*$) show a rather good agreement.

3. The resonance *4* ($\pi*+\sigma*$) that is noted in the simulation and is around twice the intensity of resonance *3* is most likely spurious.

4. The experimentally observed resonance *5* is not reproduced in the present simulation at all.

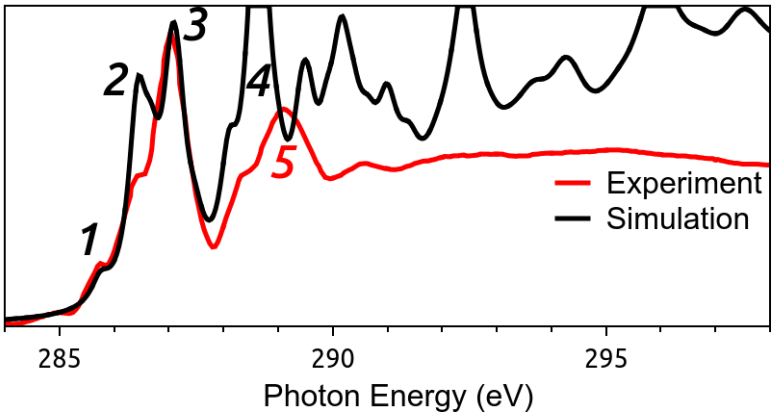

Figure 6.1: Simulated NEXAFS spectrum of perfluorinated anthracene molecule in gas phase and experimental NEXAFS spectrum of perfluoroanthracenylaminoalkane thiolate SAM on Au(111) [163].

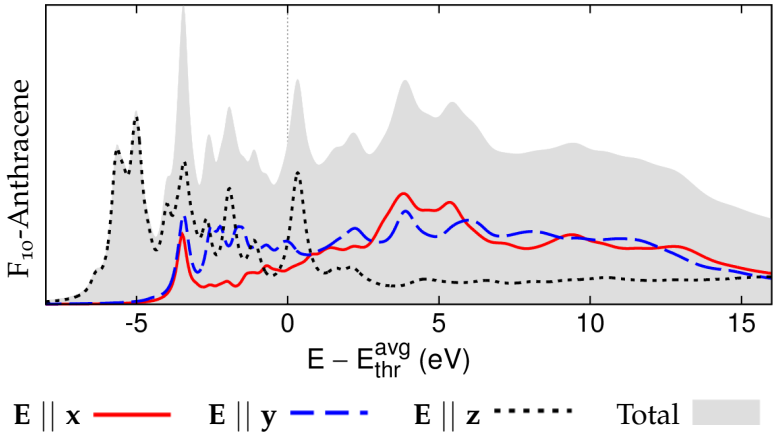

Figure 6.2: Simulated NEXAFS spectra of F_{10}-anthracene.

6.2.1 *The alkyl linker*

As a first attempt to eliminate the discrepancies, we simulated the NEXAFS spectra of the entire molecule, including the alkyl linker, that constitutes the SAM, with the sulfur atom bonded to a hydrogen atom (instead of gold). Unfortunately this lead an even poorer congruence between the experimental and the theoretical results. We note that resonance 2 becomes grows further in strength if the spectra is fit such that the other two major $\pi*$ resonances (*1* and *3*) continue agree with the experiment.

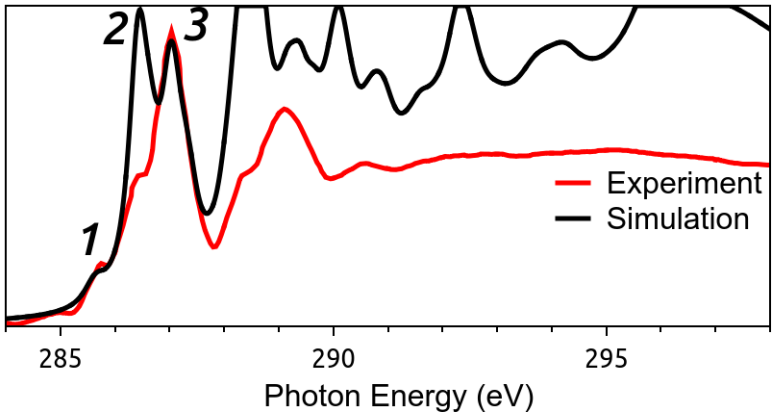

Figure 6.3: Simulated NEXAFS spectra of perfluoroanthracenylaminoalkane (H—C_3H_6—NH—(F_{14}-Anthracene) in gas phase against the experimental NEXAFS spectrum of perfluoroanthracenylaminoalkane thiolate when it is adsorbed as a SAM on Au(111). Only the fourteen carbon atoms that from the backbone are included for the simulated spectra (i.e. the three C atoms on the linker are not); however, the effect of the linker is still observed in the simulated spectrum.

6.2.2 *Presence of the metal slab*

In order to simulate the presence of the metal slab we had to simulate the complete adsorption procedure. This was done as a three step process:

1. From (high resolution XPS) experiment [163] we know that the perfluoroanthracenylaminoalkane thiolate SAM grows in a densely packed fashion with the molecules being upright standing and having a footprint of ~0.27 nm². Therefore we used a supercell with an area of 29.95 Å²[1] and introduced *only* the (hydrogen terminated) adsorbate molecule in it. Since the molecule itself is around 5.5 Å broad and the longest side of the supercell we used was 5.88 Å, the 'densely packed' resulting system was, in principle, a molecular crystal. Using FHI-aims with the PBE functional and 'tight' settings, allowed the molecule (molecular crystal) to undergo geometry relaxation so as to minimizes the forces below 0.01 eV/Å per atom.

2. We then also introduced a six atomic-layer thick Au(111) slab into the super cell, immediately below the alkyl linker of the molecule while removing a the hydrogen termination that we added to the sulfur atom. We then allowed the system to relax further which brought the sulfur in close vicinity of the gold slab (Au—S distance=~2.5 Å; with S located on bridge site). The resulting geometry, is shown in Figure 6.4b. While the usual procedure for simulating upright standing SAMs is more involved, particularly because there is a high probability of having a herringbone structure, we wanted to have a cheaply created test system purely to test the effect of a metal slab.

1 Constrained by the fact the we planned to later introduce a gold slab in exactly same supercell.

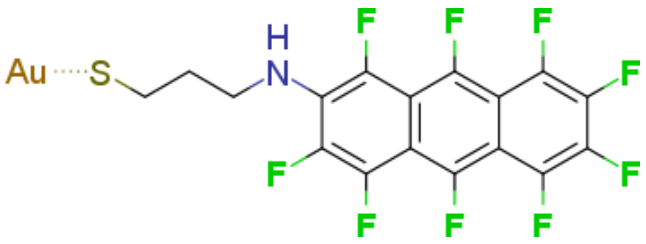

(a) Structural formula.

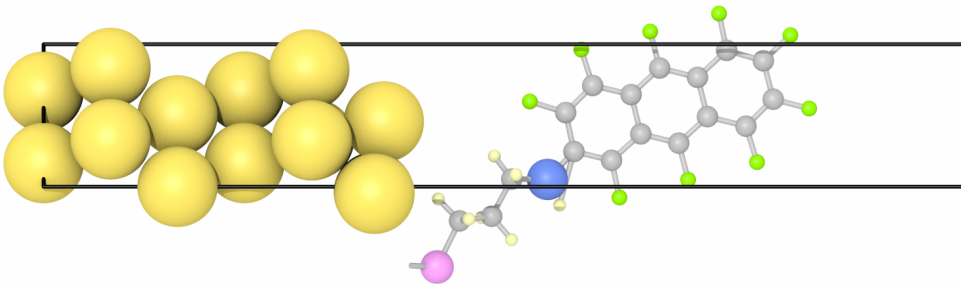

(b) In adsorbed geometry on Au(111), inside a supercell.

Figure 6.4: Perfluoroanthracenylaminoalkane thiolate that adsorbs on Au(111) surface to form a densely packed self-assembled monolayer (SAM) on a Au(111) surface. In our simulations we simplify our target system by ignoring possible excitations in the 'alkyl' linker (HN—CH_2—CH_2—CH_2—S). Nevertheless, inclusion of the metal slab meant that molecular symmetry was lost and the simulated NEXAFS spectra is an averaged contributions of fourteen carbon atoms.

3. QE makes use of periodic boundary condition. Therefore simulating photoexcitation of one atom in the supercell implies, in principle, doing the same in all periodic images of supercell. This is, of course, unnatural. The only existing method to minimize this spurious consequence of using periodic boundary condition is to use a supercell with a large lateral area. However, this risks making the supercell too big to simulate efficiently. As a compromise, we only *doubled* the supercell in the lateral direction, such that it had four molecules in it of which only one was excited in simulations.

Following this, we tried to follow the standard procedure for simulating the NEXAFS spectra. However, we had troubles in converging the calculations with a full core-hole (FCH), and therefore could not obtain core-level energy shifts for this system. As an alternative, we chose to use the core-level energy shifts that were obtained during the simulation of gas-phase NEXAFS spectra.

Figure 6.5 shows the simulated NEXAFS spectra for the perfluoroanthracenylaminoalkane thiolate adsorbed on Au(111) superimposed on that from the experiment. We see a really good agreement between the two between the energy range of 285 eV and 287.5 eV. On the other hand, we can see that the spurious feature *4* discussed in the simulated spectra of the gas phase molecule (Figure 6.1) still exists in the 'total' simulated spectra. However, if only take into consideration the spectra due to *p* polarized light (i.e. the spectra that corresponds to $\mathbf{E} \parallel \mathbf{z}$), then we see immediately see a considerably better agreement for an increased energy range — upto ~288.5 eV.

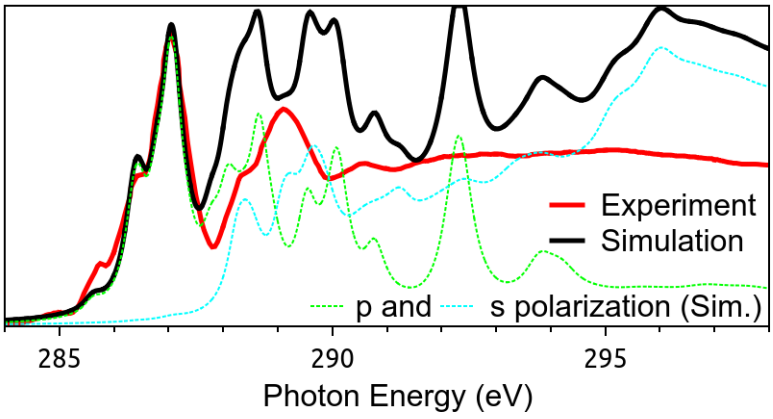

Figure 6.5: Simulated NEXAFS spectra and experimental NEXAFS spectrum [163] of perfluoroanthracenylaminoalkane thiolate SAM on Au(111).

Drawing from this, and from earlier observations about the generally better agreement of the simulated $\mathbf{E} \parallel \mathbf{z}$ spectra with *totality* of the experimental spectra at lower photon energy ranges, we hypothesized that it is the use of PBE functional (which has its spurious self-interaction error) that might lead to wrong placement of the $\sigma*$ energy levels in the spectra. Therefore, we simulated the perfluorinated anthracene molecule using the Hartree-Fock (HF) method (which does not suffer from the error) as well. We found that the the lowest lying $\sigma*$ state in the HF is place at 4.6 eV above the $\pi*$ LUMO while in when using DFT+PBE, the same state is placed at 2.2 eV.

6.2.3 *Comparison with experiment*

Drawing from this, we decided to shift *only* the *s* polarization spectra, as it is, by 2.4 eV towards higher photon energy and then scaling the energy axis (of the simulated spectra) to 1.3 times of the original. This resulted in an (acceptable) overall congruity between the experiment and the simulation (Figure 6.6).

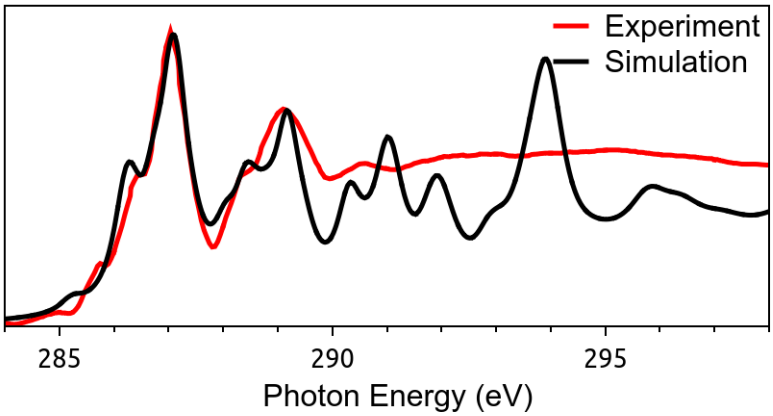

Figure 6.6: *Shifted* simulated NEXAFS spectrum and experimental NEXAFS spectrum [163] of perfluoroanthracenylaminoalkane thiolate SAM on Au(111).

6.3 CONCLUSION

While we did achieve a good level of correspondence between theory and experiment for the last system discussed here, a relatively safe strategy that can handle NEXAFS simulation of a multitude of experimental systems is a work under progress. Moreover, the present version of strategy that we use, of simulating the complete SAM with the metal slab is far from computationally efficient and needs to be improved. Finally, the findings concerning the limitations imposed by using DFT+PBE must be taken into account before further investigations.

6.4 RELATED RESULTS

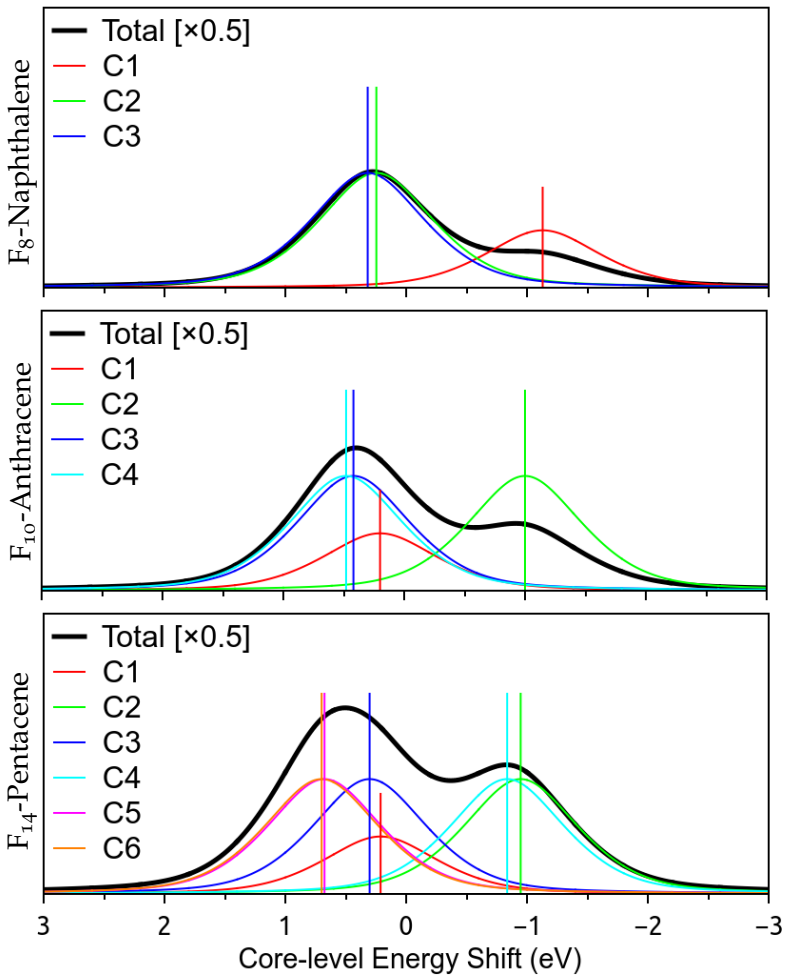

Figure 6.7: Simulated XPS spectra of three perfluorinated Acenes: F_8-naphthalene, F_{10}-anthracene and F_{14}-pentacene.

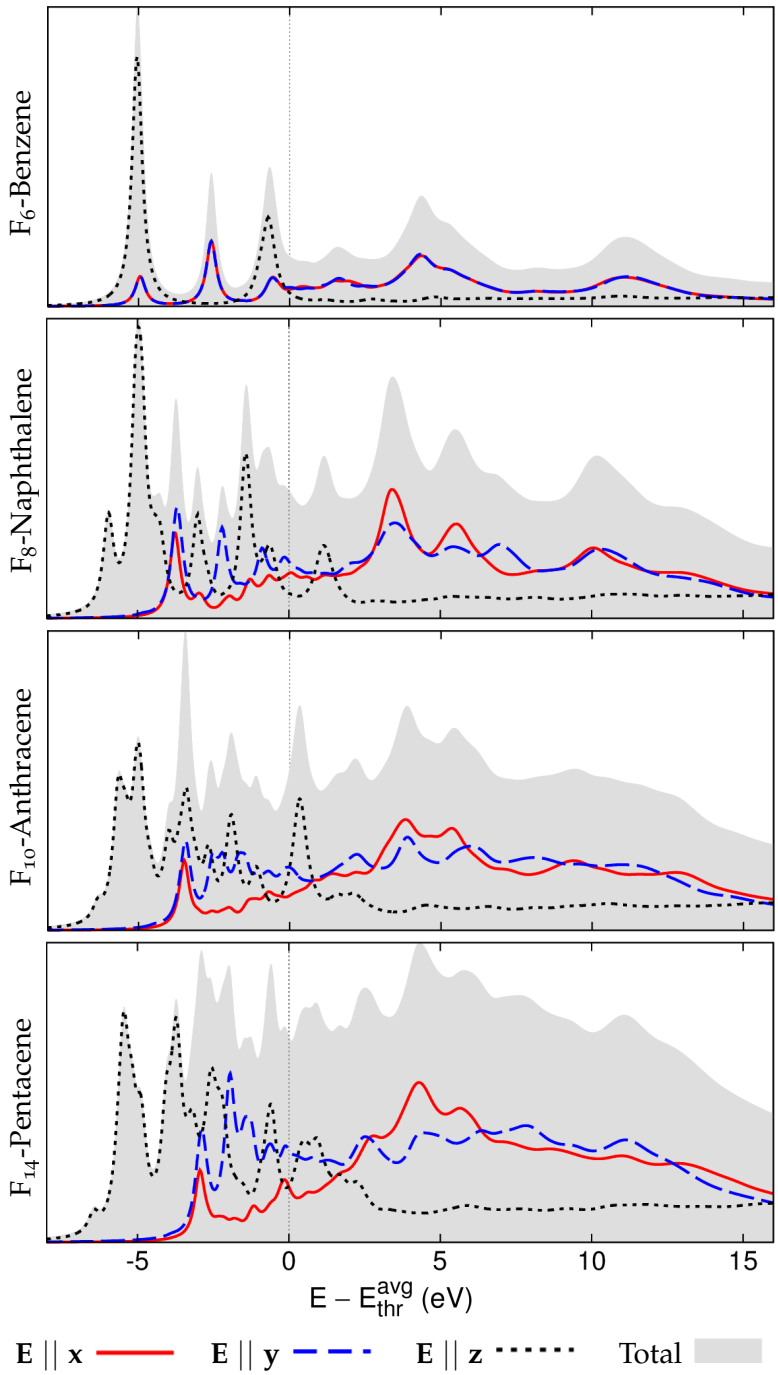

Figure 6.8: Simulated NEXAFS spectra of four perfluorinated acenes: F_6-benzene, F_8-naphthalene, F_{10}-anthracene and F_{14}-pentacene.

Part IV

METHODOLOGY

If you don't like the answer, change the question.

— Richard M. Martin
in *Electronic Structure: Basic Theory and Practical Methods*

7

METHODOLOGY

7.1 DENSITY FUNCTIONAL THEORY

7.1.1 *Hamiltonian for nuclei and electrons*

This section is largely adapted from the discussion pertaining DFT in Ref. [98].

The development of quantum theory in the early part of the twentieth century laid a solid foundation for understanding atoms and molecules. However, employing the theory to understand optoelectronic properties of a material, even at nanoscale, invariably involves numerically solving the time-independent Schrödinger equation,

$$\hat{H}\Psi = E\Psi \tag{7.1}$$

for a many-particle wavefunction Ψ. Solving this eigenvalue problem is, in fact, the goal of all electronic structure methods.

The key is to define and then, if possible, simplify the Hamiltonian, $\hat{H}$. A reasonably simple[1] Hamiltonian for a many-body interacting system with N electrons and M nuclei can be written as

$$\begin{aligned}\hat{H} = &-\frac{\hbar^2}{2m_e}\sum_{i=1}^{N}\nabla_i^2 - \frac{\hbar^2}{2}\sum_{I=1}^{M}\frac{1}{M_I}\nabla_I^2 \\ &- \sum_{i=1}^{N}\sum_{I=1}^{M}\frac{Z_I e^2}{|\mathbf{r}_i - \mathbf{R}_I|} + \frac{1}{2}\sum_{i=1}^{N}\sum_{\substack{j=1\\ j\neq i}}^{N}\frac{e^2}{|\mathbf{r}_i - \mathbf{r}_j|} + \frac{1}{2}\sum_{I=1}^{M}\sum_{\substack{J=1\\ J\neq I}}^{M}\frac{Z_I Z_J e^2}{|\mathbf{R}_I - \mathbf{R}_J|}\end{aligned} \tag{7.2}$$

where $\mathbf{r}_i$ and $\mathbf{R}_I$ (the position vectors of the electrons and the nuclei respectively) are the parameters of the wavefunction $\Psi(\mathbf{r}_1, \ldots, \mathbf{r}_N, \mathbf{R}_1, \ldots, \mathbf{R}_M)$ on which the Hamiltonian acts. The first two terms of Equation 7.2 encapsulate the kinetic energy of the electrons and of the nuclei respectively. The remaining three terms describe the attractive electrons-nuclei, the repulsive electron-electron and the repulsive internuclear interactions respectively.

The first simplification that we can make is the Born-Oppenheimer approximation [16]. Given the difference in mass of an electron and that of any of the nuclei involved, it can be assumed that the motion of these particles occur on different time-scales and, therefore, the effects (on the Hamiltonian) that emanate from the motion of electrons can be separated from those that are due to the motion of nuclei. In practice, this means that as far as the Hamiltonian for electronic structure is concerned, one can consider all the nuclei to clamped in space. Hence, one can set the nuclear kinetic energy term to zero, treat the repulsive internuclear

1 We ignore relativistic effects, magnetic fields and quantum electrodynamics.

(electrostatic) interaction term as a constant,[2] and subsume the electrons-nuclei interactions into an external potential energy term $\hat{V}_{ext}$ without influencing the description of electrons in the system. Therefore, the Equation 7.2 is rewritten as

$$\hat{H} = \hat{T} + \hat{V}_{ext} + \hat{V}_{int} \tag{7.3}$$

where $\hat{T}$ is the term representing kinetic energy of the electrons, $\hat{V}_{ext}$ holds information about the external potential energy, and $\hat{V}_{int}$ accounts for the repulsive electron-electron interactions.

7.1.2 *Hohenberg-Kohn theorems*

Having taken care of individual nuclei, the wavefunction for the Hamiltonian can be rewritten as $\Psi(\mathbf{r}_1, \ldots, \mathbf{r}_N)$. However, Ψ is still a complicated N-electron wavefunction that explicitly depends on the coordinates of all the electrons. A solution to this problem, put forth by Hohenberg and Kohn in 1964 [63], came in the form of two celebrated theorems that from the basis of density functional theory (DFT). As the name suggests, the theorems replace the N-electron wavefunction with an *electron density*

$$n(\mathbf{r}) \geq 0, \text{ such that } \int d\mathbf{r}\, n(\mathbf{r}) = N, \tag{7.4}$$

which is a scalar function that depends simply on position $\mathbf{r}$, thus making the problem tractable. Rigorously speaking, the theorems are:

THEOREM I For any system of interacting particles in an external potential $V_{ext}(\mathbf{r})$, this potential is determined uniquely, except for a constant, by the ground state particle density $n_0(\mathbf{r})$.

THEOREM II It is possible to define a *universal* functional for energy $E[n(\mathbf{r})]$ that is valid for any external potential $V_{ext}(\mathbf{r})$. Further, for any particular $V_{ext}(\mathbf{r})$, the exact ground state energy E_0 of the system is the global minimum value of $E[n(\mathbf{r})]$. The density $n(\mathbf{r})$ that yields E_0 is the exact ground state density $n_0(\mathbf{r})$.

Theorem **I** implies that the external potential $V_{ext}(\mathbf{r})$ that influences a system of interacting particles can be determined (up to a constant) from the ground state density $n_0(\mathbf{r})$ of these particles. Theorem **II** describes how this ground state density can be determined. Its first part states that, in principle, it is possible to partition $E[n(\mathbf{r})]$ into two components, one which is independent of the external potential and another which is not. Expressly, it is possible to write

$$E[n(\mathbf{r})] = F_{HK}[n(\mathbf{r})] + \int d\mathbf{r}\, V_{ext}(\mathbf{r}) n(\mathbf{r}) \tag{7.5}$$

where the second term describes the response of the electron density to external potential while F_{HK} is 'Hohenberg-Kohn' functional that incorporates all internal energies (kinetic and potential) of the interacting electrons and is thus defined as

$$F_{HK}[n(\mathbf{r})] = T[n(\mathbf{r})] + E_{int}[n(\mathbf{r})]. \tag{7.6}$$

2 It is a significant term but is ignored while solving the Hamiltonian and is only re-included in the end.

Being independent of external potential, F_{HK} is the aforementioned universal functional. The second part of theorem **II** states that one can find the ground state energy of a given system by minimizing[3] $E[n(\mathbf{r})]$ where the corresponding electron density is termed as the ground state electron density $n_0(\mathbf{r})$.

The two theorems, therefore, give an alternate *electron density dependent* framework for determining properties of a system. If a valid form of F_{HK} is known, it can be used to ascertain E_0 and n_0 for any given V_{ext} (Theorem **II**). The Hamiltonian is then uniquely determined (except for a constant) by the ground state electron density n_0 (Theorem **I**). From here, in principle, the wavefunction for any state in the system can be solved by employing the same Hamiltonian in the Schrödinger equation. Therefore all properties of the system are completely determined once $n_0(\mathbf{r})$ is known.

Whereas the Hohenberg-Kohn theorems reduce the dimensionality of the many-body problem, they suggest no explicit mechanism for constructing a reasonable F_{HK} functional that can account for electron-electron interactions.

7.1.3 *Kohn-Sham ansatz*

In a paper that followed in 1965, Kohn and Sham suggested a solution for the electron-electron interaction problem [78]. Their ansatz proposed that an equivalent *fictitious* system built with 'non-interacting' electrons can be used in place of a *physical* fully-interacting system as long as both systems have same ground state electron density; while the complicated interaction terms are packaged into a separate electron density dependent exchange-correlation (xc) functional. As a result, we can rewrite Equation 7.6 as

$$F_{HK}[n(\mathbf{r})] = T_S[n(\mathbf{r})] + E_{Hartree}[n(\mathbf{r})] + E_{xc}[n(\mathbf{r})] \tag{7.7}$$

where T_S is the kinetic energy functional for our fictitious system having non-interacting electrons and $E_{Hartree}$ is the classical interaction of these electrons with themselves, described using the following Coulombic term

$$E_{Hartree}[n(\mathbf{r})] = \frac{1}{2}\int d\mathbf{r}d\mathbf{r}' \frac{n(\mathbf{r})n(\mathbf{r}')}{|\mathbf{r}-\mathbf{r}'|}. \tag{7.8}$$

$E_{xc}[n(\mathbf{r})]$, on the other hand, is a complicated term containing the (kinetic as well as potential) energy contributions due to many-electron interactions, as can be determined by rearranging Equations 7.6 and 7.7 as follows

$$\begin{aligned} E_{xc}[n(\mathbf{r})] &= F_{HK}[n(\mathbf{r})] - (T_S[n(\mathbf{r})] + E_{Hartree}[n(\mathbf{r})]) \\ &= T[n(\mathbf{r})] + E_{int}[n(\mathbf{r})] - (T_S[n(\mathbf{r})] + E_{Hartree}[n(\mathbf{r})]) \\ &= \underbrace{T[n(\mathbf{r})] - T_S[n(\mathbf{r})]}_{\text{kinetic term}} + \underbrace{E_{int}[n(\mathbf{r})] - E_{Hartree}[n(\mathbf{r})]}_{\text{potential term}} \end{aligned} \tag{7.9}$$

The beauty of the Kohn-Sham ansatz is that it provides a set of equations that is solvable: As the fictitious system is composed of non-interacting electrons, one

3 Generally accomplished by using the variational principle.

ends up with a *solvable* time-independent Schrödinger equation for each of them. These equations can be written as follows

$$\left[-\frac{\hbar^2}{2m_e}\nabla^2 + V_{KS}(\mathbf{r})\right]\psi_i(\mathbf{r}) = \varepsilon_i\psi_i(\mathbf{r}) \tag{7.10}$$

where V_{KS} is the so-called Kohn-Sham potential that encapsulates all non-kinetic non-interacting energy terms as well as the exchange-correlation energy. It is represented as

$$\begin{aligned} V_{KS}(\mathbf{r}) &= V_{ext}(\mathbf{r}) + \frac{\delta E_{Hartree}}{\delta n(\mathbf{r})} + \frac{\delta E_{xc}[n(\mathbf{r})]}{\delta n(\mathbf{r})} \\ &= V_{ext}(\mathbf{r}) + V_{Hartree}(\mathbf{r}) + V_{xc}(\mathbf{r}). \end{aligned} \tag{7.11}$$

Equations 7.10 and 7.11 are together known as the Kohn-Sham equations which describe the fictitious system (made of *Kohn-Sham (KS) orbitals* ψ_i and having *KS energy eigenvalues* ε_i) that is linked to the physical system via the ground state electron density $n(\mathbf{r})$ in the following manner

$$n(\mathbf{r}) = \sum_i^N |\psi_i(\mathbf{r})|^2 . \tag{7.12}$$

The Kohn-Sham equations must be solved self-consistently (as they involve coupled quantities, $n(\mathbf{r})$ and $V_{KS}(\mathbf{r})$) in order to minimize the total energy of the system. The approach here is to use a reasonable guess for $n(\mathbf{r})$, say n_i, and solve it for V_{KS} which we label V_i. Then, a new density n_{i+1} is constructed using the potential V_i, followed by using the density n_{i+1} to arrive at a new potential V_{i+1}. This so called 'self-consistent field' (SCF) cycle of $n_i \rightarrow V_i \rightsquigarrow n_{i+1} \rightarrow V_{i+1} \rightsquigarrow n_{i+2} \rightarrow V_{i+2} \cdots \rightsquigarrow n_{converged} \rightarrow V_{converged}$ is continued until predefined convergence criteria are met. Generally these criteria are defined in terms of change in total energy, change in electron density or change in the sum of eigenvalues or a combination of these.

Eigenvalues derived from the Kohn-Sham fictitious system do not hold much physical meaning, with one exception: Since the ground state electron density of the fictitious system is constructed in order model the corresponding interacting system, (only) the first ionization energy of a physical system can be simply identified as the negative of energy eigenvalue of the highest occupied KS orbital i.e. $-\varepsilon_{HOMO}$ in the corresponding fictitious system [89].[4] Even though proposed by Levy *et al.*, the theorem is now widely known as the 'Koopmans' theorem in DFT' since the original Koopmans' theorem [79], proposed in context of the Hartree-Fock approximation [37], is essentially homologous to this one.

7.1.4 *Exchange-correlation functionals*

While the Kohn-Sham ansatz results in a tractable set of equations, the Pandora's box of exchange-correlation functional $E_{xc}[n(\mathbf{r})]$ that was introduced in Equation 7.7 stills needs to be tackled. As a matter of fact, an exact form the functional is

4 This is only true if an 'exact' xc functional is known, which if fact is not; see Section 7.1.4.

yet unknown and is a topic of continued research. Nevertheless, some relatively simple approximations for the xc functional were developed early on and have since been very successful, leading to the widespread use and acceptance of DFT. The functional can be represented as

$$E_{xc}[n(\mathbf{r})] = \int d\mathbf{r}\, n(\mathbf{r})\epsilon_{xc}(n(\mathbf{r}), \mathbf{r}) \tag{7.13}$$

where ϵ_{xc} is the xc energy density at a given point $\mathbf{r}$ (i.e. it is *local* in character). As a first step, one can use the Local Density Approximation (LDA) that equates $\epsilon_{xc}(n(\mathbf{r}), \mathbf{r})$ in Equation 7.13 with $\epsilon_{xc}^{heg}(n(\mathbf{r}'), \mathbf{r}')$ where the latter term is the xc energy density for an auxiliary homogeneous electron gas which has an electron density $n(\mathbf{r}')$ at $\mathbf{r}'$ that is identical to $n(\mathbf{r})$ at $\mathbf{r}$. The Generalized Gradient Approximation (GGA) further builds on this and includes not only the local electron density but also its gradient i.e. it uses $\epsilon_{xc}(n(\mathbf{r}'), \nabla n(\mathbf{r}'), \mathbf{r}')$, thus, giving better results for systems, such as molecules, in which (unlike metals) the electron density fluctuates at short length scales. Because of its widespread availability, reliability as well as totally non-empirical foundation, the Perdew-Burke-Ernzerhof (PBE) flavor [113] of GGA has been used throughout the course of this thesis.

However, it must be noted that the PBE functional has its own shortcomings: It suffers greatly from the so-called 'self-interaction error' which originates from the fact that each electron interacts with itself (coulombically) in Equation 7.8 which is, of course, spurious. While this is not a big problem for systems having delocalized electrons, the issue can lead to serious inconsistencies where electrons show a more localized behavior, such as molecules.[5] The usual practice to alleviate the problem is to use the so-called *hybrid* functionals that include a fraction of exact exchange energy from calculations done using the Hartree-Fock (HF) method [37].[6] Particularly, the commonly used hybrid functional PBE0, modifies the exchange-correlation energy to be

$$E_{xc}^{PBE0} = \frac{1}{4}E_x^{HF} + \frac{3}{4}E_x^{PBE} + E_c^{PBE}.$$

7.2 TREATING VAN DER WAALS INTERACTIONS

Most functionals used in the framework of DFT-KS ansatz are of semi-local character and, therefore, do not describe long-range (electronic) correlation effects. This means that they cannot account for van der Waals (vdW) interactions [53]. While this acceptable in cases where these forces play a trivial role (such as covalent bonding within molecules), a reasonable description of many systems — that have become technologically relevant over the last last two decades such as layered semiconductors and adsorbed SAMs — can only be achieved when vdW forces are included. Therefore, the treatment of vdW forces (and other long-range interactions) in DFT calculations is a hot topic of research and has seen some very interesting recent developments in the form of 'vdW-correction schemes' [11, 29, 35, 50–52, 72,

5 For example, the widely used PBE functional is (in)famous for predicting a smaller ionization energy and a smaller HOMO-LUMO gap than what is experimentally observed.

6 Making calculations much more computationally expensive.

92, 120, 122, 129, 143, 144, 159]. A detailed review covering these developments, as well as the basic concepts, was published in 2016 by the group of Grimme [53].

For our simulations, we chose to use the Tkatchenko-Scheffler (TS) [144] treatment of van der Waals interactions while using PBE as the xc functional, a scheme referred to as PBE+TS. When simulating the surface of some metals (namely, Cu, Ag, Au, Pd and Pt), the scheme can be customized further to use screening-corrected parameters suggested by Ruiz *et al.* [120], a combination that has been named PBE+vdW^{surf}. This setup leads to remarkable reliability when modeling the geometric [94] as well as the electronic structure [61] of metal-organic interfaces, and thus was used by us when simulating metal surfaces.

7.2.1 *The Tkatchenko-Scheffler approach*

In the PBE+TS approach (as well as the PBE+vdW^{surf} method that builds on it), the C_6 coefficient of every atom is re-parameterized 'on the fly' during any given calculation to account for the chemistry of its neighborhood. For this, the method takes the 'atom-in-molecule' approach and uses the Hirshfeld partitioning scheme [60, 72] to calculate the effective atomic volume v_i of each atom [144] as

$$v_i = \frac{\int d\mathbf{r}\, w_i(\mathbf{r}) n(\mathbf{r}) \mathfrak{r}^3}{\int d\mathbf{r}\, n_i^{free}(\mathbf{r}) \mathfrak{r}^3} \tag{7.14}$$

where $n(\mathbf{r})$ is the total electron density, n_i^{free} is the spherically averaged electron density of the reference for atom i,[7] $\mathfrak{r}^3$ is the cube of the distance from the nucleus of atom i, and w_i is the Hirshfeld weight of the atom in the presence of other atom(s) j. Formally w_i is defined to be

$$w_i(\mathbf{r}) = \frac{n_i^{free}(\mathbf{r})}{\sum_j n_j^{free}(\mathbf{r})}. \tag{7.15}$$

Reference *free-atom* data for atom species i, i.e. the homonuclear C_6 coefficient ($C_{6,ii}$) and its polarizability (α_i^{free}), are then read from existing data tables[8] and re-parameterized to adjust for the effective volume of the atom according to the relations

$$C_{6,ii} = v_i^2 C_{6,ii}^{free}, \text{ and} \tag{7.16}$$

$$\alpha_i = v_i \alpha_i^{free}. \tag{7.17}$$

Last, the C_6 coefficient between any two atoms, i and j, in the system is calculated by using the re-parameterized coefficients for each atom, $C_{6,ii}$, in the formula

$$C_{6,ij} = \frac{2 C_{6,ii} C_{6,jj}}{\frac{\alpha_j}{\alpha_i} C_{6,ii} + \frac{\alpha_i}{\alpha_j} C_{6,jj}}. \tag{7.18}$$

7 n_i^{free} is calculated using the same underlying xc functional, e.g. by using PBE when using PBE+TS.

8 These tables are present in FHI-aims as well as VASP. The data for these tables are obtained from self-interaction corrected time-dependent density functional theory calculations [26].

Effectually, the scheme works as follows: The charge distribution in any given system is determined by its geometry because the electrons arrange themselves to accommodate for the nuclei (and other electrons) while each nucleus moves in order to the minimize forces that act on it. In the TS scheme, the spatial distribution of charge density in a system, by virtue of application of Hirshfeld partitioning, becomes a factor in re-parameterizing the C_6 coefficient, and thus has a direct influence the vdW forces that are present in the system. Hence, the scheme adds *also* the influence of local chemistry[9] (via charge density dependent) C_6 coefficient to the iterative geometry optimization process discussed in Section 7.3.3.

7.2.2 *Tuning the C_6 coefficient*

Using vdW-correction schemes in systems that are dominated by ionic and covalent interactions generally has an insignificant impact on the geometry. However, in particular scenarios, such as when discussing adsorption, the attractive van der Waals forces introduced by these correction schemes can play a decisive role. For example, during physisorption these are the interactions that drive the otherwise repelled[10] adsorbate towards adsorption. This is particularly apparent for a number of physisorption cases where not including any kind of vdW-correction scheme in DFT simulations can lead to a non-congruency with experimental results. For instance, in simulations PTCDA fails to show adsorption on Ag(111) if only the PBE functional is employed [120] while room-temperature experiments show clear evidence to the contrary [48, 56].

The same is, in fact, true for the case that is discussed in Chapter 3. Interestingly, unlike any case that has been reported so far in literature,[11] the subphthalocyanine molecule (described there) tends to adsorb and interact very strongly with the Cu(111) surface (it gets electronically coupled) if a vdW-correction scheme is used while desorbing completely if no such correction is used. This results in a somewhat counter-intuitive situation where inclusion of vdW interactions (that are generally associated with physisorption) trigger a strongly interacting 'chemisorption-like' behavior. Moreover, the system gave rather unconventional results when studied employing the standard methodology of analyzing the adsorption energy vs. adsorption height curve. Therefore, in order to understand the system better, we were motivated to add an additional 'knob' for controlling the adsorption process. This was accomplished by introducing a (linearly) scaling multiplicative prefactor to the C_6 coefficient.

While such scaling of the C_6 coefficient can be used to introduce a 'knob' in virtually any vdW-correction scheme (see Section 4.1.12 for usage with the Grimme's D2 scheme [51]), it is more fruitful when used in tandem with a local-chemistry dependent correction scheme (such as TS) because then it enables a systematic exploration of the link between a system's geometry and its electronic structure. For the system discussed in Chapter 3, this turned out to be of utmost importance

9 There are now several of these local-chemistry dependent correction schemes, including a newer version from the Grimme group, known as Grimme's D3 [52].

10 In absence of covalent bonding between substrate and adsorbate, exchange interaction between the electrons of the adsorbate and of the substrate would result in a repelling interaction unless the interaction becomes dominated by the attractive vdW forces.

11 To the best of our knowledge.

for understanding the link between massive changes of molecular geometry and the charge distribution, forming the basis of most of the insights discussed in that chapter.

The technical implementation of the knob: a 'scaling parameter' S that tunes the C_6 coefficient (such that $E_{vdW} \propto SC_6$) in the TS scheme was done in the FHI-aims package (vide infra) by introducing a new input keyword to the code, as described in Section 7.5.

7.3 SIMULATING MOLECULES AND SURFACES

7.3.1 *Tools of the trade*

While a number of DFT packages are available, the following four were used during the course of this thesis:

1. Fritz Haber Institute *ab-initio* molecular simulations (FHI-aims) [13] package; versions 071914_7 and 160328_3, in some cases with modifications (see Appendix 7.5)
2. Quantum Espresso (QE) [46, 47]; version 5.4.0[12]
3. Vienna *Ab-initio* Simulation Package (VASP) [80–85]; versions 5.3.3[13] and 5.3.5
4. Gaussian09 [41]; Revision D.01

FHI-aims was used for all calculations unless noted otherwise. This choice was motivated by several scientific as well as practical factors. First, the package has been tested and benchmarked for a variety of systems and is known to be very reliable for DFT [66, 88]. Second, it has implementations for a vast number of methods, allowing for, if required, expanding beyond the standard methodology (of using GGA in tandem with vdW correction schemes) without compromising on consistency. Third, the package has been specially optimized for efficient parallelization and makes use of advanced library routines, particularly ELPA which was developed specifically to handle eigenvalue problems in electronic structure calculations [97]. Fourth, given that it uses numeric atom-centered orbitals (NAO), FHI-aims can treat systems in both, periodic as well as open boundary conditions (*vide infra*), which further adds to its employability across a number of systems.

QE was first used during a research visit to the University of Milano-Bicocca with the motivation of expanding experience with different tools as well as to make use of its accompanying utility called XSpectra [18, 49, 137] that can be used for simulating XPS and NEXAFS.[14] Hence, it is the main tool used for simulating core-level spectroscopy (CLS) of oligomers, in Chapters 5 and 6.

12 The version of XSpectra utility used was the one distributed with QE version 5.3.0. For simulation of excitations from the 1*s* shell, this should make no difference.

13 A modified version including implementation for the Tkatchenko-Scheffler vdW-correction scheme [144] was used. It was kindly made available to the group by Tomáš Bučko of the Comenius University in Bratislava. The modifications were subsequently absorbed into the standard VASP distribution starting version 5.3.4.

14 This feature is now also available in the most recent releases of FHI-aims.

VASP and Gaussian09 were used in very particular cases: Since Grimme's vdW-correction scheme is not (yet) readily implemented in FHI-aims, VASP was used for the results discussed in Section 4.1.12. Likewise, Gaussian09 was used to relax a molecular geometry in Chapter 4.

7.3.2 *Periodic boundary condition and repeated-slab approach*

In QE and VASP, the unit cell under consideration must be infinitely repeated in the three spatial directions. This prerequisite, termed as the periodic boundary condition, stems from the necessity of representing a plane wave (PW) basis set[15] in a periodic space.[16] The common practice to fulfill this requirement while simulating adsorption is to employ a suitable *supercell* (see, for example, Figure 6.4); where a supercell is basically a large unit cell (generally at least 15 Å in one of the directions) that employs the repeated slab approach [124] for simulating systems having a (two) surface(s). In a nutshell, the approach reduces the 3D periodicity of a supercell to 2D by introducing a large vacuum gap along one of the spatial directions. The adsorbate is then introduced, into the vacuum, in vicinity of the *exposed* surface. Since such a supercell is still infinitely periodic in 3D (fulfilling the periodic boundary condition), the procedure simulates the adsorption of an *infinite* number of molecules on an *infinitely* extended surface. Therefore, when simulating such systems, it is necessary to take into account the effects (such as steric hindrance and intermolecular interactions) originating from the periodic images of the adsorbate molecule. If done properly, they can be used simulate a SAM, as we do in Chapter 6.

A further question that arises is whether and how an in-vacuo molecule can be simulated in QE or VASP as they are PW basis set packages. The answer to this is, again, to use a very large unit cell that is big enough to minimize the effects originating from periodic images of the molecule. This is not particularly efficient but works nonetheless. For our QE calculations, we used unit cells that introduce a gap of at least 14 Å between the periodic images, thereby minimizing the spurious effect of using periodic boundary conditions when simulating molecules that are supposed to be in-vacuo.

7.3.3 *General procedure*

As discussed in section 7.1.3, the SCF cycle is an iterative process that tries to minimize the electronic energy of a system. Therefore, it is necessary to define a convergence criterion for energy when doing DFT calculations such that a good

15 A basis set is a set of functions that a KS DFT code uses to represent electronic wavefunction(s). The code expands ψ_i of Equation 7.12 on a basis set c_α such that $\psi_i = \sum_\alpha c_\alpha \varphi_\alpha$. While the expansion is done to make the problem more computer-friendly, the choice of basis set is usually driven by the system under consideration. For example, PW codes exploit Bloch theorem ($\varphi(\mathbf{r}) = Ae^{i\mathbf{k}\cdot\mathbf{r}}u(\mathbf{r})$ such that $u(\mathbf{r}+\mathbf{R}) = u(\mathbf{R})$) to represent periodicity in *crystals*. On the other hand, NAO codes use the (comparably) localized nature of the electron on an atom in a *molecule* to their advantage by using some form of a radially decaying ($1/r^x$) function.

16 In contrast, codes that employ numeric atom-centered orbitals (such as FHI-aims) or Gaussian-type orbitals (Gaussian09) as their basis functions can (also) be used to treat systems that are "in-vacuo" which is contrastingly referred to as the open boundary condition.

balance between available computational resources and accuracy in quantities of interest (*vide infra*) is achieved. The criteria that we used when studying particular systems are stated in the respective chapters.

Geometry Optimization

In addition to minimization of electronic energy, we also minimized the total energy of a system by allowing the atoms in it to relax under the influence of forces present in the system:[17] We started with a reasonable initial geometry and converged its electronic structure. Then, we calculated the forces on all atoms of the system and moved the atoms slightly, as if they were under influence of the calculated forces. The modified system geometry was then subjected to another SCF cycle after which the forces on each atom were recalculated and the geometry was perturbed again so as to reduce the forces on each atom. This was done iteratively[18] with the aim of minimizing the forces that act on atoms in a system, thereby reducing the total energy of a system. The convergence for this iterative process is defined in terms of 'force per atom' in the system, which is also mentioned in respective chapters.

Minimization of forces in a system, or geometry optimization as it is commonly called, is a computationally expensive procedure and its cost increases with the degrees of freedom in the system. Therefore, if reasonable, it is often prudent to reduce the number of atoms involved in a relaxation procedure. For example, in a metal slab composed of six layers of atoms, one can assume that an adsorbate would chiefly perturb the layers that are close to the exposed surface while the position of atoms that are positioned deeper in the slab would be minimally disturbed. Hence, in all systems having a (six atomic layers thick) metal slab, we demarcated lower (four atomic) layers of the metal as 'fixed' while letting rest of the system to relax as usual. This has an added advantage that the lower layers, devoid of any spurious relaxation, faithfully represent the lattice structure of the 'bulk' metal.

Quantities of Interest

Depending on the requirements of the study, various quantities in the output of an electronic structure calculation hold differing levels of importance. For example, when simulating organic SAMs on metals, the overarching motivation[19] can be to gain control over the work function of the underlying substrate; making *work function modification* the main quantity of interest. On the other hand, when studying the process of adsorption in general, and particularly when trying to determine registry between adsorbate and molecule, it is the adsorption energy of the system that is of prime importance. Since this is generally defined as in

17 In certain cases, it is actually counterproductive to do geometry optimization and was thus avoided. For example, when we wanted to determine the charge density redistribution upon adsorption in Chapter 3.

18 Employing (i) Broyden–Fletcher–Goldfarb–Shanno (BFGS) algorithm [36] when using QE, (ii) a trust radius method enhanced version of the same (based on [115]) when using FHI-aims, (iii) Berny algorithm using GEDIIS [90] when using Gaussian09, and (iv) the conjugate-gradient algorithm when using VASP.

19 Especially true for the community researching organic electronics.

Equation 1.1, it depends on the *total energy* of the system. In general, it is a good idea to converge these quantities before production calculations. For example, we converged the *work function modification* for calculations concerning the adsorption of ClB-SubPc molecules on Cu(111) to 0.02 eV. Similarly, we always used the recommended 'tight' settings when using FHI-aims for production calculations that provides for total-energy accuracy in the order of 1 meV per atom.

7.4 SIMULATING EXPERIMENTS

Over the last decade, with increased availability of computational resources, it has become possible to use *ab-initio* calculations based on DFT to simulate surfaces and other large systems (>200 atoms). This has opened up the possibility of doing *ab-initio* simulations that aim to replicate the results of experimental techniques. The benefit of doing so is that in computations one can track and pin-down the origin of simulated features, thus bringing additional clarity to the experimental results.[20] The main challenge, of course, is developing a reliable correspondence between simulated results and the experimental ones.

7.4.1 *X-ray photoelectron spectroscopy*

This section is based on the discussion in Ref. [44].

In a typical (surface science) X-ray photoelectron spectroscopy (XPS) experiment, an X-ray photon ($h\nu$ between 100 eV and 1500 eV $\approx$ λ between 12 nm and 0.82 nm) is used to excite an electron — residing in an inner shell, also called *core-level*, (K $1s$ or L_1 $2s$)[21] — of an atom such that the electron is ejected into the 'vacuum' (*knocked-out*). The energy of the incident radiation is kept fixed while the number and kinetic energies $KE_{photoelectron}$ of the photoexcited electrons are recorded. From these, it is possible to determine the XPS spectra i.e. binding energy BE vs. intensity (photoelectron count) by using the equation

$$BE = h\nu - (KE_{photoelectron} + \Phi) \tag{7.19}$$

where Φ is the work function of the sample.

Since, in general, there are atoms of different elements in a sample and the incident photons can excite any of the atoms (as long as Equation 7.19 is satisfied), the spectra shows distinct peaks corresponding to the BE of the electrons of the atoms that are present in the sample. By matching the BE peaks with known reference binding energies (from resources such as The X-Ray Data Booklet [157]), it is possible to estimate the elemental composition of a given sample. However, of greater use is the fact that very often the measured BE differs slightly from the reference value: The atoms that are (valence) electron deficient in a bonding situation have a higher effective nuclear charge making it difficult for their core-level electrons to escape, and vice-versa; resulting in deviations from the reference BE values. This

20 Though this approach is gaining prevalence for complicated experimental techniques only now, the tradition of bringing clarity to experiments by employing principles of quantum mechanics is an old one: recall the success of the Schrödinger's equation in explaining the spectral features of a hydrogen atom.

21 Here, we ignore Auger processes that give rise to photoelectrons from the L_2 $2p_{1/2}$ and L_3 $2p_{3/2}$ core-levels as they are beyond the scope of this work.

allows for sample's chemical analysis because the (local) chemical environment of the source atom also becomes a factor in the measured BE. In surface science, compositional analysis is generally useful, for example, when determining the stoichiometry of an adlayer while chemical analysis is useful for, among other things [6], estimating the strength of adsorption. Due to the strongly localized nature of core-level electrons, the chemical sensitivity of XPS as a technique is relatively good: it is possible to resolve the different orbital hybridizations (sp^2 vs. sp^3) between two carbon atoms even without high-resolution XPS [28].

ΔSCF Procedure

Evaluating the physical process that underlies X-ray photoelectron spectroscopy in the framework of DFT simulations is possible at different levels of rigor. The simplest approach, known as the initial state method, is to interpret the KS eigenvalues as for binding energies of electrons in an atom. The method completely ignores the presence of a core-hole — the absence of an electron in the core-level because of photoexcitation — as well as any changes in electronic structure of the sample after excitation.[22] Nevertheless, the approach is especially useful when the *change* in binding energy, termed as *core-level shift*, is of greater interest than the spectrum itself, for example, as seen in Ref. [138]. A more rigorous, as well as computationally expensive method for simulating XPS is the 'ΔSCF procedure' that we use in Chapters 5 and 6.

At a very basic level, the measured BE in a photoexcitation process can be expressed as

$$BE = E_{N-1} - E_N \tag{7.20}$$

where N is the total number of electrons in a neutral sample that is at ground state, while $E_{N-1} - E_N$ is the difference of energy between the ionized system and the neutral system. To simulate the XPS process, we first calculate the ground state energy E^{GS} for the system (essentially same as E_N). Then, depending on the element that is of interest, we identify every single *inequivalent atom*[23] whose excitation must be simulated in order to recover the experimental spectrum. For example, in Chapter 5, when simulating C 1*s* XPS for a terphenyl molecule, we identify six inequivalent carbon atoms (see Figure 5.8) since all other carbon atoms in the molecule are in mirror symmetry with one of those six. To simulate the photoexcited system (one that has lost a 1*s* electron), we used a specially crafted PW basis set for the photoexcited atom in form of a custom-made C pseudopotential[24] file [111] (referred to as the full core-hole (FCH) file in this thesis). The BE is then

22 In reality, the remainder of the electrons in an excited system *relax* to accommodate for alteration in the electronic structure caused by removal of an electron.

23 Inequivalent atoms are the atoms that remain in the minimum representation of a system after its *reflection symmetry(ies)* have been accounted for.

24 Pseudopotentials are a way of separating the representation of core and valence electrons in PW codes like QE. Owing to the difference in the nuclear charge they experience, the wavefunctions associated with the two kinds take significantly different forms. Hence it is generally better to separate their mathematical treatment in a PW code. Pseudopotentials for QE can be generated using the accompanying `atomic` tool while many are freely tried and tested ones are available from its webpage. The full core-hole (FCH) pseudopotential file that we used was provided by Dr. Guido Fratesi.

calculated, one inequivalent atom at a time: the energy of the system after core excitation E^{ES} is calculated self-consistently by replacing the regular pseudopotential file with the FCH file for *only* one of the inequivalent atom while assuming that the valence electrons are in the ground state i.e. they have *relaxed* in the presence of the core hole.[25] Once these calculations are done, we calculate BE_i, where i stands for every excitable atom of the element that we are interested in, by substituting E^{ES} for E_{N-1} in the Equation 7.20. Finally, in the absence of an absolute energy scale, we align these BE_i to own their average in order to quantify the chemical (core-level energy) shifts (ΔE_i^{CLS}) associated with every atom of a given element:

$$\Delta E_i^{CLS} = BE_i - \overline{BE_i} \tag{7.21}$$

7.4.2 *Near edge x-ray absorption fine structure spectroscopy*

An excellent resource on fundamental concepts of NEXAFS is the book by Prof. J. Stöhr [134] and a thorough review in context of organic thin films is Ref. [55]. Both of them were used to develop the discussion in this section.

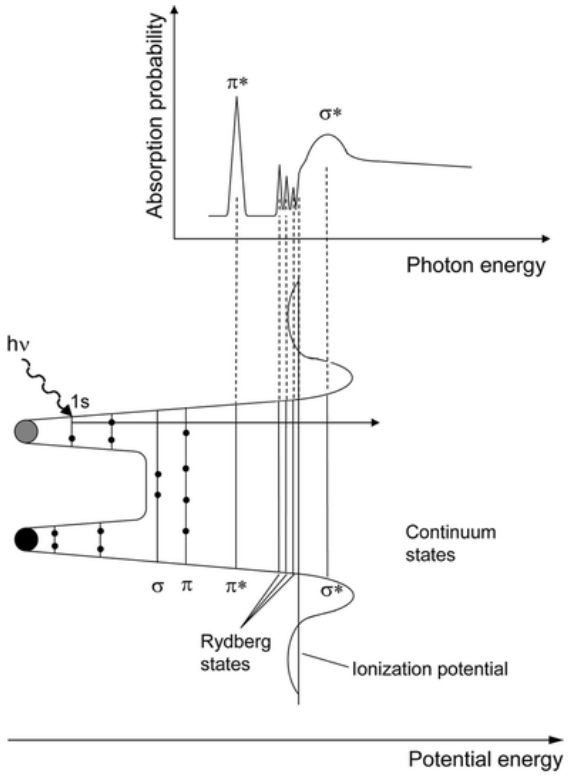

Figure 7.1: A typical NEXAFS spectrum and its origin in the electronic structure of the sample. Schematic taken from Ref. [55], © The Royal Society of Chemistry.

If XPS is a sensitive local probe, then near edge X-ray absorption fine structure (NEXAFS) spectroscopy is even more so. As an experimental tool, NEXAFS relies on using (soft) X-rays to excite electrons from the occupied core-levels to the unoccupied electronic states in a sample. Like XPS, the transitions depend on the energy of the incident radiation and are sensitive to the local chemical environment. However, in NEXAFS, instead of exciting the photoelectron to the vacuum,

25 In our methodology, we make use of the so-called 'sudden-approximation', which simply is an extension of the Born-Oppenheimer approximation (see Section 7.1.1), as it assumes that that any changes in the geometric structure occur on a much longer time scale compared to changes in the electronic structure and can, therefore, be ignored.

the sample is incident with X-ray photons that carry just enough energy so as to excite its core-level electrons into its unoccupied energy levels, resulting in absorption of the incident photons. The absorption probability of the photons at differing incident photon energies (and angles) can then be measured to identify the energy levels associated with unoccupied electronic states of the sample. A schematic for typical NEXAFS spectrum and its origin, in terms of the electronic structure of a generic diatomic molecule (and its effective potential), is shown in Figure 7.1.

If the energy of the incident photon, $h\nu$, is equal to the difference of energy between the occupied core-level ($1s$ in the figure) and one of the unoccupied levels (say $\pi*$) then the photon, with some probability (vide infra), gets absorbed by the sample. Depending on the density and electronic configuration (vide infra) of the unoccupied states, and on the *polarization* of the incident photons, one observes sharp features, (quenched) jagged features as well as relatively diffused peaks in a NEXAFS spectrum, as shown in Figure 7.1. In case of excitation from a $1s$ core-level, the sharp resonances correspond to excitation into the low-lying $\pi*$ unoccupied level(s), the jagged features (in vicinity of the ionization threshold) imply excitation into the Rydberg states and the diffused peaks indicate that the photoelectron was excited into the $\sigma*$ states.[26]

The main benefit of NEXAFS spectroscopy is that, when used with linearly polarized light, the technique can be used to obtain information about the configuration of molecular orbitals in the sample. The absorption cross-section and, therefore, the absorption probability for the photoexcitation process in a NEXAFS experiment is governed by Fermi's golden rule

$$\text{absorption probability} \propto \left|\mathbf{E} \cdot \left\langle \Psi_{final} \left|\mathbf{p}\right| \Psi_{initial} \right\rangle\right|^2 \tag{7.22}$$

where $\mathbf{E}$ is the electric field vector of the incident photon and $\mathbf{p}$ is the dipole transition operator (technically, it is the sum of linear momentum operator for all electrons.) This is the origin of the so-called *dichroism*, and the reason that NEXAFS can be used to determine the configuration of molecular orbitals in the sample: If the initial state has spherical symmetry (such as $1s$) and the final state is vector-type (i.e. it has a spatially directed orbital amplitude) then $\left\langle \Psi_{final} \left|\mathbf{p}\right| \Psi_{initial} \right\rangle$ lies in direction of the final state orbital; additionally, because of the dot product in Equation 7.22, absorption is maximized if $\mathbf{E}$ is also in the same direction. To quote from Ref. [55], "Bonds and the associated molecular orbitals are highly directional and the spatial orientation of an orbital, i.e. the direction of maximum orbital amplitude on the excited atom, determines the angular dependence of the K-shell spectra. Therefore, the transition intensities depend on the orientation of the electric field vector relative to the orientation of the molecule. Note that $\sigma*$-orbitals have a maximum orbital amplitude along the bond axis while $\pi*$-orbitals have maximum amplitude normal to the bond direction."
Hence, by measuring the spectra for different angles of incident radiation, one can determine the orientation of the sample (generally an adsorbate molecule on a surface) in a NEXAFS experiment [110]. A summary of results for most common

26 The order of unoccupied levels, as described here, is not fixed. It depends on the sample. One should also note that the creation of a core-hole shifts and often alters the order of the occupied and unoccupied energy levels in the sample.

molecular orientations and the two possible extremes[27] of incident radiation is summarized in Figure 7.2 as well as Table 7.1. The common experimental practice is report the spectra for $\theta = 20°$, $55°$ (the magic angle) and $90°$ as well as (sometimes) the difference of spectra as $90° - 20°$.

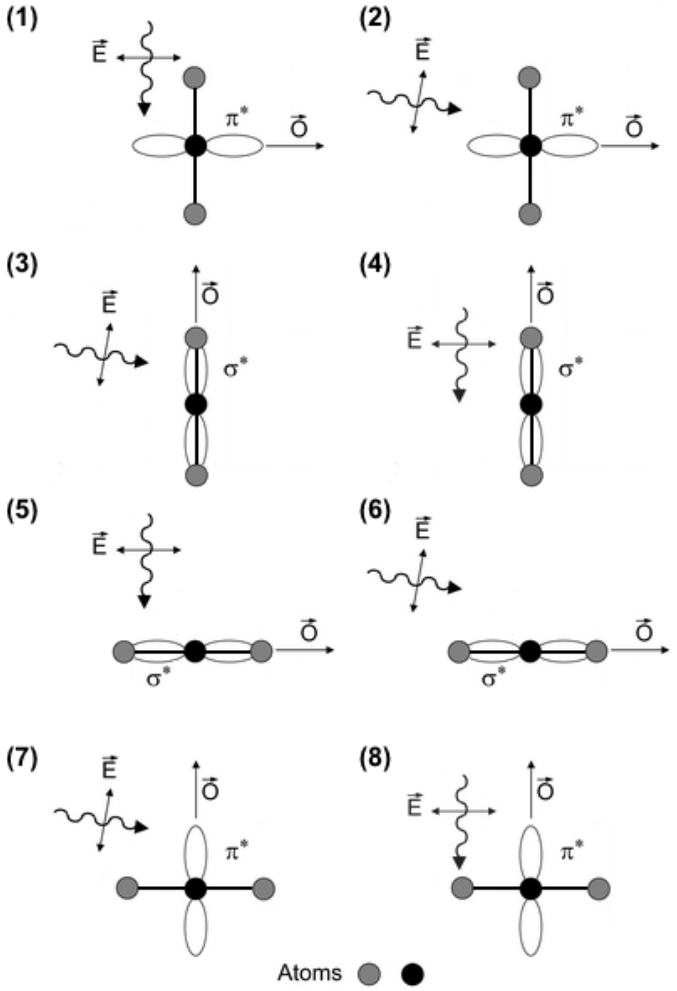

Figure 7.2: A schematic depicting the origin of angular dependence of NEXAFS resonances in π-conjugated systems. The bold black line represents the backbone while orbitals are shown as gray ellipses attached to either-side of the central (black) atom. $\rightsquigarrow$ represents the direction of incident photon while $\updownarrow$ represents the direction of its electric field **E**. The vector **O** represents the direction of the final state orbital Ψ_{final}, defined as the direction of maximum orbital amplitude on the excited atom. For maximization of the resonances, **E** and **O** should be parallel.
Panels (1) to (4): π-conjugated molecule standing upright (on a substrate). Panels (5) to (8): π-conjugated molecule lying flat (on a substrate). Left column (odd numbered panels): maximized resonances and right column (even numbered panels): minimized resonances. Panels (1) and (7): maximized $\pi*$ resonances when **E** is at 0° and ~90° respectively. Panels (3) and (5): maximized $\sigma*$ resonances when **E** is at ~90° and 0° respectively. Figure adapted and expanded from Ref. [55]. Original figure © The Royal Society of Chemistry.

27 While the angle of incident light, at its least, is supposed to be 0°, the actual value achieved in experiments, because of technical reasons, is generally only as low as ~20° (grazing angle).

Light (angle θ with respect to substrate)	$\boldsymbol{E}$	Strength of $s \rightarrow \pi*$	Orientation of molecule
Grazing (~0°)	at ~90°	Maximum (7)	Flat-lying on substrate
		Minimum (2)	Upright on substrate
Normal (90°)	at 0°	Maximum (1)	Upright on substrate
		Minimum (8)	Flat-lying on substrate

(a) Determining orientation from strength of $s \rightarrow \pi*$ resonances.

Light (angle θ with respect to substrate)	$\boldsymbol{E}$	Strength of $s \rightarrow \sigma*$	Orientation of molecule
Grazing (~0°)	at ~90°	Minimum (6)	Flat-lying on substrate
		Maximum (3)	Upright on substrate
Normal (90°)	at 0°	Minimum (4)	Upright on substrate
		Maximum (5)	Flat-lying on substrate

(b) Determining orientation from strength of $s \rightarrow \sigma*$ resonances.

Table 7.1: Determining adsorbate's orientation using NEXAFS. The number in the second column, in brackets, corresponds to the panels in Figure 7.2.

The discussion here follows the one found in Ref. [38]. In this thesis, we use the same methodology to simulate NEXAFS.

Transition-potential approach

Simulating NEXAFS is a multi-step process which is slightly more involved than that for XPS since the excited electron does not leave the sample. Mathematically, the process underlying NEXAFS spectroscopy can be written as

$$h\nu = E_f^{tot}(N; n_i = 0; n_f = 1) - E_i^{tot}(N; n_i = 1; n_f = 0) \tag{7.23}$$

where N is the total number of electrons in the system, $n_{i\,(f)}$ is the occupation of the initial (final) state and $E_{i\,(f)}$ is the total energy of the system before (after) the excitation process. Therefore, the first term on right hand side represents the excited system while the second term represents the ground state system.

While the KS eigenvalues yielded by DFT do not have a direct physical meaning, under the purview of Janak's Theorem [70], one can use the difference in the KS eigenvalues[28] for an N particle system and an $N-1$ particle system to determine the difference in energy of two such systems as long as it is the HOMO which undergoes the loss of electron. In practice, the treatment is extended to removal of an electron from a core energy level as well. Hence, the Equation 7.23 can be rewritten in terms of energy eigenvalues of the initial (ε_i) and the final state (ε_f) as

$$h\nu = \varepsilon_f(N; n_i = 0; n_f = 1) - \varepsilon_i(N; n_i = 1; n_f = 0). \tag{7.24}$$

We then follow Slater to represent the initial and the final states with half-occupied orbitals (the transition-state theorem) [130]. The assumption here being that it is

28 Independent of the xc functional used.

safe to neglect the second-order response of orbitals to the change in their occupation. This allows us to reframe Equation 7.24 as

$$h\nu = \varepsilon_f(N;\, n_i = 1/2;\, n_f = 1/2) - \varepsilon_i(N;\, n_i = 1/2;\, n_f = 1/2). \tag{7.25}$$

However, solving this requires a separate calculation for all the possible final states making its calculation cumbersome for small systems and infeasible for larger ones. Hence, we make yet another assumption, as proposed by Triguero *et al.* [149], and ignore the fractional occupation in the final state, thereby reducing Equation 7.25 to

$$h\nu = \varepsilon_f(N - 1/2;\, n_i = 1/2;\, n_f = 0) - \varepsilon_i(N - 1/2;\, n_i = 1/2;\, n_f = 0). \tag{7.26}$$

In this equation, the second term on right hand side (with its sign) is essentially the same as the core-level shifts calculated when simulating the XPS.[29] Hence, we can rewrite Equation 7.26 as

$$h\nu = \varepsilon_f(N - 1/2;\, n_i = 1/2;\, n_f = 0) + \Delta E_i^{CLS} + E_i^{ref}. \tag{7.27}$$

where ΔE_i^{CLS} is defined in Equation 7.21 (chemical shift of the atom) while E_i^{ref} is a constant that may be set to zero if only a relative energy scale is desired or to an arbitrary value in order to bring the simulated spectra in alignment with experimental results.

The method that we have detailed here is called the transition-potential or the half core-hole (HCH) approach as it places a "half-electron" in the core-hole.[30] This is because the first term of Equation 7.27, $\varepsilon_f(N - 1/2;\, n_i = 1/2;\, n_f = 0)$, is calculated by doing SCF calculation using a half core-hole (HCH) pseudopotential file[31] that removes half of an electron from the core-level. As we describe above (building from Equations 7.23 through 7.27), doing such a SCF calculation (and therefore relaxing the electronic structure in absence of 1/2 of a core-level electron) captures the effects of the photoexcitation process (that happens in NEXAFS) on the electronic structure of the sample. Hence, the Density of States (DoS) calculated for such a calculation can be used to determine the density and electronic structure of the unoccupied levels. This is the first requirement for simulating the NEXAFS spectra as it tells us at what energies can we expect to see the resonances.

The other requirement is then to calculate the expectation value of $\mathbf{p}$ in order to determine the strength of these resonances i.e. the absorption probability of an incident photon when it encounters the sample, as defined by Equation 7.22. This is done using the XSpectra utility of QE in which the direction of $\mathbf{E}$ is provided as an input and the energy range of the 'simulated' incident photons is based on the species of element being excited. For example, for simulating excitation from carbon 1*s* level, this is a range of values around -284.2 eV, which is the core-level energy of a carbon atom [157]. The wavefunction of the initial state, $\Psi_{initial}$ is reconstructed from the HCH pseudopotential file, using a tool called `upf2plotcore.sh`

29 Note that the final product of an excitation process associated with XPS can be similarly expressed as: $N - 1;\, n_i = 1;\, n_f = 0$.

30 It must be noted that this is, by far, not the only approach that can be taken and other approaches are also used, varying in levels of accuracy and expensiveness.

31 Provided for carbon by Dr. Guido Fratesi.

that is provided alongside XSpectra. On the other hand, the wavefunction of the final state, Ψ_{final} is made available from the results of the calculations done to obtain the first term (on right hand side) of Equation 7.26; the wavefunction is reconstructed from the output charge density. Last, the expectation value of $\mathbf{p}$ is then solved recursively using the Lanczos procedure [87] for solving eigenvalue problems. This is then (usually) repeated for three mutually orthogonal directions of $\mathbf{E}$ in order to obtain a spectrum for each direction.

The entire exercise produces the spectrum for only one inequivalent atom in the system and, thus, must be repeated over for all such atoms in order to produce a composite spectrum that is directly comparable with that of experiments. This last step, of making a composite spectrum, is implemented in the Fortran program called nexafsanalysis[32] which aligns all the spectra from inequivalent atoms to account for their respective system's Fermi levels/vacuum level[33] and the core-level shifts.

7.4.3 *Scanning tunneling microscopy*

Scanning Tunneling Microscopy (STM) is a surface imaging technique that can resolve features at an atomic-scale. The fundamental idea behind the technique is to introduce a biased conducting probe (*tip*) in the vicinity (but not in contact) of an analyte such that the quantum tunneling barrier for electrons — that might tunnel between the analyte and the tip — is significantly reduced. Whatever tunneling results as a consequence of the (known) applied bias voltage in this setup can then be measured and is called the tunneling current. This current depends essentially on four factors: (i) bias between the tip and the analyte, (ii) vertical and lateral position of the tip with respect to the analyte, (iii) the local DoS within the analyte, and (iv) the DoS in the tip.

Since, in principle, all these factors can be accounted for in electronic structure calculations, theoretical models to emulate experimental STM images were conceived relatively quickly. Between 1983 and 1989, in three papers [140–142], Tersoff and Hamann laid down a method for *calculating* STM images. The approach approximates the tip's geometry as well as its electronic structure with a spherical *s*-wavefunction of finite radius and a constant density of states,[34] and arrives at the result that the STM images with constant tunneling current can be approximated by integrating the Local Density of States (LDoS) of the analyte in vacuum,

$$LDoS(\mathbf{r}; E) = \sum_i |\psi_i(\mathbf{r})|^2 \, \delta(E - \varepsilon_i), \tag{7.28}$$

32 ©Guido Fratesi.

33 For gas-phase calculations, the results might be aligned to the vacuum-level while for molecule-adsorbed-on-metal systems, it might be aligned to the Fermi level of the adsorbed system.

34 The role of electronic structure inside the tip and that of tip's geometry was subject to some improvements after Tersoff and Hamann laid down their approach. In their first paper in 1983 [141], Tersoff and Hamann noted that results obtained from different kinds of tips (W, Mo and stainless steel) all give similar results and used this as the basis for representing the tip with a simple spherical potential. However, this was further expanded (particularly to account for certain discrepancies that became apparent only later) by Chen to include non-spherical tip wavefunctions [23, 24]. Nevertheless, we rely on the original definitions since using the simplistic spherical tip is suffice for our purpose, as evident from the simulation results presented in Chapter 1.

between Fermi energy E_F of the system and the tip bias V_{tip}. Here, ψ_i is a Kohn-Sham orbital of the analyte with ε_i being its energy eigenvalue and E is the energy of the tip in absence of any tunneling [57].

For the results presented in Chapter 1, the initial STM data-grids output by FHI-aims were very dense and therefore the corresponding simulated STM images carried an unnaturally high contrast.[35] Therefore, in a fashion similar to that outlined by Heimel *et al.* [57], we 'blurred' the output cube files to take into account the tip's finite size. To this end we made use of a similar hypothetical spherical tip with a diameter of 2 Å and an active-area height of 1 Å, resulting in the hypothetical tip *touching* 625 data-points when placed at any given position in the cube file.[36] Using this setup, new "blurred" cube files were created by overwriting their every data-point with an averaged value (calculated from the corresponding 625 data-points). From these "blurred" data-grids, we plotted[37] the constant-current maps (0.001 as the isovalue parameter and 0.9 as the z axis fractional coordinate)[38] presented in Chapter 1.

7.5 IMPLEMENTATION OF C_6 SCALING IN FHI-AIMS

The implementation[39] described here was done in FHI-aims version 071914_7,[40] and should remain applicable to near-future versions of the package as well unless the code underlying FHI-aims is significantly revised. A big thanks to Oliver for helping with the task of integrating a new keyword into the code. Since the purpose of this keyword is to scale the C_6 coefficient, we agreed to name it (rather unimaginatively) `vdW_scaling`.

The only *scientific* change in the code was made to the file `vdW_corrections.f90`. The execution of its content is responsible for determining and including the effect of van der Waals (vdW) forces on the system that is being calculated. The file receives and modifies system's attributes as such as its energy and the forces acting in it to account for vdW interactions.

VDW_CORRECTIONS.F90: In the `calc_vdw_hirshfeld` subroutine, all instances of

```
rphi = -C6/(dist6*aexp)
```

were replaced with

35 Unnatural because even if the experimental STM tip is effectively only a single tungsten atom, its lateral area would still be ~14 Å². On the other hand, the calculated data grid had a lateral density of ~125 data points per Å².

36 We say that the blurring was done in a similar (and not in the same) fashion because, Heimel *et al.* made use of the LDoS of the system while we made use of the STM data-grid calculator that is natively available in FHI-aims which leads to some (technical) dissimilarities. Furthermore, the original tools used in 2006 were lost, and new code had to be written by Oliver T. Hofmann in order to fill the gap. The new code is now a part of Oliver's `Toolbox Cube` package.

37 Again, using the `Toolbox Cube`.

38 This is equal to $z = 18$ Å which is 2 Å above the highest atom (chlorine) of the adsorbed molecule.

39 This implementation was only tested for the TS-vdW correction scheme as described in Ref.[144]. Caution is advised before expanding its scope to any other vdW correction scheme.

40 The `vdw_corrections.f90` file in the latest stable release has since been modified. Nevertheless, the changes was also successfully implemented in FHI-aims version 160328_3 using the procedure described here.

```
rphi = -C6/(dist6*aexp)*vdW_scaling
```

where `rphi` is the term that represents Equation 1 of Ref.[144].[41] By doing so, we modified that equation to be

$$E_{vdW} = -\frac{1}{2}\sum_{A,B} f_{damp}(R_{AB}, R_A^0, R_B^0) S C_{6AB} R_{AB}^{-6}$$

where S is the newly introduced scaling factor.

The part of code that modifies the forces in the system (to account for vdW interactions) receives the C_6 coefficient embedded inside the identifier `rphi`. Therefore, only modifying `rphi` is enough to include the effects of scaling parameter in the calculation.

The following three files were modified for the purpose of introducing the new keyword:

READ_CONTROL.F90: This file parses the input file `control.in` file to read and check all the keywords. Therefore, the following piece of code was included in the main `if` loop of the `readfile` subroutine.

```
case('vdW_scaling')
        read(inputline,*,end=88,err=99) desc_str, vdW_scaling
        write(info_str,'(2X,2A)') &
                'Using a scaling factor for vdW: ', &
                vdW_scaling
```

DIMENSIONS.F90: The `parse_control` subroutine of this file also parses the input file `control.in` and any unknown keyword in the file can mangle execution. Therefore the following code was included in the file by searching for the string '`all other keywords`' and placing the following code snippet above the `then` statement that occurs immediately above the searched string.

```
(desc_str.eq."vdW_scaling") .or. &
```

RUNTIME_CHOICES.F90: This file provides the default value for all keywords in case they are not set in the `control.in` file. Since, we wanted FHI-aims to treat C_6 'normally' in case the keyword is not explicitly defined, we set the default for `vdW_scaling` to be `1`. To achieve this, the following code was included after the header statements in the file.

```
real*8 :: vdW_scaling=1.0
```

Please note that the above procedure, especially that for introducing a new keyword, can change significantly in future versions of the package. Therefore, rudimentary knowledge of Fortran (or help from someone more experienced) is suggested if one is trying to implement the above changes.

41 Identifier `C6` represents C_{6AB}, identifier `dist6` represents R_{AB}^{-6} while identifier `aexp` represents f_{damp}.

As a closing remark we note that this exercise is not required when scaling the C_6 coefficient in VASP for use in tandem with Grimme's D2 vdW correction approach.[51] This is because VASP already provides a keyword (that acts on the C_6 coefficient) called `VDW_S6`, albeit for a different reason, that can be manipulated to achieve the same purpose.[42] The value of `VDW_S6` defaults to 0.75 if PBE is used and must be overwritten if any other functional is used (see VASP manual). One can, therefore, simply use this keyword and force overwrite its value to be $X \times S$, where X is the recommended value (e.g. 0.75 for PBE) and S is the scaling factor as defined in Chapter 3. For instance to achieve $S = 0.4$ when using PBE, we set `VDW_S6` to be 0.3 ($= 0.75 \times 0.4$).

42 This keyword replaces the `VDW_SCALING` keyword which was available between VASP versions 5.2.11 and 5.3.3.

Part V

CONCLUSION AND OUTLOOK

CONCLUSION AND OUTLOOK

The underlying theme developed during the course of this thesis is the necessity of an ongoing dialogue between experiment and theory, especially in the realm of surface science which finds extensive application when trying to better the interfaces in organic electronic devices. With ongoing advancement and expansion of experimental research techniques as well as significant improvements in simulation methods, it is now more possible than ever to achieve a two-fold understanding for a number of research questions. As we realized often during this work, the result of using them in tandem is generally more than a mere sum of the two.

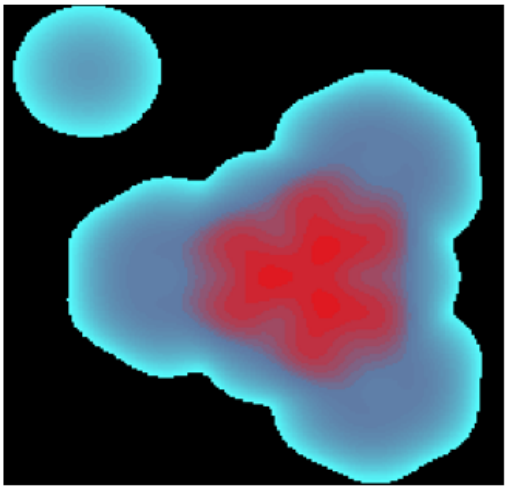

Simulated STM image of the dechlorinated ClB-SubPc molecule.

In Chapter 1, we open with the question of a non-planar molecule's registry with a metal surface. In our density functional theory (DFT) simulations, we found that the triangular arrangement of nitrogen atoms in the molecule reduces the number of possible registries to one, a observation that was also suggested by scanning tunneling microscopy (STM) images. We then focused on the origin of the two species that are observed experimentally. Contrary to a previously held notion, we stipulated the molecule undergoes dechlorination upon adsorption on Cu(111). We then simulated the STM images for such a dechlorinated molecule (as well as other possible configurations) and compared them with experimental ones. Based on this comparison as well as thermodynamic considerations, we were able to confirm our hypothesis of the dechlorination process.

However, this left us with an open question regarding the fate of the chlorine atom that results from the dechlorination process which still needs to resolved. (Another hypothesis that has been suggested since the study was published is that the Cl atom diffuses into the substrate.) Another interesting aspect of the system that warrants exploration is the exact chemical mechanism that leads to the dechlorination of the molecule.

In Chapter 3, we discuss the evolution of the interfacial electronic of the system. We found that the standard methodology of studying adsorption phenomena falls short of providing a detailed understanding. We therefore presented a novel technique of scaling the C_6 coefficient to tune the van der Waals (vdW) interactions in the system. By linearly increasing the coefficient, we found that adsorption of ClB-SubPc is a two-staged process with the first stage corresponding to a physisorped system while the second stage has features that are characteristic of a chemisorptive adsorption — an observation that we corroborated with results of ultraviolet photoelectron (UP) spectroscopy. Interestingly, the second regime, that involves considerable planarization of the molecule's heterocycle, is enabled by the vdW interactions between the molecule and the metal slab — making this an unusual case of van der Waals (vdW)-forces triggered strong electronic interaction. We note here that the merits of using of this technique, of scaling the C_6 coefficient, beyond the subphthalocyanine/Cu(111) system are yet to explored.

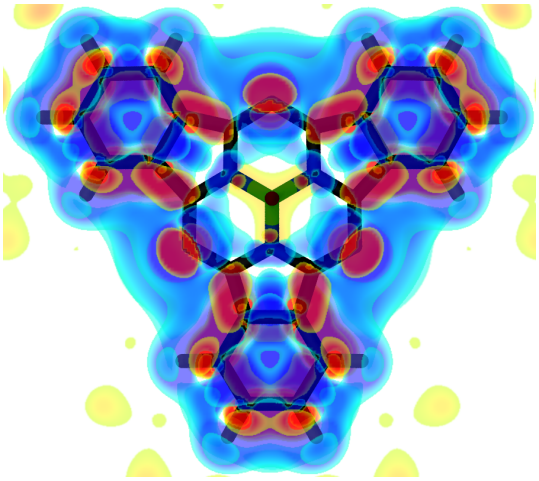

Charge rearrangements around the ClB-SubPc molecule upon adsorption on Cu(111).

In Chapters 5, we change our approach and focus more on testing the capability of state-of-the-art DFT methods to simulate X-ray photoelectron spectroscopy (XPS) and near edge X-ray absorption fine structure (NEXAFS) spectroscopy. We were met with mixed success as the results were comparable with the experiment to varying degrees. For acenes, we were able to replicate previously published results and found relatively good correspondence between experiments and theory for the para-thioterphenyl self-assembled monolayer (SAM) on Au(111) even though we compare the experimental spectra with the simulated spectra of a gas phase terphenyl molecule. For the perfluoroterphenyl-substituted alkanethiol self-assembled monolayer (SAM), also on Au(111), the agreement was poorer.

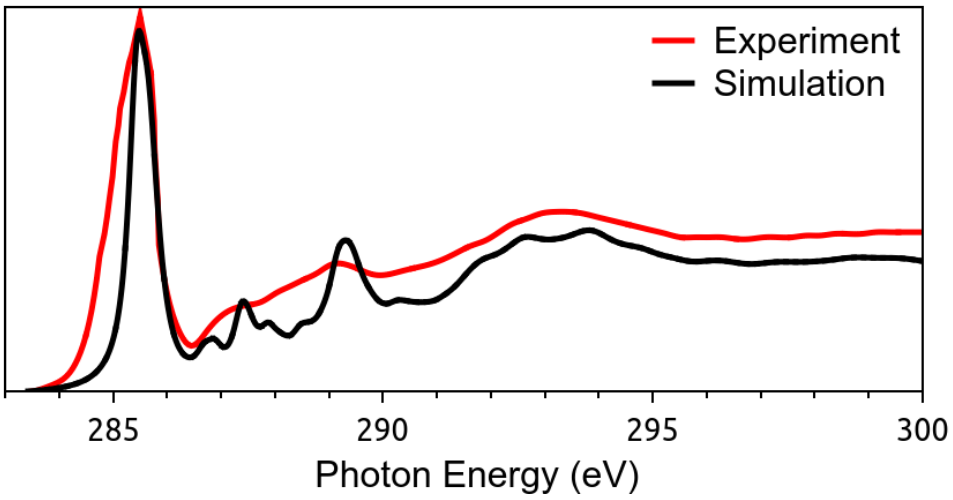

para-Thioterphenyl SAM on Au(111): Comparing experiment and theory.

In 6, we then moved onto another experimentally relevant perfluorinated system, that of perfluoroanthracenylaminoalkane thiolate self-assembled monolayer (SAM) on Au(111): We began by comparing the experimental spectra with that of the gas phase molecule and found very poor agreement. Then, after introducing an Au(111) slab and accounting for the inherent limits of the methodology used, we were able to reproduce a remarkably good correspondence between simulation and theory. However, the employed methodology is far from being widely applicable and significant improvements are needed before confidence in simulated NEXAFS spectra can be built.

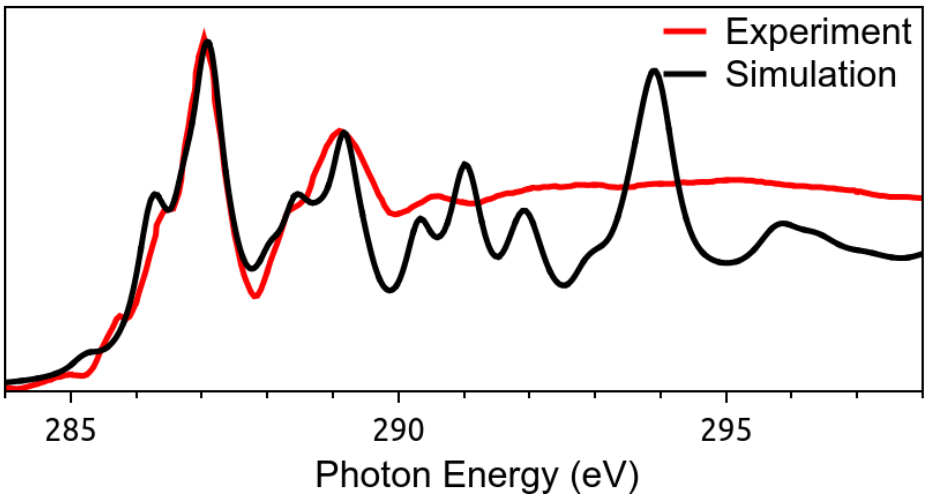

Perfluoroanthracenylaminoalkane thiolate SAM on Au(111): Comparing experiment and theory.

Part VI

BIBLIOGRAPHY

BIBLIOGRAPHY

[1] H. Adler, M. Paszkiewicz, J. Uihlein, M. Polek, R. Ovsyannikov, T. V. Basova, T. Chassé, and H. Peisert. "Interface Properties of VOPc on Ni(111) and Graphene/Ni(111): Orientation-Dependent Charge Transfer." In: *The Journal of Physical Chemistry C* 119.16 (Apr. 2015), pp. 8755–8762. DOI: 10.1021/acs.jpcc.5b01485 (cit. on pp. 8, 11).

[2] B. Andryushechkin, K. Eltsov, and V. Shevlyuga. "Domain-wall mechanism of "(n$\sqrt{3}$×n$\sqrt{3}$)R30°" incommensurate structure formation in chemisorbed halogen layers on Cu(111)." In: *Surface Science* 470.1 (Dec. 2000), pp. L63–L68. DOI: 10.1016/S0039-6028(00)00896-7 (cit. on p. 19).

[3] E. Annese, J. Fujii, I. Vobornik, and G. Rossi. "Structure and Electron States of Co-phthalocyanine Interacting With the Cu(111) Surface." In: *The Journal of Physical Chemistry C* 115.35 (Sept. 2011), pp. 17409–17416. DOI: 10.1021/jp203200s (cit. on p. 35).

[4] A. Baby, G. Fratesi, S. R. Vaidya, L. L. Patera, C. Africh, L. Floreano, and G. P. Brivio. "Anchoring and Bending of Pentacene on Aluminum (001)." In: *The Journal of Physical Chemistry C* 119.7 (Feb. 2015), pp. 3624–3633. DOI: 10.1021/jp512337y (cit. on p. 36).

[5] P. S. Bagus, K. Hermann, and C. Wöll. "The interaction of C_6H_6 and C_6H_12 with noble metal surfaces: Electronic level alignment and the origin of the interface dipole." In: *The Journal of Chemical Physics* 123.18 (Nov. 2005), p. 184109. DOI: 10.1063/1.2107647 (cit. on p. 32).

[6] P. S. Bagus, F. Illas, G. Pacchioni, and F. Parmigiani. "Mechanisms responsible for chemical shifts of core-level binding energies and their relationship to chemical bonding." In: *Journal of Electron Spectroscopy and Related Phenomena* 100.1 (Oct. 1999), pp. 215–236. DOI: 10.1016/S0368-2048(99)00048-1 (cit. on p. 98).

[7] P. S. Bagus, V. Staemmler, and C. Wöll. "Exchangelike Effects for Closed-Shell Adsorbates: Interface Dipole and Work Function." In: *Physical Review Letters* 89 (9 Aug. 2002), p. 096104. DOI: 10.1103/PhysRevLett.89.096104 (cit. on p. 42).

[8] J. D. Baran, J. A. Larsson, R. A. J. Woolley, Y. Cong, P. J. Moriarty, A. A. Cafolla, K. Schulte, and V. R. Dhanak. "Theoretical and experimental comparison of SnPc, PbPc, and CoPc adsorption on Ag(111)." In: *Physical Review B* 81 (7 Feb. 2010), p. 075413. DOI: 10.1103/PhysRevB.81.075413 (cit. on p. 35).

[9] J. D. Baran and J. A. Larsson. "Structure and Energetics of Shuttlecock-Shaped Tin-Phthalocyanine on Ag(111): A Density Functional Study Employing Dispersion Correction." In: *The Journal of Physical Chemistry C* 116.17 (May 2012), pp. 9487–9497. DOI: 10.1021/jp210771d (cit. on pp. 35, 36).

[10] J. V. Barth. "Molecular Architectonic on Metal Surfaces." In: *Annual Review of Physical Chemistry* 58 (May 2007), pp. 375–407. DOI: 10.1146/annurev.physchem.56.092503.141259 (cit. on p. 8).

[11] A. D. Becke and E. R. Johnson. "A density-functional model of the dispersion interaction." In: *The Journal of Chemical Physics* 123.15 (Oct. 2005), p. 154101. DOI: 10.1063/1.2065267 (cit. on pp. 39, 91).

[12] S. Berner, M. de Wild, L. Ramoino, S. Ivan, A. Baratoff, H.-J. Güntherodt, H. Suzuki, D. Schlettwein, and T. A. Jung. "Adsorption and two-dimensional phases of a large polar molecule: Sub-phthalocyanine on Ag(111)." In: *Physical Review B* 68.11 (Sept. 2003). DOI: 10.1103/PhysRevB.68.115410 (cit. on pp. 9, 13, 19, 20, 32).

[13] V. Blum, R. Gehrke, F. Hanke, P. Havu, V. Havu, X. Ren, K. Reuter, and M. Scheffler. "Ab initio molecular simulations with numeric atom-centered orbitals." In: *Computer Physics Communications* 180.11 (Nov. 2009), pp. 2175–2196. DOI: 10.1016/j.cpc.2009.06.022 (cit. on pp. 9, 33, 56, 94).

[14] M. L. Blumenfeld, M. P. Steele, N. Ilyas, and O. L. Monti. "Interfacial electronic structure of vanadyl naphthalocyanine on highly ordered pyrolytic graphite." In: *Surface Science* 604.19 (Sept. 2010), pp. 1649–1657. DOI: 10.1016/j.susc.2010.06.009 (cit. on p. 8).

[15] M. L. Blumenfeld, M. P. Steele, and O. L. Monti. "Near- and Far-Field Effects on Molecular Energy Level Alignment at an Organic/Electrode Interface." In: *The Journal of Physical Chemistry Letters* 1.1 (Jan. 2010), pp. 145–148. DOI: 10.1021/jz9000517 (cit. on p. 19).

[16] M. Born and R. Oppenheimer. "Zur Quantentheorie der Molekeln." In: *Annalen der Physik* 389.20 (1927), pp. 457–484. DOI: 10.1002/andp.19273892002 (cit. on p. 87).

[17] S. Braun, W. R. Salaneck, and M. Fahlman. "Energy-Level Alignment at Organic/Metal and Organic/Organic Interfaces." In: *Advanced Materials* 21.14-15 (Mar. 2009), pp. 1450–1472. DOI: 10.1002/adma.200802893 (cit. on pp. 3, 32).

[18] O. Bunău and M. Calandra. "Projector augmented wave calculation of x-ray absorption spectra at the $L_{2,3}$ edges." In: *Physical Review B* 87 (20 May 2013), p. 205105. DOI: 10.1103/PhysRevB.87.205105 (cit. on p. 94).

[19] Y. Cai and X. Qiao. "Adsorption and reconstruction of metal-phthalocyanine molecules on Pt(001) investigated by density functional theory." In: *Surface Science* 630 (Dec. 2014), pp. 202–207. DOI: 10.1016/j.susc.2014.08.016 (cit. on p. 35).

[20] J. Carrasco, W. Liu, A. Michaelides, and A. Tkatchenko. "Insight into the description of van der Waals forces for benzene adsorption on transition metal (111) surfaces." In: *The Journal of Chemical Physics* 140.8 (Feb. 2014), p. 084704. DOI: 10.1063/1.4866175 (cit. on p. 39).

[21] H. B. G. Casimir and D. Polder. "The Influence of Retardation on the London-van der Waals Forces." In: *Physical Review* 73 (4 Feb. 1948), pp. 360–372. DOI: 10.1103/PhysRev.73.360 (cit. on p. 40).

[22] S.-H. Chang, S. Kuck, J. Brede, L. Lichtenstein, G. Hoffmann, and R. Wiesendanger. "Symmetry reduction of metal phthalocyanines on metals." In: *Physical Review B* 78.23 (Dec. 2008), p. 233409. DOI: 10.1103/PhysRevB.78.233409 (cit. on p. 8).

[23] C. J. Chen. "Tunneling matrix elements in three-dimensional space: The derivative rule and the sum rule." In: *Physical Review B* 42 (14 Nov. 1990), pp. 8841–8857. DOI: 10.1103/PhysRevB.42.8841 (cit. on p. 104).

[24] C. J. Chen. "Effects of m$\neq$ 0 tip states in scanning tunneling microscopy: The explanations of corrugation reversal." In: *Physical Review Letters* 69 (11 Sept. 1992), pp. 1656–1659. DOI: 10.1103/PhysRevLett.69.1656 (cit. on p. 104).

[25] F. Chesneau, B. Schupbach, K. Szelagowska-Kunstman, N. Ballav, P. Cyganik, A. Terfort, and M. Zharnikov. "Self-assembled monolayers of perfluoroterphenyl-substituted alkanethiols: specific characteristics and odd-even effects." In: *Physical Chemistry Chemical Physics* 12 (38 Oct. 2010), pp. 12123–12137. DOI: 10.1039/C0CP00317D (cit. on pp. 69, 74, 75).

[26] X. Chu and A. Dalgarno. "Linear response time-dependent density functional theory for van der Waals coefficients." In: *The Journal of Chemical Physics* 121.9 (Sept. 2004), pp. 4083–4088. DOI: 10.1063/1.1779576 (cit. on p. 92).

[27] R. Cuadrado, J. I. Cerdá, Y. Wang, G. Xin, R. Berndt, and H. Tang. "CoPc adsorption on Cu(111): Origin of the C4 to C2 symmetry reduction." In: *The Journal of Chemical Physics* 133.15 (Oct. 2010), p. 154701. DOI: 10.1063/1.3502682 (cit. on p. 35).

[28] J. Díaz, G. Paolicelli, S. Ferrer, and F. Comin. "Separation of the sp^3 and sp^2 components in the C1s photoemission spectra of amorphous carbon films." In: *Physical Review B* 54 (11 Sept. 1996), pp. 8064–8069. DOI: 10.1103/PhysRevB.54.8064 (cit. on p. 98).

[29] M. Dion, H. Rydberg, E. Schröder, D. C. Langreth, and B. I. Lundqvist. "Van der Waals Density Functional for General Geometries." In: *Physical Review Letters* 92 (24 June 2004), p. 246401. DOI: 10.1103/PhysRevLett.92.246401 (cit. on p. 91).

[30] S. Duhm, A. Gerlach, I. Salzmann, B. Bröker, R. Johnson, F. Schreiber, and N. Koch. "PTCDA on Au(111), Ag(111) and Cu(111): Correlation of interface charge transfer to bonding distance." In: *Organic Electronics* 9.1 (Feb. 2008), pp. 111–118. DOI: 10.1016/j.orgel.2007.10.004 (cit. on p. 36).

[31] J. Endres, I. Pelczer, B. P. Rand, and A. Kahn. "Determination of Energy Level Alignment within an Energy Cascade Organic Solar Cell." In: *Chemistry of Materials* 28.3 (Feb. 2016), pp. 794–801. DOI: 10.1021/acs.chemmater.5b03857 (cit. on p. 36).

[32] M. Eremtchenko, J. A. Schaefer, and F. S. Tautz. "Understanding and tuning the epitaxy of large aromatic adsorbates by molecular design." In: *Nature* 425 (Oct. 2003), pp. 602–605. DOI: 10.1038/nature01901 (cit. on p. 8).

[33] I. Fernandez-Torrente, S. Monturet, K. J. Franke, J. Fraxedas, N. Lorente, and J. I. Pascual. "Long-Range Repulsive Interaction between Molecules on a Metal Surface Induced by Charge Transfer." In: *Physical Review Letters* 99.17 (Oct. 2007), p. 176103. DOI: 10.1103/PhysRevLett.99.176103 (cit. on p. 8).

[34] A. Ferretti, C. Baldacchini, A. Calzolari, R. Di Felice, A. Ruini, E. Molinari, and M. G. Betti. "Mixing of Electronic States in Pentacene Adsorption on Copper." In: *Physical Review Letters* 99 (4 July 2007), p. 046802. DOI: 10.1103/PhysRevLett.99.046802 (cit. on p. 36).

[35] N. Ferri, R. A. DiStasio, A. Ambrosetti, R. Car, and A. Tkatchenko. "Electronic Properties of Molecules and Surfaces with a Self-Consistent Interatomic van der Waals Density Functional." In: *Physical Review Letters* 114.17 (Apr. 2015), p. 176802. DOI: 10.1103/PhysRevLett.114.176802 (cit. on p. 91).

[36] R. Fletcher. *Practical Methods of Optimization*. Wiley, 2013 (cit. on p. 96).

[37] V. Fock. "Näherungsmethode zur Lösung des quantenmechanischen Mehrkörperproblems." In: *Zeitschrift für Physik* 61.1 (Jan. 1930), pp. 126–148. DOI: 10.1007/BF01340294 (cit. on pp. 90, 91).

[38] G. Fratesi, V. Lanzilotto, L. Floreano, and G. P. Brivio. "Azimuthal Dichroism in Near-Edge X-ray Absorption Fine Structure Spectra of Planar Molecules." In: *The Journal of Physical Chemistry C* 117.13 (Apr. 2013), pp. 6632–6638. DOI: 10.1021/jp312569q (cit. on pp. 67, 68, 102).

[39] G. Fratesi, V. Lanzilotto, L. Floreano, and G. P. Brivio. "Correction to "Azimuthal Dichroism in Near-Edge X-ray Absorption Fine Structure Spectra of Planar Molecules"." In: *The Journal of Physical Chemistry C* 118.4 (Jan. 2014), pp. 2236–2236. DOI: 10.1021/jp412420s (cit. on p. 68).

[40] S. Frey, V. Stadler, K. Heister, W. Eck, M. Zharnikov, M. Grunze, B. Zeysing, and A. Terfort. "Structure of Thioaromatic Self-Assembled Monolayers on Gold and Silver." In: *Langmuir* 17.8 (Apr. 2001), pp. 2408–2415. DOI: 10.1021/la001540c (cit. on p. 74).

[41] M. J. Frisch et al. *Gaussian 09 Revision D.01* (cit. on pp. 56, 94).

[42] C. .-.-L. Fu and K. .-.-M. Ho. "First-principles calculation of the equilibrium ground-state properties of transition metals: Applications to Nb and Mo." In: *Physical Review B* 28 (10 Nov. 1983), pp. 5480–5486. DOI: 10.1103/PhysRevB.28.5480 (cit. on p. 34).

[43] H. Fukagawa, H. Yamane, S. Kera, K. K. Okudaira, and N. Ueno. "Experimental estimation of the electric dipole moment and polarizability of titanyl phthalocyanine using ultraviolet photoelectron spectroscopy." In: *Physical Review B* 73 (4 Jan. 2006), p. 041302. DOI: 10.1103/PhysRevB.73.041302 (cit. on p. 35).

[44] S. García-Gil, A. García, and P. Ordejón. "Calculation of core level shifts within DFT using pseudopotentials and localized basis sets." In: *The European Physical Journal B* 85.7 (July 2012), p. 239. DOI: 10.1140/epjb/e2012-30334-5 (cit. on p. 97).

[45] A. Gerlach, T. Hosokai, S. Duhm, S. Kera, O. T. Hofmann, E. Zojer, J. Zegenhagen, and F. Schreiber. "Orientational Ordering of Nonplanar Phthalocyanines on Cu(111): Strength and Orientation of the Electric Dipole Moment." In: *Physical Review Letters* 106.15 (Apr. 2011), p. 156102. DOI: 10.1103/PhysRevLett.106.156102 (cit. on pp. 8, 19).

[46] P. Giannozzi et al. "QUANTUM ESPRESSO: a modular and open-source software project for quantum simulations of materials." In: *Journal of Physics: Condensed Matter* 21.39 (Sept. 2009), p. 395502. DOI: 10.1088/0953-8984/21/39/395502 (cit. on p. 94).

[47] P. Giannozzi et al. "Advanced capabilities for materials modelling with Quantum ESPRESSO." In: *Journal of Physics: Condensed Matter* 29.46 (Nov. 2017), p. 465901. DOI: 10.1088/1361-648X/aa8f79 (cit. on p. 94).

[48] K. Glöckler, C. Seidel, A. Soukopp, M. Sokolowski, E. Umbach, M. Böhringer, R. Berndt, and W.-D. Schneider. "Highly ordered structures and submolecular scanning tunnelling microscopy contrast of PTCDA and DM-PBDCI monolayers on Ag(111) and Ag(110)." In: *Surface Science* 405.1 (May 1998), pp. 1–20. DOI: 10.1016/S0039-6028(97)00888-1 (cit. on p. 93).

[49] C. Gougoussis, M. Calandra, A. P. Seitsonen, and F. Mauri. "First-principles calculations of x-ray absorption in a scheme based on ultrasoft pseudopotentials: From α-quartz to high-T_c compounds." In: *Physical Review B* 80 (7 Aug. 2009), p. 075102. DOI: 10.1103/PhysRevB.80.075102 (cit. on p. 94).

[50] S. Grimme. "Accurate description of van der Waals complexes by density functional theory including empirical corrections." In: *Journal of Computational Chemistry* 25.12 (June 2004), pp. 1463–1473. DOI: 10.1002/jcc.20078 (cit. on p. 91).

[51] S. Grimme. "Semiempirical GGA-type density functional constructed with a long-range dispersion correction." In: *Journal of Computational Chemistry* 27.15 (Nov. 2006), pp. 1787–1799. DOI: 10.1002/jcc.20495 (cit. on pp. 58, 91, 93, 107).

[52] S. Grimme, J. Antony, S. Ehrlich, and H. Krieg. "A consistent and accurate ab initio parametrization of density functional dispersion correction (DFT-D) for the 94 elements H-Pu." In: *The Journal of Chemical Physics* 132.15 (Apr. 2010), p. 154104. DOI: 10.1063/1.3382344 (cit. on pp. 39, 58, 91, 93).

[53] S. Grimme, A. Hansen, J. G. Brandenburg, and C. Bannwarth. "Dispersion-Corrected Mean-Field Electronic Structure Methods." In: *Chemical Reviews* 116.9 (May 2016), pp. 5105–5154. DOI: 10.1021/acs.chemrev.5b00533 (cit. on pp. 91, 92).

[54] J. Guilleme, L. Martínez-Fernández, D. González-Rodríguez, I. Corral, M. Yáñez, and T. Torres. "An Insight into the Mechanism of the Axial Ligand Exchange Reaction in Boron Subphthalocyanine Macrocycles." In: *Journal of the American Chemical Society* 136.40 (Oct. 2014), pp. 14289–14298. DOI: 10.1021/ja508181b (cit. on p. 20).

[55] G. Hahner. "Near edge X-ray absorption fine structure spectroscopy as a tool to probe electronic and structural properties of thin organic films and liquids." In: *Chemical Society Reviews* 35 (12 June 2006), pp. 1244–1255. DOI: 10.1039/B509853J (cit. on pp. 99–101).

[56] A. Hauschild, R. Temirov, S. Soubatch, O. Bauer, A. Schöll, B. C. C. Cowie, T.-L. Lee, F. S. Tautz, and M. Sokolowski. "Normal-incidence x-ray standing-wave determination of the adsorption geometry of PTCDA on Ag(111): Comparison of the ordered room-temperature and disordered low-temperature phases." In: *Physical Review B* 81 (12 Mar. 2010), p. 125432. DOI: 10.1103/PhysRevB.81.125432 (cit. on p. 93).

[57] G. Heimel, L. Romaner, J.-L. Brédas, and E. Zojer. "Organic/metal interfaces in self-assembled monolayers of conjugated thiols: A first-principles benchmark study." In: *Surface Science* 600.19 (Oct. 2006), pp. 4548–4562. DOI: 10.1016/j.susc.2006.07.023 (cit. on pp. 10, 105).

[58] G. Heimel, L. Romaner, E. Zojer, and J.-L. Bredas. "The Interface Energetics of Self-Assembled Monolayers on Metals." In: *Accounts of Chemical Research* 41.6 (June 2008), pp. 721–729. DOI: 10.1021/ar700284q (cit. on p. 41).

[59] B. W. Heinrich, G. Ahmadi, V. L. Müller, L. Braun, J. I. Pascual, and K. J. Franke. "Change of the Magnetic Coupling of a Metal–Organic Complex with the Substrate by a Stepwise Ligand Reaction." In: *Nano Letters* 13.10 (Oct. 2013), pp. 4840–4843. DOI: 10.1021/nl402575c (cit. on pp. 17, 20).

[60] F. L. Hirshfeld. "Bonded-atom fragments for describing molecular charge densities." In: *Theoretica chimica acta* 44.2 (June 1977), pp. 129–138. DOI: 10.1007/BF00549096 (cit. on p. 92).

[61] O. T. Hofmann, V. Atalla, N. Moll, P. Rinke, and M. Scheffler. "Interface dipoles of organic molecules on Ag(111) in hybrid density-functional theory." In: *New Journal of Physics* 15 (Dec. 2013), p. 123028. DOI: 10.1088/1367-2630/15/12/123028 (cit. on pp. 10, 42, 92).

[62] O. T. Hofmann, D. A. Egger, and E. Zojer. "Work-Function Modification beyond Pinning: When Do Molecular Dipoles Count?" In: *Nano Letters* 10.11 (Nov. 2010), pp. 4369–4374. DOI: 10.1021/nl101874k (cit. on pp. 20, 42).

[63] P. Hohenberg and W. Kohn. "Inhomogeneous Electron Gas." In: *Physical Review* 136 (3B Nov. 1964), B864–B871. DOI: 10.1103/PhysRev.136.B864 (cit. on p. 88).

[64] I. Horcas, R. Fernández, J. M. Gómez-Rodríguez, J. Colchero, J. Gómez-Herrero, and A. M. Baro. "WSXM: A software for scanning probe microscopy and a tool for nanotechnology." In: *Review of Scientific Instruments* 78.1 (Jan. 2007), p. 013705. DOI: 10.1063/1.2432410 (cit. on p. 9).

[65] Y. L. Huang, W. Chen, F. Bussolotti, T. C. Niu, A. T. S. Wee, N. Ueno, and S. Kera. "Impact of molecule-dipole orientation on energy level alignment at the submolecular scale." In: *Physical Review B* 87.8 (Feb. 2013), p. 085205. DOI: 10.1103/PhysRevB.87.085205 (cit. on pp. 8, 19).

[66] W. P. Huhn and V. Blum. "One-hundred-three compound band-structure benchmark of post-self-consistent spin-orbit coupling treatments in density functional theory." In: *Physical Review Materials* 1 (3 Aug. 2017), p. 033803. DOI: 10.1103/PhysRevMaterials.1.033803 (cit. on p. 94).

[67] N. Ilyas, S. S. Harivyasi, P. Zahl, R. Cortes, O. T. Hofmann, P. Sutter, E. Zojer, and O. L. A. Monti. "Sticking with the Pointy End? Molecular Configuration of Chloro Boron-Subphthalocyanine on Cu(111)." In: *The Journal of Physical Chemistry C* 120.13 (Apr. 2016), pp. 7113–7121. DOI: 10.1021/acs.jpcc.5b11799 (cit. on pp. 32, 34, 36, 42, 49).

[68] N. Ilyas and O. L. A. Monti. "Interplay of local and global interfacial electronic structure of a strongly coupled dipolar organic semiconductor." In: *Physical Review B* 90.12 (Sept. 2014), p. 125435. DOI: 10.1103/PhysRevB.90.125435 (cit. on pp. 9, 19, 20, 32, 36).

[69] H. Ishii, K. Sugiyama, E. Ito, and K. Seki. "Energy Level Alignment and Interfacial Electronic Structures at Organic/Metal and Organic/Organic Interfaces." In: *Advanced Materials* 11.8 (June 1999), pp. 605–625. DOI: 10.1002/(SICI)1521-4095(199906)11:8<605::AID-ADMA605>3.0.CO;2-Q (cit. on pp. 3, 32, 42).

[70] J. F. Janak. "Proof that $\frac{\partial E}{\partial n_i} = \epsilon$ in density-functional theory." In: *Physical Review B* 18 (12 Dec. 1978), pp. 7165–7168. DOI: 10.1103/PhysRevB.18.7165 (cit. on p. 102).

[71] N. Jiang, Y. Wang, Q. Liu, Y. Zhang, Z. Deng, K.-H. Ernst, and H.-J. Gao. "Polymorphism and chiral expression in two-dimensional subphthalocyanine crystals on Au(111)." In: *Physical Chemistry Chemical Physics* 12.6 (Feb. 2010), pp. 1318–1322. DOI: 10.1039/B918278K (cit. on pp. 9, 13, 19, 32).

[72] E. R. Johnson and A. D. Becke. "A post-Hartree–Fock model of intermolecular interactions." In: *The Journal of Chemical Physics* 123.2 (July 2005), p. 024101. DOI: 10.1063/1.1949201 (cit. on pp. 91, 92).

[73] S. Kera, H. Yamane, H. Honda, H. Fukagawa, K. Okudaira, and N. Ueno. "Photoelectron fine structures of uppermost valence band for well-characterized ClAl-phthalocyanine ultrathin film: UPS and MAES study." In: *Surface Science* 566-568 (Oct. 2004), pp. 571–578. DOI: 10.1016/j.susc.2004.05.110 (cit. on p. 35).

[74] M. E. El-Khouly, J.-H. Kim, J.-H. Kim, K.-Y. Kay, and S. Fukuzumi. "Subphthalocyanines as Light-Harvesting Electron Donor and Electron Acceptor in Artificial Photosynthetic Systems." In: *The Journal of Physical Chemistry C* 116.37 (Sept. 2012), pp. 19709–19717. DOI: 10.1021/jp3066103 (cit. on p. 32).

[75] M. Klues, P. Jerabek, T. Breuer, M. Oehzelt, K. Hermann, R. Berger, and G. Witte. "Understanding the F 1s NEXAFS Dichroism in Fluorinated Organic Semiconductors." In: *The Journal of Physical Chemistry C* 120.23 (June 2016), pp. 12693–12705. DOI: 10.1021/acs.jpcc.6b04048 (cit. on p. 77).

[76] N. Koch. "Organic Electronic Devices and Their Functional Interfaces." In: *ChemPhysChem* 8.10 (July 2007), pp. 1438–1455. DOI: 10.1002/cphc.200700177 (cit. on pp. 3, 32).

[77] N. Koch et al. "Adsorption-Induced Intramolecular Dipole: Correlating Molecular Conformation and Interface Electronic Structure." In: *Journal of the American Chemical Society* 130.23 (June 2008), pp. 7300–7304. DOI: 10.1021/ja800286k (cit. on p. 38).

[78] W. Kohn and L. J. Sham. "Self-Consistent Equations Including Exchange and Correlation Effects." In: *Physical Review* 140 (4A Nov. 1965), A1133–A1138. DOI: 10.1103/PhysRev.140.A1133 (cit. on p. 89).

[79] T. Koopmans. "Über die Zuordnung von Wellenfunktionen und Eigenwerten zu den Einzelnen Elektronen Eines Atoms." In: *Physica* 1.1 (1934), pp. 104–113. DOI: 10.1016/S0031-8914(34)90011-2 (cit. on p. 90).

[80] G. Kresse and J. Furthmüller. "Efficiency of ab-initio total energy calculations for metals and semiconductors using a plane-wave basis set." In: *Computational Materials Science* 6.1 (July 1996), pp. 15–50. DOI: 10.1016/0927-0256(96)00008-0 (cit. on p. 94).

[81] G. Kresse and J. Furthmüller. "Efficient iterative schemes for ab initio total-energy calculations using a plane-wave basis set." In: *Physical Review B* 54 (16 Oct. 1996), pp. 11169–11186. DOI: 10.1103/PhysRevB.54.11169 (cit. on p. 94).

[82] G. Kresse and J. Hafner. "Ab initio molecular dynamics for liquid metals." In: *Physical Review B* 47 (1 Jan. 1993), pp. 558–561. DOI: 10.1103/PhysRevB.47.558 (cit. on p. 94).

[83] G. Kresse and J. Hafner. "Ab initio molecular-dynamics simulation of the liquid-metal–amorphous-semiconductor transition in germanium." In: *Physical Review B* 49 (20 May 1994), pp. 14251–14269. DOI: 10.1103/PhysRevB.49.14251 (cit. on p. 94).

[84] G. Kresse and J. Hafner. "Norm-conserving and ultrasoft pseudopotentials for first-row and transition elements." In: *Journal of Physics: Condensed Matter* 6.40 (Oct. 1994), p. 8245. DOI: 10.1088/0953-8984/6/40/015 (cit. on p. 94).

[85] G. Kresse and D. Joubert. "From ultrasoft pseudopotentials to the projector augmented-wave method." In: *Physical Review B* 59 (3 Jan. 1999), pp. 1758–1775. DOI: 10.1103/PhysRevB.59.1758 (cit. on p. 94).

[86] M. Lackinger and M. Hietschold. "Determining adsorption geometry of individual tin–phthalocyanine molecules on Ag(111)—a STM study at submonolayer coverage." In: *Surface Science* 520.1-2 (Nov. 2002), pp. L619–L624. DOI: 10.1016/S0039-6028(02)02269-0 (cit. on pp. 8, 11, 19).

[87] C. Lanczos. "An Iteration Method for the Solution of the Eigenvalue Problem of Linear Differential and Integral Operators." In: *Journal of Research of the National Bureau of Standards* 49.255 (1947) (cit. on p. 104).

[88] K. Lejaeghere et al. "Reproducibility in density functional theory calculations of solids." In: *Science* 351.6280 (Mar. 2016). DOI: 10.1126/science.aad3000 (cit. on p. 94).

[89] M. Levy, J. P. Perdew, and V. Sahni. "Exact differential equation for the density and ionization energy of a many-particle system." In: *Physical Review A* 30 (5 Nov. 1984), pp. 2745–2748. DOI: 10.1103/PhysRevA.30.2745 (cit. on p. 90).

[90] X. Li and M. J. Frisch. "Energy-Represented Direct Inversion in the Iterative Subspace within a Hybrid Geometry Optimization Method." In: *Journal of Chemical Theory and Computation* 2.3 (May 2006), pp. 835–839. DOI: 10.1021/ct050275a (cit. on p. 96).

[91] Z. Li, B. Li, J. Yang, and J. G. Hou. "Single-Molecule Chemistry of Metal Phthalocyanine on Noble Metal Surfaces." In: *Accounts of Chemical Research* 43.7 (July 2010), pp. 954–962. DOI: 10.1021/ar9001558 (cit. on p. 8).

[92] O. A. von Lilienfeld, I. Tavernelli, U. Rothlisberger, and D. Sebastiani. "Optimization of Effective Atom Centered Potentials for London Dispersion Forces in Density Functional Theory." In: *Physical Review Letters* 93 (15 Oct. 2004), p. 153004. DOI: 10.1103/PhysRevLett.93.153004 (cit. on p. 91).

[93] W. Liu, J. Carrasco, B. Santra, A. Michaelides, M. Scheffler, and A. Tkatchenko. "Benzene adsorbed on metals: Concerted effect of covalency and van der Waals bonding." In: *Physical Review B* 86 (24 Dec. 2012), p. 245405. DOI: 10.1103/PhysRevB.86.245405 (cit. on pp. 32, 39).

[94] W. Liu, A. Tkatchenko, and M. Scheffler. "Modeling Adsorption and Reactions of Organic Molecules at Metal Surfaces." In: *Accounts of Chemical Research* 47.11 (Nov. 2014), pp. 3369–3377. DOI: 10.1021/ar500118y (cit. on pp. 10, 92).

[95] N. Lorente, M. F. G. Hedouin, R. E. Palmer, and M. Persson. "Chemisorption of benzene and STM dehydrogenation products on Cu(100)." In: *Physical Review B* 68 (15 Oct. 2003), p. 155401. DOI: 10.1103/PhysRevB.68.155401 (cit. on p. 36).

[96] S. Mannsfeld, H. Reichhard, and T. Fritz. "LEED and STM investigation of chloro(subphthalocyaninato)boron on Au(111)." In: *Surface Science* 525.1 (Feb. 2003), pp. 215–221. DOI: 10.1016/S0039-6028(02)02562-1 (cit. on pp. 9, 19, 32).

[97] A. Marek, V. Blum, R. Johanni, V. Havu, B. Lang, T. Auckenthaler, A. Heinecke, H.-J. Bungartz, and H. Lederer. "The ELPA library: scalable parallel eigenvalue solutions for electronic structure theory and computational science." In: *Journal of Physics: Condensed Matter* 26.21 (May 2014), p. 213201. DOI: 10.1088/0953-8984/26/21/213201 (cit. on p. 94).

[98] R. M. Martin. *Electronic Structure: Basic Theory and Practical Methods*. Cambridge University Press, 2004. DOI: 10.1017/CBO9780511805769 (cit. on p. 87).

[99] B. Maughan, P. Zahl, P. Sutter, and O. L. A. Monti. "Configuration-specific electronic structure of strongly interacting interfaces: TiOPc on Cu(110)." In: *Physical Review B* 96 (23 Oct. 2017), p. 235133. DOI: 10.1103/PhysRevB.96.235133 (cit. on p. 35).

[100] H. J. Monkhorst and J. D. Pack. "Special points for Brillouin-zone integrations." In: *Physical Review B* 13.12 (June 1976), pp. 5188–5192. DOI: 10.1103/PhysRevB.13.5188 (cit. on p. 10).

[101] O. L. A. Monti and M. P. Steele. "Influence of electrostatic fields on molecular electronic structure: insights for interfacial charge transfer." In: *Physical Chemistry Chemical Physics* 12 (39 Oct. 2010), pp. 12390–12400. DOI: 10.1039/C0CP01039A (cit. on p. 32).

[102] G. E. Morse and T. P. Bender. "Boron Subphthalocyanines as Organic Electronic Materials." In: *ACS Applied Materials & Interfaces* 4.10 (Oct. 2012), pp. 5055–5068. DOI: 10.1021/am3015197 (cit. on p. 32).

[103] K. Motai, T. Hashizume, H. Shinohara, Y. Saito, H. W. Pickering, Y. Nishina, and T. Sakurai. "C_60 Grown on the Cu(111)1×1 Surface." In: *Japanese Journal of Applied Physics* 32.3B (Mar. 1993), p. L450. DOI: 10.1143/JJAP.32.L450 (cit. on p. 36).

[104] K. Müller, A. Kara, T. K. Kim, R. Bertschinger, A. Scheybal, J. Osterwalder, and T. A. Jung. "Multimorphism in molecular monolayers: Pentacene on Cu(110)." In: *Physical Review B* 79.24 (June 2009), p. 245421. DOI: 10.1103/PhysRevB.79.245421 (cit. on p. 8).

[105] K. Müller, A. P. Seitsonen, T. Brugger, J. Westover, T. Greber, T. Jung, and A. Kara. "Electronic Structure of an Organic/Metal Interface: Pentacene/Cu(110)." In: *The Journal of Physical Chemistry C* 116.44 (Nov. 2012), pp. 23465–23471. DOI: 10.1021/jp308058u (cit. on p. 36).

[106] J. Neugebauer and M. Scheffler. "Adsorbate-substrate and adsorbate-adsorbate interactions of Na and K adlayers on Al(111)." In: *Physical Review B* 46.24 (Dec. 1992), pp. 16067–16080. DOI: 10.1103/PhysRevB.46.16067 (cit. on pp. 10, 34).

[107] T. Niu, J. Zhang, and W. Chen. "Molecular Ordering and Dipole Alignment of Vanadyl Phthalocyanine Monolayer on Metals: The Effects of Interfacial Interactions." In: *The Journal of Physical Chemistry C* 118.8 (Feb. 2014), pp. 4151–4159. DOI: 10.1021/jp4101653 (cit. on pp. 8, 11, 19, 23).

[108] T. Niu, C. Zhou, J. Zhang, S. Zhong, H. Cheng, and W. Chen. "Substrate Reconstruction Mediated Unidirectionally Aligned Molecular Dipole Dot Arrays." In: *The Journal of Physical Chemistry C* 116.21 (May 2012), pp. 11565–11569. DOI: 10.1021/jp301510a (cit. on p. 19).

[109] T. Niu, M. Zhou, J. Zhang, Y. Feng, and W. Chen. "Dipole Orientation Dependent Symmetry Reduction of Chloroaluminum Phthalocyanine on Cu(111)." In: *The Journal of Physical Chemistry C* 117.2 (Jan. 2013), pp. 1013–1019. DOI: 10.1021/jp310196k (cit. on pp. 8, 11, 35).

[110] D. A. Outka, J. Stöhr, J. P. Rabe, and J. D. Swalen. "The orientation of Langmuir-Blodgett monolayers using NEXAFS." In: *The Journal of Chemical Physics* 88.6 (Mar. 1988), pp. 4076–4087. DOI: 10.1063/1.453862 (cit. on p. 100).

[111] E. Pehlke and M. Scheffler. "Evidence for site-sensitive screening of core holes at the Si and Ge (001) surface." In: *Physical Review Letters* 71 (14 Oct. 1993), pp. 2338–2341. DOI: 10.1103/PhysRevLett.71.2338 (cit. on p. 98).

[112] S. Peljhan and A. Kokalj. In: *The Journal of Physical Chemistry C* 113.32 (Aug. 2009), pp. 14363–14376. DOI: 10.1021/jp902273k (cit. on pp. 17, 19).

[113] J. P. Perdew, K. Burke, and M. Ernzerhof. "Generalized Gradient Approximation Made Simple." In: *Physical Review Letters* 77.18 (Oct. 1996), pp. 3865–3868. DOI: 10.1103/PhysRevLett.77.3865 (cit. on pp. 10, 33, 91).

[114] R. Potz †, M. Göldner, H. Hückstädt, U. Cornelissen, A. Tutaß, and H. Homborg. "Synthese und strukturelle Charakterisierung von Borsubphthalocyaninaten." In: *Zeitschrift für anorganische und allgemeine Chemie* 626.2 (Feb. 2000), pp. 588–596. DOI: 10.1002/(SICI)1521-3749(200002)626:2<588::AID-ZAAC588>3.0.CO;2-B (cit. on p. 20).

[115] W. Press, S. Teukolsky, W. Vetterling, and B. Flannery. *Numerical Recipes 3rd Edition: The Art of Scientific Computing*. Cambridge University Press, 2007 (cit. on p. 96).

[116] B. del Rey, U. Keller, T. Torres, G. Rojo, F. Agulló-López, S. Nonell, C. Martí, S. Brasselet, I. Ledoux, and J. Zyss. "Synthesis and Nonlinear Optical, Photophysical, and Electrochemical Properties of Subphthalocyanines." In: *Journal of the American Chemical Society* 120.49 (Dec. 1998), pp. 12808–12817. DOI: 10.1021/ja980508q (cit. on p. 32).

[117] M. Robin, I. Ishii, R. McLaren, and A. Hitchcock. "Fluorination effects on the inner-shell spectra of unsaturated molecules." In: *Journal of Electron Spectroscopy and Related Phenomena* 47 (1988), pp. 53–92. DOI: https://doi.org/10.1016/0368-2048(88)85005-9 (cit. on p. 77).

[118] T. Roman and A. Groß. "Periodic Density-Functional Calculations on Work-Function Change Induced by Adsorption of Halogens on Cu(111)." In: *Physical Review Letters* 110.15 (Apr. 2013), p. 156804. DOI: 10.1103/PhysRevLett.110.156804 (cit. on p. 19).

[119] L. Romaner, D. Nabok, P. Puschnig, E. Zojer, and C. Ambrosch-Draxl. "Theoretical study of PTCDA adsorbed on the coinage metal surfaces, Ag(111), Au(111) and Cu(111)." In: *New Journal of Physics* 11.5 (May 2009), p. 053010. DOI: 10.1088/1367-2630/11/5/053010 (cit. on pp. 32, 36).

[120] V. G. Ruiz, W. Liu, E. Zojer, M. Scheffler, and A. Tkatchenko. "Density-Functional Theory with Screened van der Waals Interactions for the Modeling of Hybrid Inorganic-Organic Systems." In: *Physical Review Letters* 108.14 (Apr. 2012), p. 146103. DOI: 10.1103/PhysRevLett.108.146103 (cit. on pp. 10, 33, 92, 93).

[121] A. Sastre, T. Torres, M. A. Díaz-García, F. Agulló-López, C. Dhenaut, S. Brasselet, I. Ledoux, and J. Zyss. "Subphthalocyanines: Novel Targets for Remarkable Second-Order Optical Nonlinearities." In: *Journal of the American Chemical Society* 118.11 (Mar. 1996), pp. 2746–2747. DOI: 10.1021/ja9533050 (cit. on p. 32).

[122] T. Sato and H. Nakai. "Density functional method including weak interactions: Dispersion coefficients based on the local response approximation." In: *The Journal of Chemical Physics* 131.22 (Dec. 2009), p. 224104. DOI: 10.1063/1.3269802 (cit. on pp. 39, 92).

[123] A. Scarfato, S.-H. Chang, S. Kuck, J. Brede, G. Hoffmann, and R. Wiesendanger. "Scanning tunneling microscope study of iron(II) phthalocyanine growth on metals and insulating surfaces." In: *Surface Science* 602.3 (Feb. 2008), 677–683". DOI: j.susc.2007.11.011 (cit. on p. 23).

[124] M. Schlüter, J. R. Chelikowsky, S. G. Louie, and M. L. Cohen. "Self-consistent pseudopotential calculations for Si (111) surfaces: Unreconstructed (1×1) and reconstructed (2×1) model structures." In: *Physical Review B* 12 (10 Nov. 1975), pp. 4200–4214. DOI: 10.1103/PhysRevB.12.4200 (cit. on pp. 33, 95).

[125] A. Scholl, L. Kilian, Y. Zou, J. Ziroff, S. Hame, F. Reinert, E. Umbach, and R. H. Fink. "Disordering of an Organic Overlayer on a Metal Surface Upon Cooling." In: *Science* 329.5989 (July 2010), pp. 303–305. DOI: 10.1126/science.1189106 (cit. on p. 8).

[126] M. Schwarze et al. "Band structure engineering in organic semiconductors." In: *Science* 352.6292 (June 2016), pp. 1446–1449. DOI: 10.1126/science.aaf0590 (cit. on p. 32).

[127] K. Shen et al. "On-surface manipulation of atom substitution between cobalt phthalocyanine and the Cu(111) substrate." In: *RSC Advances* 7 (23 2017), pp. 13827–13835. DOI: 10.1039/C7RA00636E (cit. on p. 35).

[128] X.-Q. Shi, Y. Li, M. A. Van Hove, and R.-Q. Zhang. "Interactions between Organics and Metal Surfaces in the Intermediate Regime between Physisorption and Chemisorption." In: *The Journal of Physical Chemistry C* 116.44 (Nov. 2012), pp. 23603–23607. DOI: 10.1021/jp310007v (cit. on p. 36).

[129] P. L. Silvestrelli. "Van der Waals Interactions in DFT Made Easy by Wannier Functions." In: *Physical Review Letters* 100 (5 Feb. 2008), p. 053002. DOI: 10.1103/PhysRevLett.100.053002 (cit. on p. 92).

[130] J. C. Slater, J. B. Mann, T. M. Wilson, and J. H. Wood. "Nonintegral Occupation Numbers in Transition Atoms in Crystals." In: *Physical Review* 184 (3 Aug. 1969), pp. 672–694. DOI: 10.1103/PhysRev.184.672 (cit. on p. 102).

[131] C. Stadler, S. Hansen, I. Kröger, C. Kumpf, and E. Umbach. "Tuning intermolecular interaction in long-range-ordered submonolayer organic films." In: *Nature Physics* 5.2 (Feb. 2009), pp. 153–158. DOI: 10.1038/nphys1176 (cit. on p. 8).

[132] M. P. Steele, M. L. Blumenfeld, and O. L. A. Monti. "Image states at the interface with a dipolar organic semiconductor." In: *The Journal of Chemical Physics* 133.12 (Sept. 2010), p. 124701. DOI: 10.1063/1.3481783 (cit. on p. 8).

[133] M. P. Steele, L. L. Kelly, N. Ilyas, and O. L. A. Monti. "Resonance and localization effects at a dipolar organic semiconductor interface." In: *The Journal of Chemical Physics* 135.12 (Sept. 2011), p. 124702. DOI: 10.1063/1.3637051 (cit. on p. 8).

[134] J. Stöhr. *NEXAFS Spectroscopy*. Springer Series in Surface Sciences. Springer, 1992 (cit. on p. 99).

[135] A. Stukowski. "Visualization and analysis of atomistic simulation data with OVITO–the Open Visualization Tool." In: *Modelling and Simulation in Materials Science and Engineering* 18.1 (Jan. 2010), p. 015012. DOI: 10.1088/0965-0393/18/1/015012. URL: www.ovito.org (cit. on p. 10).

[136] E. C. H. Sykes, B. A. Mantooth, P. Han, Z. J. Donhauser, and P. S. Weiss. "Substrate-Mediated Intermolecular Interactions: A Quantitative Single Molecule Analysis." In: *Journal of the American Chemical Society* 127.19 (May 2005), pp. 7255–7260. DOI: 10.1021/ja0472331 (cit. on p. 8).

[137] M. Taillefumier, D. Cabaret, A.-M. Flank, and F. Mauri. "X-ray absorption near-edge structure calculations with the pseudopotentials: Application to the K edge in diamond and α-quartz." In: *Physical Review B* 66 (19 Nov. 2002), p. 195107. DOI: 10.1103/PhysRevB.66.195107 (cit. on p. 94).

[138] T. C. Taucher, I. Hehn, O. T. Hofmann, M. Zharnikov, and E. Zojer. "Understanding Chemical versus Electrostatic Shifts in X-ray Photoelectron Spectra of Organic Self-Assembled Monolayers." In: *The Journal of Physical Chemistry C* 120.6 (Feb. 2016), pp. 3428–3437. DOI: 10.1021/acs.jpcc.5b12387 (cit. on p. 98).

[139] F. Tautz. "Structure and bonding of large aromatic molecules on noble metal surfaces: The example of PTCDA." In: *Progress in Surface Science* 82.9 (Sept. 2007), pp. 479–520. DOI: 10.1016/j.progsurf.2007.09.001 (cit. on p. 32).

[140] J. Tersoff. "Method for the calculation of scanning tunneling microscope images and spectra." In: *Physical Review B* 40 (17 Dec. 1989), pp. 11990–11993. DOI: 10.1103/PhysRevB.40.11990 (cit. on p. 104).

[141] J. Tersoff and D. R. Hamann. "Theory and Application for the Scanning Tunneling Microscope." In: *Physical Review Letters* 50 (25 June 1983), pp. 1998–2001. DOI: 10.1103/PhysRevLett.50.1998 (cit. on p. 104).

[142] J. Tersoff and D. R. Hamann. "Theory of the scanning tunneling microscope." In: *Physical Review B* 31.2 (Jan. 1985), pp. 805–813. DOI: 10.1103/PhysRevB.31.805 (cit. on pp. 10, 104).

[143] A. Tkatchenko, R. A. DiStasio, R. Car, and M. Scheffler. "Accurate and Efficient Method for Many-Body van der Waals Interactions." In: *Physical Review Letters* 108 (23 June 2012), p. 236402. DOI: 10.1103/PhysRevLett.108.236402 (cit. on p. 92).

[144] A. Tkatchenko and M. Scheffler. "Accurate Molecular Van Der Waals Interactions from Ground-State Electron Density and Free-Atom Reference Data." In: *Physical Review Letters* 102.7 (Feb. 2009), p. 073005. DOI: 10.1103/PhysRevLett.102.073005 (cit. on pp. 10, 39, 92, 94, 105, 106).

[145] M. Toader, P. Shukrynau, M. Knupfer, D. R. T. Zahn, and M. Hietschold. "Site-Dependent Donation/Backdonation Charge Transfer at the CoPc/Ag(111) Interface." In: *Langmuir* 28.37 (Sept. 2012), pp. 13325–13330. DOI: 10.1021/la302792z (cit. on p. 8).

[146] K. Toyoda, I. Hamada, K. Lee, S. Yanagisawa, and Y. Morikawa. "Density functional theoretical study of pentacene/noble metal interfaces with van der Waals corrections: Vacuum level shifts and electronic structures." In: *The Journal of Chemical Physics* 132.13 (Apr. 2010), p. 134703. DOI: 10.1063/1.3373389 (cit. on pp. 32, 36).

[147] K. Toyoda, Y. Nakano, I. Hamada, K. Lee, S. Yanagisawa, and Y. Morikawa. "First-principles study of benzene on noble metal surfaces: Adsorption states and vacuum level shifts." In: *Surface Science* 603.18 (Sept. 2009), pp. 2912–2922. DOI: 10.1016/j.susc.2009.07.039 (cit. on p. 32).

[148] M. Trelka et al. "Subphthalocyanine-based nanocrystals." In: *Chemical Communications* 47.36 (Sept. 2011), pp. 9986–9988. DOI: 10.1039/c1cc11658d (cit. on pp. 9, 15, 19, 23, 32).

[149] L. Triguero, L. G. M. Pettersson, and H. Ågren. "Calculations of near-edge x-ray-absorption spectra of gas-phase and chemisorbed molecules by means of density-functional and transition-potential theory." In: *Physical Review B* 58 (12 Sept. 1998), pp. 8097–8110. DOI: 10.1103/PhysRevB.58.8097 (cit. on p. 103).

[150] A. Ugolotti, S. S. Harivyasi, A. Baby, M. Dominguez, A. L. Pinardi, M. F. López, J. Á. Martín-Gago, G. Fratesi, L. Floreano, and G. P. Brivio. "Chemisorption of Pentacene on Pt(111) with a Little Molecular Distortion." In: *The Journal of Physical Chemistry C* 121.41 (Oct. 2017), pp. 22797–22805. DOI: 10.1021/acs.jpcc.7b06555 (cit. on p. 36).

[151] T. Ules, D. Lüftner, E. M. Reinisch, G. Koller, P. Puschnig, and M. G. Ramsey. "Orbital tomography of hybridized and dispersing molecular overlayers." In: *Physical Review B* 90 (15 Oct. 2014), p. 155430. DOI: 10.1103/PhysRevB.90.155430 (cit. on p. 36).

[152] D. van Vörden, M. Lange, J. Schaffert, M. C. Cottin, M. Schmuck, R. Robles, H. Wende, C. A. Bobisch, and R. Möller. "Surface-Induced Dechlorination of FeOEP—Cl on Cu(111)." In: *ChemPhysChem* 14.15 (Oct. 2013), pp. 3472–3475. DOI: 10.1002/cphc.201300497 (cit. on pp. 17, 20).

[153] Y. Wang, J. Kröger, R. Berndt, and W. Hofer. "Structural and Electronic Properties of Ultrathin Tin-Phthalocyanine Films on Ag(111) at the Single-Molecule Level." In: *Angewandte Chemie International Edition* 48.7 (Feb. 2009), pp. 1261–1265. DOI: 10.1002/anie.200803305 (cit. on pp. 8, 11, 19).

[154] Y. Wang, J. Kröger, R. Berndt, and W. A. Hofer. "Pushing and Pulling a Sn Ion through an Adsorbed Phthalocyanine Molecule." In: *Journal of the American Chemical Society* 131.10 (Mar. 2009), pp. 3639–3643. DOI: 10.1021/ja807876c (cit. on p. 28).

[155] Y. Wei, S. W. Robey, and J. E. Reutt-Robey. "Flux-Selected Titanyl Phthalocyanine Monolayer Architecture on Ag (111)." In: *The Journal of Physical Chemistry C* 112.47 (Nov. 2008), pp. 18537–18542. DOI: 10.1021/jp8063678 (cit. on p. 8).

[156] M. Willenbockel, R. J. Maurer, C. Bronner, M. Schulze, B. Stadtmuller, S. Soubatch, P. Tegeder, K. Reuter, and F. Stefan Tautz. "Coverage-driven dissociation of azobenzene on Cu(111): a route towards defined surface functionalization." In: *Chemical Communications* 51.83 (Oct. 2015), pp. 15324–15327. DOI: 10.1039/C5CC05003K (cit. on p. 15).

[157] G. P. Williams. *X-Ray Data Booklet*. Ed. by A. Thompson and D. Vaughan. Lawrence Berkeley National Laboratory, University of California, Oct. 2009. URL: http://xdb.lbl.gov (cit. on pp. 97, 103).

[158] E. Wruss, O. T. Hofmann, D. A. Egger, E. Verwüster, A. Gerlach, F. Schreiber, and E. Zojer. "Adsorption Behavior of Nonplanar Phthalocyanines: Competition of Different Adsorption Conformations." In: *The Journal of Physical Chemistry C* 120.12 (Mar. 2016), pp. 6869–6875. DOI: 10.1021/acs.jpcc.6b00312 (cit. on pp. 19, 20, 35).

[159] Q. Wu and W. Yang. "Empirical correction to density functional theory for van der Waals interactions." In: *The Journal of Chemical Physics* 116.2 (Jan. 2002), pp. 515–524. DOI: 10.1063/1.1424928 (cit. on p. 92).

[160] H. Yamane, H. Honda, H. Fukagawa, M. Ohyama, Y. Hinuma, S. Kera, K. Okudaira, and N. Ueno. "HOMO-band fine structure of OTi- and Pb-phthalocyanine ultrathin films: effects of the electric dipole layer." In: *Journal of Electron Spectroscopy and Related Phenomena* 137-140 (July 2004), pp. 223–227. DOI: 10.1016/j.elspec.2004.02.054 (cit. on p. 8).

[161] P. Zahl, M. Bierkandt, S. Schröder, and A. Klust. "The flexible and modern open source scanning probe microscopy software package GXSM." In: *Review of Scientific Instruments* 74.3 (Mar. 2003), pp. 1222–1227. DOI: 10.1063/1.1540718 (cit. on p. 9).

[162] P. Zahl, T. Wagner, R. Möller, and A. Klust. "Open source scanning probe microscopy control software package GXSM." In: *Journal of Vacuum Science & Technology B, Nanotechnology and Microelectronics: Materials, Processing, Measurement, and Phenomena* 28.3 (May 2010), C4E39–C4E47. DOI: 10.1116/1.3374719 (cit. on p. 9).

[163] Z. Zhang, T. Wächter, M. Kind, S. Schuster, J. W. Bats, A. Nefedov, M. Zharnikov, and A. Terfort. "Self-Assembled Monolayers of Perfluoroanthracenylaminoalkane Thiolates on Gold as Potential Electron Injection Layers." In: *ACS Applied Materials & Interfaces* 8.11 (Mar. 2016), pp. 7308–7319. DOI: 10.1021/acsami.6b00532 (cit. on pp. 77–79, 81).

[164] L. Zoppi, A. Garcia, and K. K. Baldridge. "Theoretical Investigation of the Binding Process of Corannulene on a Cu(111) Surface." In: *The Journal of Physical Chemistry A* 114.33 (Aug. 2010), pp. 8864–8872. DOI: 10.1021/jp102662t (cit. on p. 36).

Stories never end, it is the narrator who tires.
— Yours truly!

COLOPHON

This document was typeset using the typographical look-and-feel `classicthesis` developed by André Miede. The style was inspired by Robert Bringhurst's seminal book on typography *"The Elements of Typographic Style"*. `classicthesis` is available for both LaTeX and LyX:

https://bitbucket.org/amiede/classicthesis/

The LyX port was used for this work. Porting was initially done by Nicholas Mariette in March 2009 and continued by Ivo Pletikosić in 2011.

Completed on May/Mai 3, 2018 in Graz.